Electrodynamics of Nearly Ferroelectric Superconductors in the local London and non-local Pippard limits

by

Upali Aparajita

A dissertation submitted to the Graduate Faculty in Physics in partial fulfillment of the requirements for the degree of Doctor of Philosophy, The City University of New York.

2010

This manuscript has been read and accepted for the Graduate Faculty in Physics in satisfaction of the dissertation requirements for the degree of Doctor of Philosophy.

(Professor Sultan Catto)

Date — Chair of Examining Committee

(Professor Steven G. Greenbaum)

Date — Executive Officer

Distinguished Professor Joseph L. Birman

Professor Alexander Kheyfits

Professor Tobias Schaefer

Supervisory Committee

THE CITY UNIVERSITY OF NEW YORK

Abstract

Electrodynamics of Nearly Ferroelectric Superconductors in the local London and non-local Pippard limits

by

Upali Aparajita

Advisor: Distinguished Professor Joseph L. Birman

In this work, electrodynamics of a Nearly Ferroelectric Superconducting (NFE-SC) material in local London limit and nonlocal Pippard limit is reported. NFE-SC materials exhibit superconductivity and are in a nearly-ferroelectric state. One example of such materials is n or p doped $SrTiO_3$. The structure of a single vortex in an NFE-SC thin film is explored. Taking $n - SrTiO_3$ as our sample of choice, the frequency dependent magnetic field and current within the sample are calculated. The expulsion of the vortex from the sample at resonances is observed. The interaction between two vortices due to the presence of high background dielectric is explored. The effect of finite thickness on the vortex structure is explored for an NFE-SC

film. With increase in film thickness, the resonances become sharper and as a result the system undergoes oscillatory transition between ferroelectric, superconducting and Meissner-like states.

Nonlocal effects in the NFE-SC thin film are explored in the Pippard limit. Specular Reflection and Random scattering are studied. Analytical as well as numerical methods are used to investigate the nature of the material and solve for the current and magnetic field within the sample. The current is found to be non-zero within the sample. The material properties can be manipulated to enhance or expel the current from within the sample with the change in frequency. The material shows complex transitions between Type-I, Type-II superconducting as well as Dielectric states. Numerical codes developed for the solution of the integro-differential equations are given.

Preface

We discuss the electrodynamics of a Nearly-Ferroelectric Superconducting (NFE-SC) material in the local London approximation and non-local Pippard limit. An NFE-SC material exhibits superconductivity and is in a nearly ferroeletric (NFE) state. An example of such materail is n or p doped $SrTiO_3$.

In the first chapter, we give an overview of Ferroeltricity and in the second chapter we discuss Superconductivity. These two review chapters provide the necessary background physics behind the Neraly-Ferroelectric Superconductors. In the third chapter, the initial work done on the electrodynamics of NFE-SC materials by Birman and Zimbovskaya are discussed which gives us an understanding of this novel material. In the fourth and fifth chapter we discuss the new work we have done on the vortex structure inside an NFE-SC thin film and film of finite thickness in the London limit as well as extend and explore the physics behind it in the non-local Pippard limit.

Acknowledgments

I extend my sincere thanks to my thesis advisor Professor Joseph L. Birman for his guidance and support. I am very grateful to Professor Sultan Catto for being there for me through out this journey. Special thanks to my dear friends Francesca Gianferrara and Oleksiy Roslyak for the much needed moral support and for not giving upon me. Going through this Ph.D. has been a learning and life changing experience. It would not have been possible without the understanding and encouragement of my family whom I can not thank enough. This thesis work was partly supported by PSC-CUNY grant.

Contents

List of Figures

Chapter 1

FERROELECTRICITY

1.1 Introduction

The unusual dielectric properties of Rochelle salt (Sodium potassium tartrate tetrahydrate,$NaKC_4H_4O_{6.}4H_2O$) were reported by Pockels in 1894 (Kanzing, 1957). But after J. Valesek in 1920 reported that the dielectric properties of the Rochelle salt were analogous to the magnetic properties of the ferromagnetic materials the interest in Ferroelectrics intensified. Ferromagnetism was already known at that time. Ferroelectricity is named in analogy with ferromagnetism which occurs in such materials as iron.

The term ferromagnetism is used for materials that exhibit spontaneous magnetization or a net magnetic moment in the absence of an external magnetic field. For example, consider the case of iron atoms. They are tiny magnets which spontaneously align themselves in clusters called ferromag-

netic domains below some transition temperature called T_c. These domains can be oriented in a particular direction by application of an external magnetic field.

Similarly, in ferroelectric materials, the crystal has a net macroscopic polarization even in the absence of an externally applied field. Ferroelectric materials, for example, Barium Titanate ($BaTiO_3$) and Rochelle Salt are composed of crystals in which the structural units are tiny electric dipoles. In each of these units the centers of positive charges and those of the negative charges are slightly separated. In some crystals, these dipoles spontaneously align themselves into domains which are basically clusters of dipoles. In ferroelectric crystals these domains can be oriented predominantly in a particular direction by the application of a strong external electric field.

Due to the similarity between properties, presence of net magnetic moment in ferromagnets and net dipole moment in ferroelectrics, the prefix 'ferro', which means iron, was used to describe the property despite the fact that most ferroelectric materials do not have iron in their lattice.

To understand how ferroelectricity arises, we should look at the molecular structure of the ferroelectric materials[14] . A centro-symmetrical molecule such as methane (CH_4) has no dipole, but many molecules are not symmetric (e.g., H_2O) and have a dipole moment.

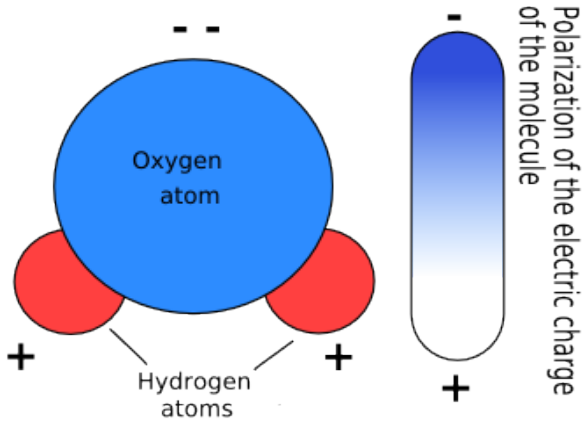

Figure 1.1: Water Molecule

Dipole moment is defined as

$$\mathbf{p} = \int \rho(\mathbf{r})\mathbf{r}dv \tag{1.1}$$

where $\rho(\mathbf{r})$ is the charge density of the molecule.

If we consider atoms as the point charges Q_i at positions $\vec{R}_i$, then the polarization can be written as

$$\mathbf{p} = \sum Q_i \mathbf{R}_i \tag{1.2}$$

To understand the origin of ferroelectricity, its necessary to understand the concept of electric polarization. Appearance of ferroelectricity can be found in crystallized nonconducting substances having at least one polar axis. These type of materials have no center of symmetry. Lets consider the following situations to understand the concept of polar axis[15]. If the two

directions of a line can be distinguished then its considered polar. A polar line has a 'head' and a 'tail'. Similarly, a plane is called polar if its two surfaces are not equivalent. Polarity of the plane arises from having a 'front' and a 'back'. This definition of polarity is different than charge separation. A sheet of paper with one side painted is polar with respect to its color and a vertical line on Earth's surface is polar with respect to gravity. An axis is polar if its two ends are not brought into coincidence by the symmetry transformations of the symmetry group of its figure. Polarity is excluded if a symmetry group includes a center of symmetry. When a centrosymmetric figure under goes inversion, a directed line or a segment of a face changes direction. In the case of the absence of a center of symmetry, there will be at least one directed line or face which is not accompanied by its parallel counterparts reversed in direction,[1].

The significance of polar axis is clear in crystal morphology. Fig. (1.3)(a) shows two centrosymmetric *acetanilide* crystals, following Curtin and Paul[16] . The faces occur in parallel pairs in both habits. On the other hand, the *p-chloroacetanilide* crystal shown in Fig. (1.3)(b) is noncentrosymmetric, and some of the faces occur without parallel ones at the opposite end of the crystal. This crystal has a polar axis parallel to its long direction.

Polar axis is not exclusive to complicated systems. Very simple systems

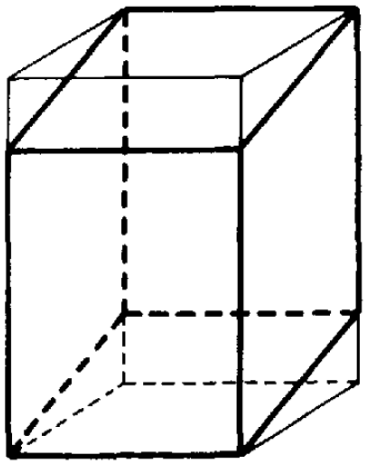

Figure 1.2: Diagram of a Parallelepiped, an object with a center of symmetry[1].

can also form polar crystals. For example, lets consider a polar crystal composed of diatomic molecules AB[16]. The molecular axis will be oriented more along the polar direction of the crystal than perpendicular to it. The crystal has an $ABAB$.. array. In order to have polar axis, the spacings between the atom A and the two adjacent atoms B must be unequal as demonstrated in fig. 1.4. One can try to understand this concept from the point of view of a submicroscopic traveller proceeding along this array of atoms . The traveller is able to determine the direction due to the difference in spacings. The distance is always longer from atom B to atom A and shorter from atom A to the next atom B in one direction whereas the reverse is true in the opposite

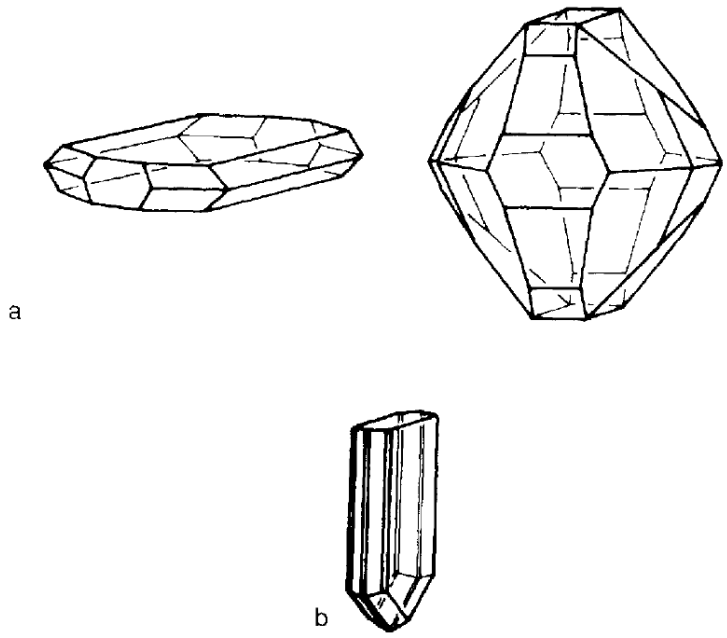

Figure 1.3: (a) Centrosymmetric rhombic hipyramidal acetanilide; (b) Non centrosymmetric rhombic pyramidal *p*-chloroacetanilide,[1]

A B A B A B . . .

Figure 1.4: Polar crystal composed of diatomic molecules AB,[1]

direction [1].

Polar crystals exhibit important physical properties such as pyroelectricity, piezoelectricity and ferroelectricity. The primitive cell of a pyroelectric crystal possesses a dipole moment. The separation of the centers of the positive and negative charges changes upon heating. In this process the two charges migrate to the two ends of the polar axis. Piezoelectricity is the separation of the positive and negative charges upon expansion/compression of the crystal.

Presence of a center of symmetry prohibits ferroelectricity. Ferroelectric crystals have one polar axis and show a spontaneous ferroelectric polarization. Crystals with more than one polar axis can have induced electrical polarization by the application of elastic stress. Such crystals are called piezoelectrics. Extension or compression will induce electrical polarization of opposite signs. Ferroelectric materials have a noncentrosymmetric unit cell and a spontaneous electrical polarization at room temperature. The direction of the spontaneous polarization can be switched by applying an external electric field. This aligns the dipoles so that the total dipole moment can be written as[14]

$$\mathbf{p} = \sum_{\mathbf{molecules}} \mathbf{p}_{\mathbf{molecule}} \tag{1.3}$$

Defining the dipole moment per unit volume as $\mathbf{P}$ we can write $\mathbf{P}$ as

$$\mathbf{P} = \frac{\mathbf{p}}{V} \tag{1.4}$$

where V is the total volume of the system(though it should be noted that for ultrasmall systems, the boundaries of the system are not sharp) .

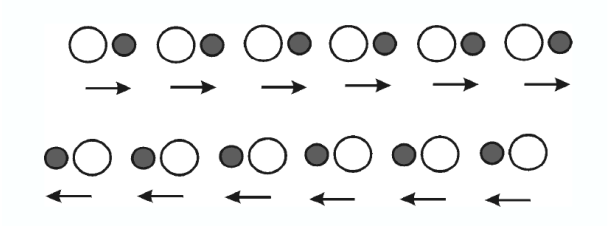

Figure 1.5: Model crystal,[2],[3]

A defining property of the ferroelectric crystals is the switching between different metastable states by the application and removal of an electric field. To better understand the properties of ferroelectrics let us consider a one-dimensional crystal made up of two atoms of opposite charge as seen in fig.(1.5). The system can be manipulated so that all the dipoles point to the right or to the left. This does not make a difference to the structure or energy of the system except the signs of the dipole moments will have opposite signs [2],[3].

When the crystal undergoes a change in polarization, provided it is stable in both polarized states, there exists an energy barrier between the two states. A curve for the energy as a function of polarization is given in Fig. (1.6)

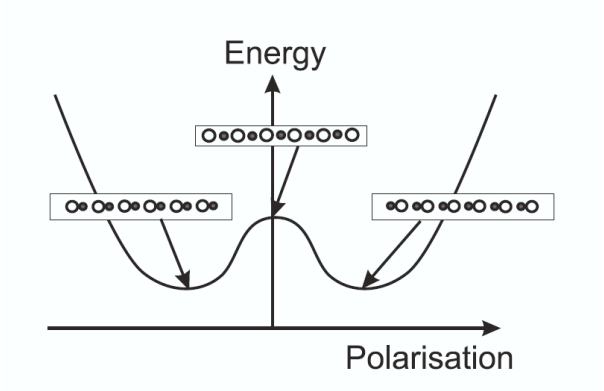

Figure 1.6: Schematic potential well,[2],[3]

If an electric field **E** is applied to this crystal, the two stable states will no longer have the same energy because of the electric polarization energy $-\mathbf{P}\cdot\mathbf{E}$. The wells in the energy vs. polarization curve are no longer balanced, they become rather tilted. A small electric filed will not act immediately to overcome the energy barrier needed to reverse the polarization. In the ideal ferroelectric, where all the dipoles have to be overturned together, there will be hysteresis schematically demonstrated in Fig. (1.7).

1.2 Macroscopic Properties of Ferroelectrics

1.2.1 Ferroelectric Phase Transitions

Generally above the Curie temperature T_c, ferroelectric materials exist in a non-polar state. They also have high static dielectric constants close to the Curie temperature. In certain temperature regions, one can observe hystere-

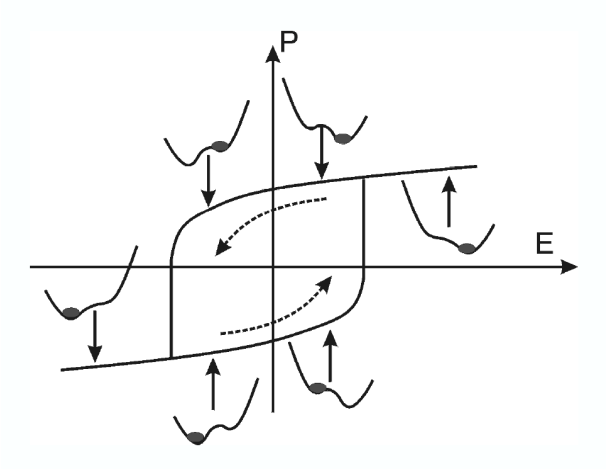

Figure 1.7: Hysteresis in an idealized ferroelectric,[2],[3]

sis loops. For $T > T_C$, the crystal exhibits dielectric behavior. Figure(1.8) represents the variation of dielectric constant vs. temperature. As we can see from this figure, there is a sharp increase in the dielectric constant at T_c. The dielectric constant ε_r is said to have an 'anomalous value' in the neighborhood of T_c. For $T > T_c$, this anomalous behavior follows the Curie-Weiss relation

$$\varepsilon_r = \frac{C}{T - T_c} \tag{1.5}$$

where C is the Curie constant. In general, anomalous behavior is observed near any point of phase transition, [2],[3].

One of the identifying characteristics of a ferroelectric material is the non-zero value of polarization in the absence of an externally applied electric field.

It can be said that the ferroelectric materials have spontaneous polarization. The direction of the polarization can be reversed by reversing the direction of the applied field. The value of the spontaneous polarization increases rapidly once the transition point is crossed, then gradually reaches a saturation point at a lower temperature. The polarization P shows non-linear behavior and hysteresis w.r.t. the applied electric field E as shown in the figure(1.9) . These are the most prominent features of a ferroelectric material, [4].

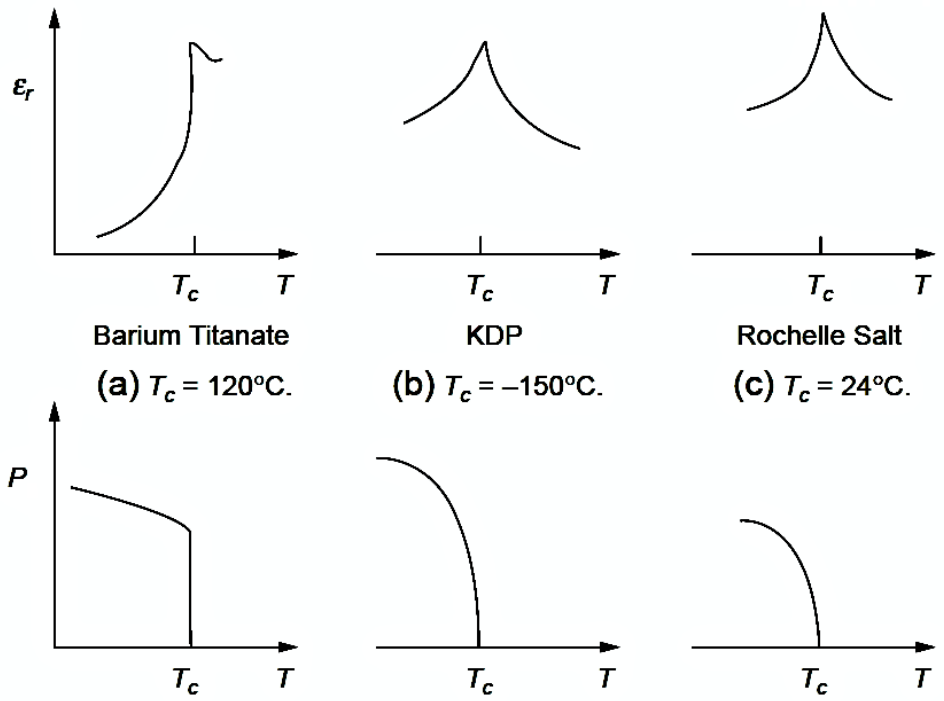

Figure 1.8: Variation of the dielectric constant ε_r and polarization P w.r.t. temperature T,[4]

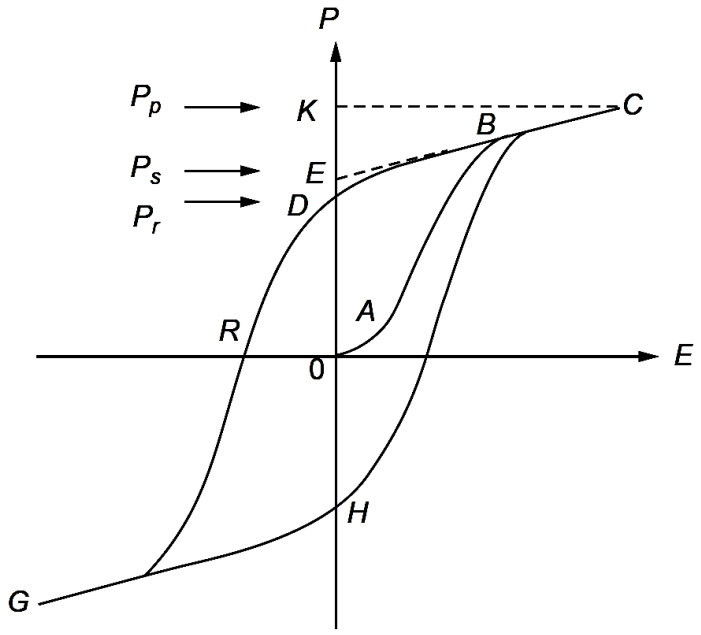

Figure 1.9: Hysteresis curve,[4]

As shown in the figure (1.9), the value of polarization increases linearly with the applied electric field. The reason behind it is that the applied field is not strong enough to cause orientation of the domains (portion OA). As the strength of the applied field increases, the domains start to orient themselves along the direction of the applied filed and the increase in polarization shows non-linearity (portion AB). With further increase in the field, the polarization reaches a saturation (portion BC) where most of the domains have aligned themselves along the filed. If the value of the electric field is gradually decreased to zero, the polarization decreases following the path CBD.

OE represents spontaneous polarization P_s and OD represents the remnant polarization P_r. $P_r < P_s$ because when the field is reduced and goes to zero, some domains return to their original orientation hence reducing their contributions to the net polarization The electric field required to make P zero is called the 'coercive field', E_c (portion OR). This coercive field depends on the temperature as well as the frequency and the wave form of the applied field. The area of the hysteresis loop gives the energy dissipated in the form of heat inside the specimen during each cycle. The measurements for hysteresis are generally done with low frequency(60 Hz or lower) AC fields so as not to heat the specimen [4].

In ceramics which are polycrystalline materials composed of crystallites, ferroelectricity is harder to demonstrate due to the random orientation of the crystallites. Ferroelectricity is rather easily detected in single crystal specimen. In these materials the change in polarization is abrupt thus creating a square hysteresis loop as shown in the figure (1.10)(a). In case of ceramics, the reversal of polarization is sluggish which makes the hysteresis loop rounded as shown in the figure (1.10)(b), [4].

Ferroelectric materials are not polar above T_c. The shape of a hysteresis loop depends on temperature. Figure (1.11) represents the hysteresis loop for Rochelle salt for two different temperatures. For $T > T_c$, the loop

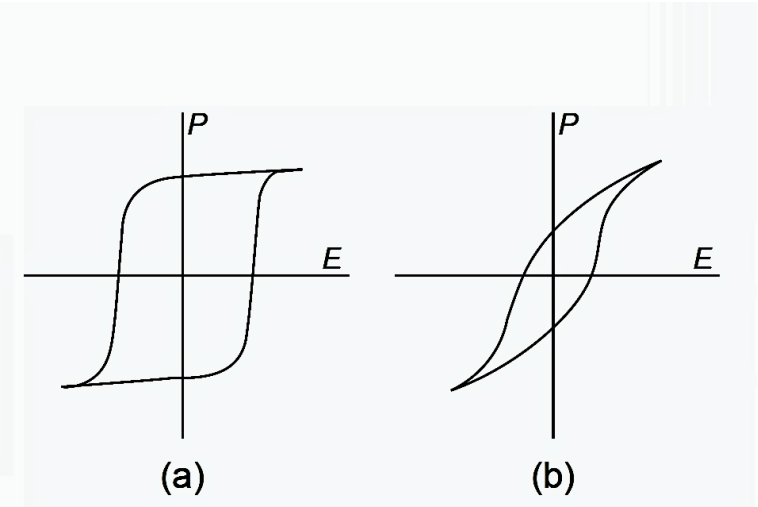

Figure 1.10: Schematic diagram of 'square' and 'rounded' hysteresis loops,[4]

becomes diminished and then eventually degenerates to a straight line for temperatures much greater than T_c. At this temperature, the ferroelectricity is completely destroyed. The applied electric field affects the appearance of ferroelectrics. A paraelectric material ,which exists at a temperature greater than T_c, can be driven into the ferroelectric state by increasing the applied electric field beyond a critical value E_t. This shifts the Curie point to a higher temperature [4].

In a crystal lattice the size of the unite cells a well as the force of ions are temperature dependent. At the transition temperature or critical temperature, the structure of the crystal becomes unstable which paves the path for transition to a more stable structure. The small ionic movements involved

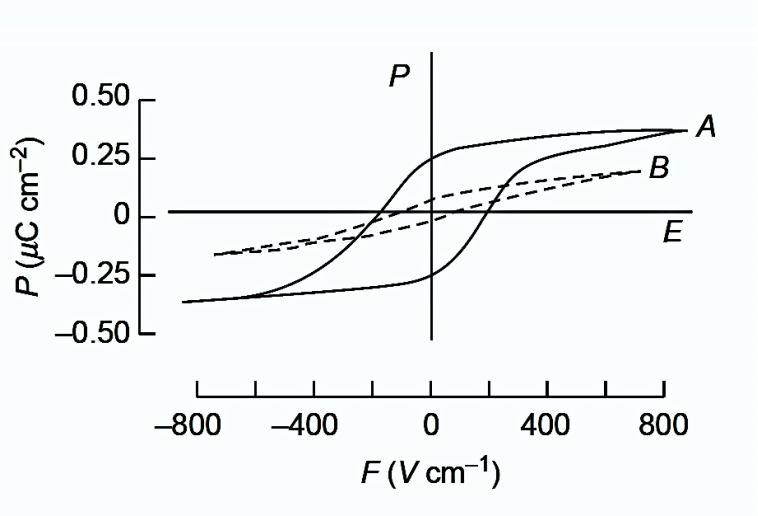

Figure 1.11: Temperature dependence of the hysteresis loop for Rochelle salt,[4]

in the transition create internal stresses in the material. If the magnitude of the stresses is strong enough it can cause internal cracks. Transition from one crystal structure to another generally involves changes in volume and entropy. When the spontaneous polarization goes from zero to a finite value or from one finite value to another, the change in polarization can be continuous or discontinuous. If discontinuity is involved, then the transition is called a 'first order transition' as in $BaTiO_3$ and $KNbO_3$. In case of first order transitions, the change in entropy occurs at a constant temperature. Latent heat also changes during the transition. If the change in polarization is continuous, this is a 'second order transition' as in KH_2PO_4 and Rochelle salt. Entropy and latent heat do no change at the transition temperature [4].

1.2.2 Ferroelectric Materials

Ferroelectricity was first discovered in hydrogen-bonded materials Rochelle Salt and KDP . The 1949 discovery of ferroelectricity in the perovskite oxide $BaTiO_3$ revolutionized the understanding of the phenomenon. Perovskites are now widely studied and $BaTiO_3$ is a typical example of this family. The simplicity of the perovskite structure provides a better understanding of the origin of ferroelectricity. Additional examples of ferroelectric materials involve intergrowth of perovskite layers with other oxides. Also some additional ferroelectric oxides exist which are not related to perovskites.

1.2.3 Perovskite Oxides

Perovskite oxides are the materials which have the same type of crystal structure as $CaTiO_3$, known as the perovskite structure. Perovskites take their name from this compound which was first discovered in the Ural mountains of Russia by Gustav Rose in 1839 and is named after Russian mineralogist L.A. Perovski (1792-1856). A brief discusiion of the perovskite crystal structure is given here due to our interest in perovskite like materials in the study of Nearly Ferroelectric Superconductors (discussed in Chapter 3).

Ideal perovskites are simple cubic in structure. There are five atoms in unit cell. Its structure can be compared to that of the molecular struture

of the family ABO_3. In an ideal unit cell of such compund, the cube corner position (0,0,0) is occupied by an A atom, whereas the bodycenter position (1/2,1/2,1/2) is occupied by a B atom and the (1/2,1/2,0) or the face centered position is taken by the oxygen atom [3],[17].

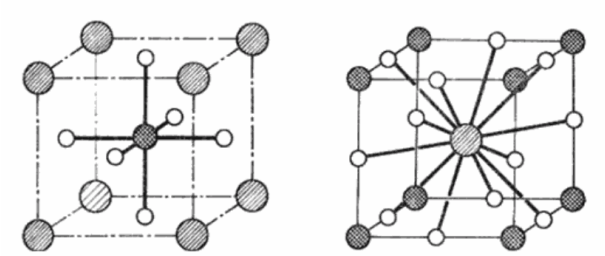

Figure 1.12: Two different views of the unit cell of the ABO_3 ideal cubic perovskite structure. The B atom (grilled pattern) is at the center of an octahedron composed of oxygen atoms (white pattern). The A atom (dashed pattern) has 12 oxygen first neighbors,[3]

The B atom is the center of six oxygen first neighbors occupying the corners of a regular octahedron as shown in the figure (1.12). The octahedras are connected at their corners thus making a simle cubic network and enclosing large holes that are occupied by A atoms. each A atom is surrounded by twelve oxygen atoms.The arrangement and size requirement for the atoms to maintain stability are quite strict. Any slight distortion or bulking can produce lower symmetry distorted versions where the coordination numbers of A and B are both reduced. There is empirical criterion for the stability of perovskite-like structures, as proposed by Goldschmidt in 1926. Ionic radius

plays a big role in Goldschmidt's model. The rules are : "(i) a cation will be surrounded by as many anions as can touch it, but no more; (ii) all the anions must touch the cations and the anion-cation distance is obtained as the sum of their ionic radii." [3]. The relationship between ionic radii follows from these rules as

$$r_A + r_O = \sqrt{2}\,(r_B + r_O) \tag{1.6}$$

An ideal cubic perovskite structure does not satisfy this condition. Introduction of 'tolerance factor' takes care of the deviation from this condition. The tolerance factor t is defined as

$$t = \frac{r_A + r_O}{\sqrt{2}\,(r_B + r_O)} \tag{1.7}$$

$t \approx 1$ is suitable condition for the formation of perovskites. For $t > 1$, a small disrotion develops in the material. This occurs due to the imposition of the $A - O$ distance and the Perovskite structure is formed when $t \approx 1$. When $t > 1$, the structure develops a small polar distortion, because the structure is imposed by the $A - O$ distance and the B atom is too small for the oxygen octahedron. An example is $BaTiO_3$. When $t < 1$, the atom A is small compared to the hole in the octahedra and it cannot effectively bond with all 12 of its neighboring O atoms. If t is only slightly less than one, the oxygen octahedra undergo rotation and tilting as in $SrTiO_3$ and $CaTiO_3$.

For smaller t, the compound favors a strongly distorted structure with only six neighbors for the A atoms as in $LiNbO_3$. If the value of t is very different than one, the perovskite structure is not favorable [3].

The first perovskite oxide compound identified as being ferroelectric was $BaTiO_3$. It is a ferroelectric ceramic material with piezoelectric properties. It has different phases as solid depending on the temperature. At high temperature, it has a paraelectric cubic perovskite structure. As the temperature is lowered, at 393 K, it transforms from a cubic phase to a ferroelectric tetragonal phase. This phase remains stable until 278 K, where there is a second transformation to a ferroelectric phase of orthorhombic symmetry. The last transition occurs at 183 K. The low-temperature ferroelectric phase is rhombohedral. All of the structures exhibit ferroelectricity except the cubic structure. $KNbO_3$ is isostructural with $BaTiO_3$, exhibiting the same sequence of phases, though the transition temperatures are different; 701 K for cubic to tetragonal, 488 K for tetragonal to orthorhombic and 210 to 265 K for orthorhombic to rhombohedral [3].

Another widely studied material of interest is $SrTiO_3$. It is a centrosymmetric paraelectric material with a perovskite structure. At room temperature it exists in the cubic form, but transforms into the tetragonal ferroelectric structure at temperatures close to 120 K.As the temperature is

lowered a structural phase transition occurs at 120 K in which the oxygen octahedra rotate around a cartesian axis to lower the symmetry to tetragonal and Ti ion is no longer in the center. At very low temperature $SrTiO_3$ exhibits piezoelectric and superconducting characteristics. Strontium titanate also exhibits a very large dielectric constant (300).

1.2.4 Landau-Devonshire Theory

The study of the critical phenomena which occur very close to a second order phase transition is rather interesting. The apparent close similarity of critical behavior in widely different physical contexts is noteworthy. For example the behavior of a ferromagnet near its Curie point is very similar to that of a liquid near its critical point. Many similarities can be noticed between a superconducting transition and a second order ferroelectric transition[18]. The simplest view of a phenomena near a critical point is universal in character and attributes certain common characteristics to all phase transitions. Landau theory was introduced by Lev Landau in an attempt to formulate a general theory of second-order phase transition[19]. Landau's symmetry-based treatment of phase transitions was first applied to the case of ferroelectrics by *Devonshire*[20].

Thermodynamical variables such as temperature T, entropy S, electric

field E, polarization P, stress σ and strain s can completely define the thermodynamic equilibrium state of a crystal[14]. The external variables are the externally applied electric field and the the elastic stress. The polarization and the strain are the internal variables.

The free energy F can be expressed as a function of ten variables; three components of polarization, six components of the stress tensor and temperature. Values of the dependent variables in thermal equilibrium are obtained at the minimum of the free energy. The free energy can be expanded in terms of the dependent variables and the coefficients of expansion can be obtained from experimental data or microscopic theory. If we take a free, unpolarized and unstrained crystal, the origin of energy for such a crystal can be taken as zero, hence

$$F_P = \frac{1}{2}aP^2 + \frac{1}{4}bP^4 + \frac{1}{6}cP^6 + ... - EP \tag{1.8}$$

Here E is the electric field. The unknown coefficients $a, b, c..$ etc are temperature dependent and can be of either positive or negative sign. At equilibrium

$$\frac{\partial F}{\partial P} = 0 \tag{1.9}$$

The free energy has a minimum at the origin for $E = 0$ when the coefficients are all positive. If we ignore the higher order terms, the induced polarization

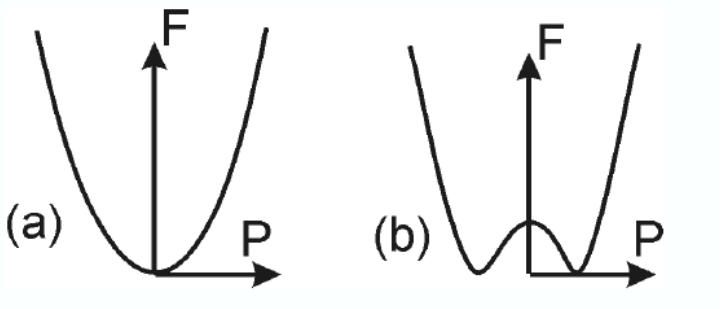

Figure 1.13: Schematic diagram of the Free energy vs Polarization for (a) Paraelectric material and (b) Ferroelectric material,[2],[3]

can be obtained from

$$\frac{\partial F}{\partial P} = aP - E = 0 \tag{1.10}$$

The dielectric susceptibilty can be obtained from (1.10) such as

$$\chi = \frac{P}{E} = \frac{1}{a} \tag{1.11}$$

Spontaneous polarization occurs when $a < 0$ but $b, c > 0$. Here the free enrgy shows a minimum at a finite polarization P as shown in the figure (1.13 (b)). In this case the material is ferroelecric. At the Curie point T_0, $a(T)$ changes sign and varies linerly with temperature as $a' \times (T - T_0)$. When it comes to predicting the behaviour of free energy, polarization and susceptibility, this is an useful phenomenological theory, as shown in figure (1.14), [2],[3].

When $b < 0$, but c is positive, the free energy may have a subsidiary min-

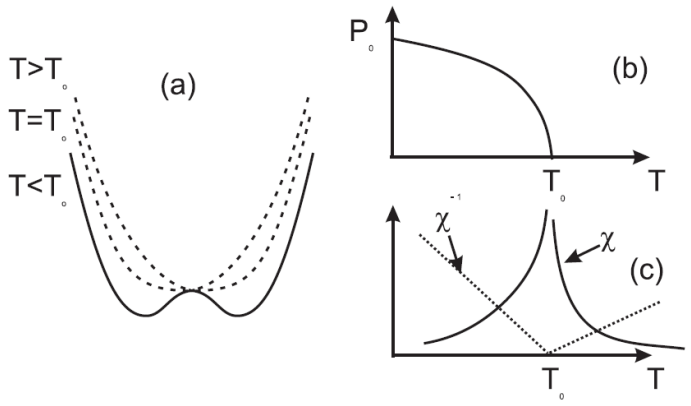

Figure 1.14: Second order phase transition. (a) Free energy as a function of the polarization at $T > T_0$,$T = T_0$ and $T < T_0$; (b) Spontaneous polarization,[2],[3]

imum abruptly at non-zero P as shown in the figure (1.15). When the value of a goes down with lowering of the temperature, the minimum of energy drops below that of the unpolarized state and is favoured thermodynamically. This happens at the Curie temperature T_c. Within the temperature range T_c and T_0, the unpolarized phase exista as a local minimum of the free energy. Here its noteworthy that the order parameter jumps discontinuously to zero at T_c. Such phase transitions are called first-order phase transition. A common example of such transition is solid-liquid transition [2],[3].

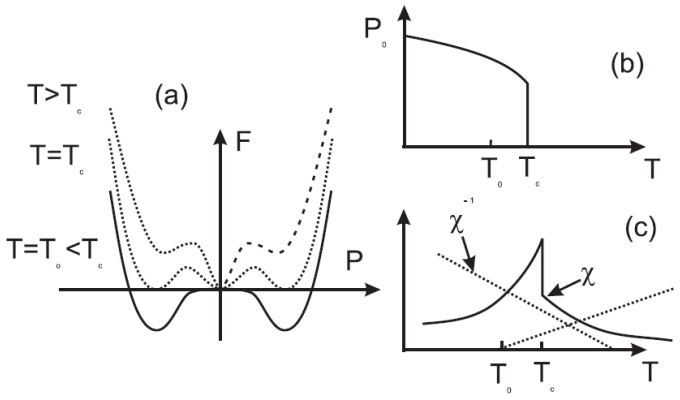

Figure 1.15: First order phase transition. (a) Free energy as a function of the polarization at $T > T_c$,$T = T_c$ and $T = T_0 < T_c$; (b) Spontaneous polarization as a function of temperature (c) Susceptibility χ,[2],[3]

Effect of Strain

Elastic stress strongly affects ferroelectric materials. To understand the effect of strain, a related term can be added to equation (1.8). For a uniaxial ferroelectric the equation can be written as

$$F_s = \frac{1}{2}Ks^2 + dsP^2 + ... - s\sigma \tag{1.12}$$

Here s represents a componet of the strain field. The first term of this expansion can be recognised as Hooke's law. K is the elastic constant. The second term of this equation gives us the soupling between the polarization P and the elastic strain s. If we consider the variation of displacement **u** of

a point in the solid with position $\mathbf{r}$, the strain can be written as

$$s_{ij} = \frac{1}{2}\left(\frac{\partial u_i}{\partial r_j} + \frac{\partial u_j}{\partial r_i}\right) \tag{1.13}$$

Here i,j mean the x,y,z components of the vectors. s is therefore a 3x3 symmetric matrix, with six independent components. Generally polarizationcan couple to one or more type of starin. In a cubic crystal such as $BatiO_3$ polarization can point along one of the six orthogonal cubic directions [2],[3].

The free energy can now be written as a combination of the terms from (1.8) and (1.12) , $F = F_P + F_s$. At equlibrium, the properties of the free energy can be determined by minimizing it with respect t the plarization P and strain s, such as

$$\frac{\partial F\left(P,s\right)}{\partial P} = \frac{\partial F\left(P,s\right)}{\partial s} = 0 \tag{1.14}$$

From the minimisation of free energy w.r.t. s, we obtain

$$\frac{\partial F\left(P,s\right)}{\partial s} = Ks + dP^2 - \sigma \tag{1.15}$$

When $P = 0$, this becomes Hook's law where $s = \sigma/K$. If there is no external stress applied so that ($\sigma = 0$), then one obtains

$$s = -dP^2/K \tag{1.16}$$

This implies that a "spontaneous (tetragonal strain) occurs proportional to the square of the polarization".

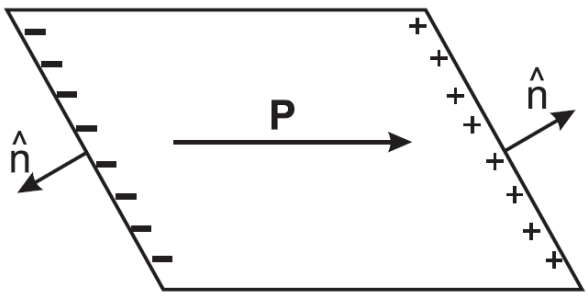

Figure 1.16: Surface charge density generated by a bulk polarization at an interface,[2],[3]

Substituting the strain s as a fucntion of the polarization P in the expansion of free energy, we obtain

$$F\left(P, s\left(P\right)\right) = \frac{1}{2}aP^2 + \frac{1}{4}\left(b - 2d^2/K\right)P^4 + \frac{1}{6}cP^6 + ... - EP \qquad (1.17)$$

If we compare the expression for free energy without strain (clamped system) to this expression with strain, we that there is no dependence on the sign of d. For a first order transition where $b < 0$, the transition is even more first-order and the value of T_c goes up [2],[3].

1.2.5 Domains

Ferroelectrics do not always have uniform polarization throughout. The reasons for the non-uniform polarization can be attributed to defects on a microscopic level, the material undergoing non-uniform strain and the thermal

and electrical history of the sample. Even the most ideal ferroelectric crystals can have domains. The polarization in the bulk is the result of separation or displacement of the positive charge with respect to the negative charge. This can produce net positive and negative charge density on the opposite sides of the crystal(Fig. 1.16). We can write the surface charge density per unit area as

$$\sigma = \mathbf{P} \cdot \mathbf{n} \tag{1.18}$$

where $\mathbf{n}$ is the vector normal to the boundary. The charges accumulated on the surface produce fields internal and external to the material. These fields store energy in the manner of a capacitor [2],[3].

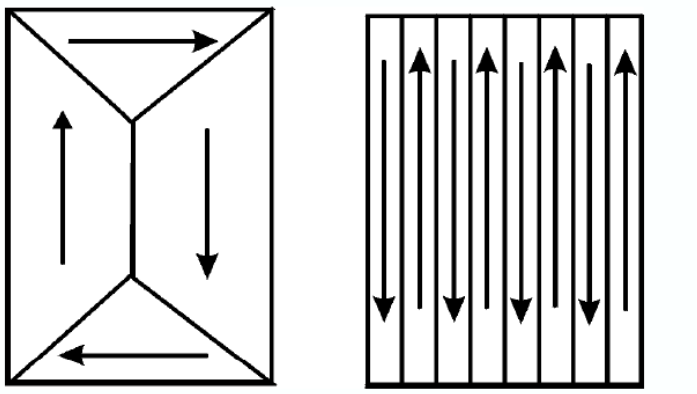

Figure 1.17: Ideal domain configuration in a single crystal of cubic ferroelectric material, where the coupling strain is negligible. On the right is the configuration adopted when strain affects are important,[2],[3]

The system tries to minimize its energy by getting rid of the charges on

the surface. For example in a ferroelectric thin film the polarization vector would 'prefer' to be oriented 'lying down' in the plane of the film rather than 'standing up' or pointing towards the direction which is perpendicular to the film. In a thick crystal, where all the dimensions are considerable in size, polarization is always oriented along the direction that is parallel to the crystal surface. Domains walls can be introduced in such case. This produces polarization charges unless the walls are appropriately oriented [2],[3].

The charge density between the interface of two neighboring domains can be written as, analogous to the formula for charge density at a free surface,

$$\sigma = (\mathbf{P}_1 - \mathbf{P}_2) \cdot \mathbf{n} \tag{1.19}$$

where $\mathbf{P}_1$, $\mathbf{P}_2$ are the polarizations of the two domains, and $\mathbf{n}$ is a unit vector normal to the interface. We can see from this equation that the surface charge density will vanish when the polarizations are oriented in opposite directions of each other or are anti parallel to each other and are parallel to the domain walls or a 180° domain wall. σ also goes to zero when the domain wall bisects the angle between two domains pointing 'head to tail'. In most common variety of crystals, the possible polarizations are perpendicular to each other, called a 90° domain wall. Both 90° and the 180° domain walls are shown in figure (1.17), [2],[3].

The ferroelectric domains walls differ from the magnetic domain walls when its comes to 'charge screening'. Since magnetic monopoles do not exist, the (fictious) magnetic charges generated on the magnetic boundaries can not be screened. In ferroelectric materials, the surface polarization charges are screened by electrical charges from impurieties, defects and wandering ions. Domains, their motion, 'pinning' and 'switing' are very interesting topics for discussion. This review is an introdution on the topic [2],[3].

1.3 Microscopic Properties

1.3.1 Phonons

A phonon is a quantum mechanical description of a special type of vibrational motion, known as normal modes in classical mechanics, in which a lattice uniformly oscillates at the same frequency. In this section phonons are discussed from a microscopic point of view. The principles of lattice vibrations are described by the use of a simple one-dimensional crystal model.

One-dimensional mono atomic chain

The atomic model is composed of atoms that are identical and are connected to each other by springs. Its illustrated in figure (1.18) [14], [7].

At the equilibrium position, the atoms in the crystal are separated from each other by distance a . The atoms exhibit harmonic motion about the

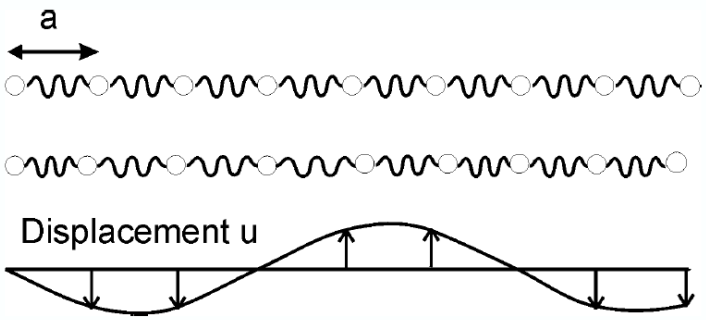

Figure 1.18: A one dimensional linear chain. The atoms are shown in their equally spaced equilibrium conditions in the top row, and with a periodic distortion below. The bottom figure plots the displacements u_n as arrows, and the curve shows how this is a sine-wave of period $6a$, in this case,[2],[3]

equilibrium position during oscillations. The restoring force acting on an atom here is directly proportional to its displacement from the mean position. Considering the position of the nth atom to be $r_n = na$ and the its displacement from the equilibrium position to be u_n, its equation of motion can be written as

$$m\frac{\partial^2 u_n}{\partial t^2} = K\left(u_{n+1} - u_n\right) + K\left(u_{n-1} - u_n\right) \tag{1.20}$$

The trial solution is taken as a wave of the form

$$u_n\left(t\right) = u_0 \cos\left(qr_n - \omega\left(q\right)t\right) \tag{1.21}$$

The wavelength of the wave is $\lambda = 2\pi/q$, and the period is $T = 2\pi/\omega\left(q\right)$ The solution equation (1.21) exists provided that

$$m\omega^2\left(q\right) = 2K\left(1 - \cos\left(qa\right)\right) = 4K\sin^2\left(\frac{qa}{2}\right) \tag{1.22}$$

so that

$$\omega(q) = 2(K/m)^{1/2} \sin\left(\frac{qa}{2}\right) \tag{1.23}$$

Equation (1.23) gives us the relationship between the frequency of the mode and its wave vector or the relationship between the wavelength and the period. This is called a dispersion relation [2],[3].

The wave vector q and the wavelength are inversely proportional to each other. When one considers the long wavelength mode for which $q \to 0$, the relationship between the wave vector and the wavelength is linear,

$$\omega(q) = (K/m)^{1/2}(qa) \tag{1.24}$$

This expression is comparable to a wire with tension Ka and density m/a. For $q \to 0$ or the long wave length limit, one obtains sound waves traveling with a velocity $v = a(K/m)^{1/2}$. These modes are called acoustic modes because of their similarity to the sound wave.

As the value of q gets larger, the dispersion gets periodic and is not linear anymore (Fig. 1.19). The periodic behavior can be understood by recalling equation (1.21). For $q = 2\pi/a$,

$$qr_n = \frac{2\pi}{a} \times na = 2\pi n \tag{1.25}$$

From this equation, it can be concluded that the all the atoms in the

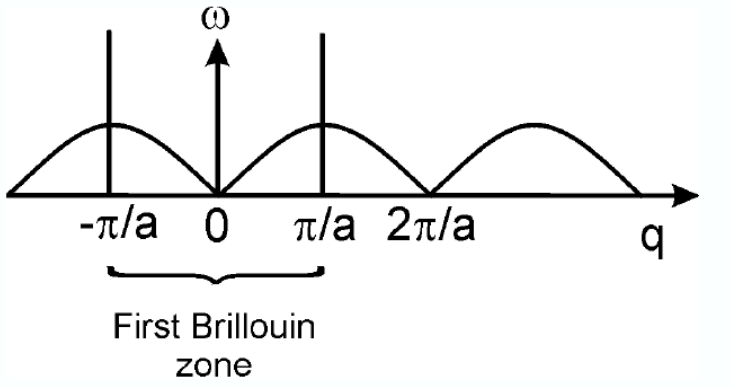

Figure 1.19: Dispersion relation between frequency and wave vector for a one-dimensional monatomic chain,[2],[3]

crystal displace together, similar to the situation when $q = 0$. The displacements do not change even if q is replaced by $q + 2\pi na$. Hence the discussion can be simplified by using only q vectors in the range

$$-\frac{\pi}{a} \leqslant q \leqslant \frac{\pi}{a} \tag{1.26}$$

This is the first Brillouin zone [2],[3].

One-dimensional diatomic chain

A monoatomic chain model adequately explains the principles behind dispersion of lattice vibrations in solids. However, to fully understand the physics of a ferroelectric material one needs to have a diatomic basis.

This model, though similar to that of a ball and chain model as seen in the previous section, has two different atoms in a unit cell. These atoms

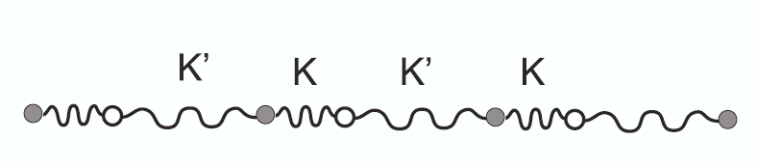

Figure 1.20: Diatomic chain,[2],[3]

differ from each other in terms of mass and spring constant. Different spring constants can be obtained by unequally spaced atoms as shown in Fig.(1.20). The equations of motion for the two types of atoms can be written as [2],[3]

$$\begin{aligned} m_A \frac{\partial^2 u_{n,A}}{\partial t^2} &= K\left(u_{n,B} - u_{n,A}\right) + K'\left(u_{n-1,B} - u_{n,A}\right) \\ m_B \frac{\partial^2 u_{n,B}}{\partial t^2} &= K'\left(u_{n+1,A} - u_{n,B}\right) + K\left(u_{n,A} - u_{n,B}\right) \end{aligned} \tag{1.27}$$

If the two atoms are strongly bound to each other (Fig.1.20) , then one can consider $K \gg K'$ and to a first approximation the pairs can be treated as independent molecules. In this case, when the atoms in the molecule oscillate out of phase with each other, each molecule will have a vibrational mode where the frequency of the mode

$$\omega_0^2 = 2K/m \tag{1.28}$$

The corresponding coordinate which undergoes this oscillation is

$$u_{opt}\left(q = 0\right) = u_A - u_B \tag{1.29}$$

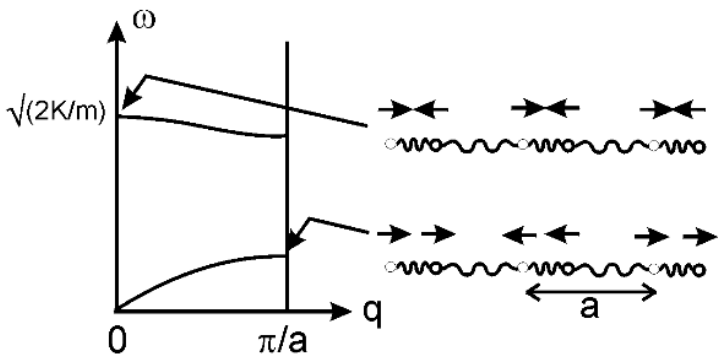

Figure 1.21: Dispersion of the optical and acoustic phonon branches in a diatomic chain, and a schematic picture of the atomic displacements in the optical mode at $q = 0$,[2],[3]

A wave-like solution can be found by choosing the correct phase relationship from one unit cell to the next, (Fig.1.21). If $K' \ll K$, restoring force does not undergo any noticeable change. In this case the frequency of the optical phonon mode is nearly independent of q. As shown in the figure (1.22), the dispersion curve now has two branches. The frequency vanishes linearly with the wave vector along one branch. The other mode has a finite frequency as $q \rightarrow 0$(Fig. 1.22). These phonons can interact with light via absorption or scattering at these long wavelengths. Hence the name "Optical Phonon" [2],[3].

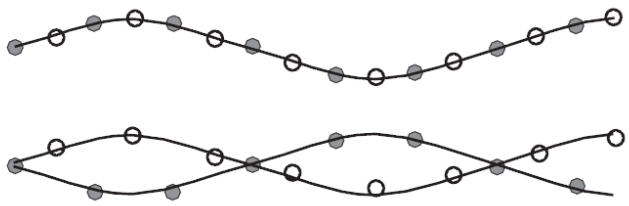

Figure 1.22: Pattern of atomic displacements for an acoustic and optical phonon of the same wave vector,[2],[3]

Phonons in three-dimensional solids

The one dimensional theory discussed so far can be generalized for three dimensional solids. To express the waves traveling in different directions in the three dimensional solid, $\omega\left(\vec{k}\right)$ takes the place of the one dimensional wave vector k. There are transverse or shear waves in addition to the longitudinal or compressional waves giving rise to new dispersion relation. For each atom in the unit cell, there are three (two transverse and one longitudinal) branches of phonons. There are three acoustic branches. Hence a solid with N atoms in the unit cell will have $3(N-1)$ optical modes. Each optical mode is then separated into two transverse branches and one longitudinal branch.

1.3.2 Soft modes

Lets go back to the discussion of ferroelectric phase transitions (as in fig.1.6). When the temperature reaches the transition temperature, the free energy exhibits a double minima. The behavior of phonons at this transition point

is quite interesting. In the previous sections, the motions of the atoms about their equilibrium position were considered harmonic. The amplitude of the vibrations are considered to be very small, hence the potential can be expanded about the minimum of the free energy. The spring constant K is found by assuming that the elastic energy stored in the spring or in the bond between the atoms obeys Hooke's law [2],[3],

$$u\left(x\right) = \frac{1}{2}Kx^2 \tag{1.30}$$

A relationship between the stiffness constant for the $q = 0$ optic phonon above the transition temperature and the coefficient $a(T)$ (from Landau Theory) can be found when one substitutes the internal energy in the above equation with the free energy from Landau Theory.

The polarization P and the amplitude of the corresponding lattice displacement are directly related to each other. Hence the free energy in equation (1.8) can be expanded as a function of the lattice displacement u. The displacement coordinate for a diatomic chain is same as the amplitude of the optical phonon,

$$u_{opt} = u_A - u_B \tag{1.31}$$

Polarization P is related to the optical phonon amplitude as

$$P = \frac{1}{V_{cell}} \left(e_T^* u_{opt} + O\left(u_{opt}^3\right) \right) \tag{1.32}$$

Here e_T^* is called the "transverse effective charge". It signifies that for rigid ions with charge $\pm Ze$ the dipole moment is Zeu_{opt} . In the harmonic approximation, the frequency of the $q = 0$ optical phonon vanishes as it approaches the transition. This is because

$$m\frac{\partial^2 u_{opt}}{\partial t^2} = -\frac{\partial F}{\partial u_{opt}} \propto -a\left(T\right) u_{opt} \tag{1.33}$$

Hence,

$$\omega\left(q=0\right)^2 \propto \frac{1}{\chi} \tag{1.34}$$

This relationship (1.34) is valid in many materials. An example for $SrTiO_3$ is given in figure (1.23)

Landau theory takes into account only the uniform components of the polarization and works well when $q = 0$. From the simple harmonic model of ball and springs, $K \rightarrow 0$ at transition temperature. One can conclude that all the phonons, both acoustic and optical, for all the momenta would soften to zero frequency at transition. This, however, is not correct.

Fig (1.24) shows the phonon spectra of $SrTiO_3$. Here the lowest optical phonon branch is soft near the origin. However the stiffness of the branch sharply increases as q becomes larger. The softening of the modes happen

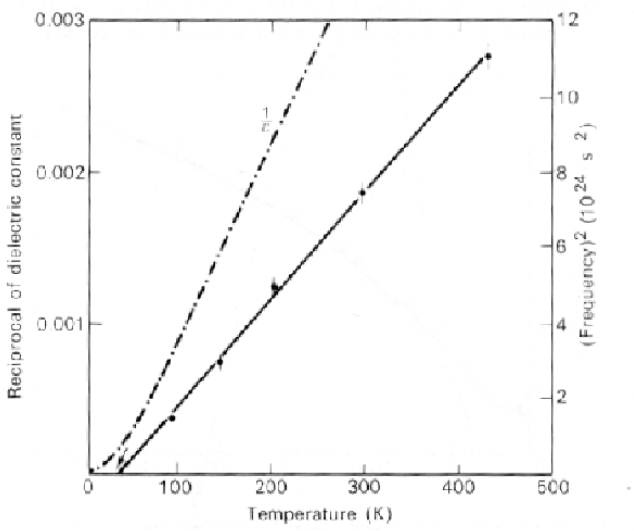

Figure 1.23: Comparision of the temperature dependence of the square of an optic phonon frequency with the inverse of the dielectric susceptibility in $SrTiO_3$,[2],[3]

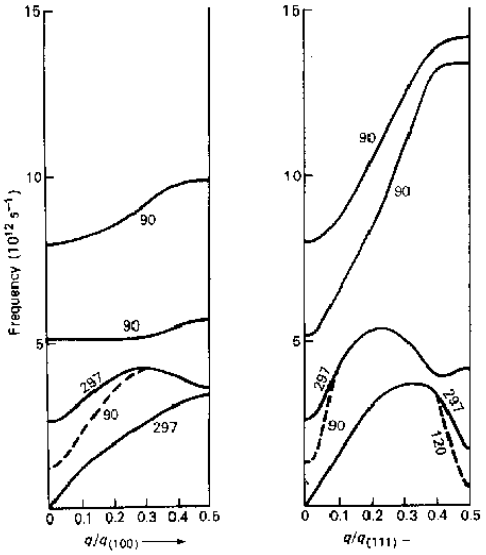

Figure 1.24: Phonon dispersion relation for $SrTiO_3$ at different temperatures for those modes where a considerable change with temperature is seen,[2],[3]

only for the long wavelength mode over a small part of the zone. The modes are strongly dependent on temperature. Fig.(1.24) shows the softening of an acoustic mode at the zone edge. It is important to note that the acoustic mode goes soft in $SrTiO_3$ which is not quite a ferroelectric even at high dielectric constant. Here the zone boundary has a periodicity of two lattice constants in each of the x-,y-, and z- directions. It corresponds to a soft mode where the articulated octahedra rotate alternately in opposite directions [2],[3].

1.3.3 A microscopic mean field theory

The role of Mean field theory in ferroelectricity can be compared to that of Weiss theory in ferromagnetism. The ions in solids are themselves polarizable in an electric field. In addition to the polarization caused by displacement of ions from their lattice sites, there is an electric polarization which is generated by the electric field inside the solid.

To understand this we can again consider the diatomic ball and spring model. In the paraelectric phase the ions are at equidistance from each other. If inside each unit cell the ions undergo the displacement **u** with respect to each other, the induced polarization can be written as

$$\mathbf{P} = \frac{1}{\Omega_0}\left[Ze\mathbf{u} + \alpha\mathbf{E}_{loc}\right] \tag{1.35}$$

Here the ions have charges $\pm Ze$, Ω_0 is the volume of the unit cell and α is the ionic polarizability. $\mathbf{E_{loc}}$ is the local electric field which is the field at the site of the atom and is produced by the dipoles throughout the rest of the solid. This local field can be estimated by a simpler method called the 'cavity method'. If the dipoles are at a large distance from the site where the field is calculated, they are treated as a continuum with uniform polarization $\mathbf{P}$ and a small imaginary sphere is considered around the site. In bulk polarization, the discontinuity is accounted for by the surface charge density $\sigma = \mathbf{P} \cdot \mathbf{n}$. This approach works in the case of this imaginary sphere as well. One can have a non-uniform charge density on the surface of the small sphere (Fig. 1.25). The field produced by this charge density is in the same direction as that of the polarization. The electric field inside the sphere is given by

$$\mathbf{E}_{loc} = \mathbf{P}/3\varepsilon_0 \tag{1.36}$$

($\varepsilon_0 \approx 9 \times 10^{-12} Fm^{-1}$ is the permittivity of free space). Substituting this expression in equation (1.31), and solving for $\mathbf{P}$, gives

$$\mathbf{P} = \frac{Ze\mathbf{u}/\Omega_0}{[1 - \alpha/3\varepsilon_0\Omega_0]} = \frac{Z^* e\mathbf{u}}{\Omega_0} \tag{1.37}$$

The polarizability of the ions adds to the effective charge Z^*. In this case $Z^* > Z$, where Z is the bare charge. With sufficiently large α, the

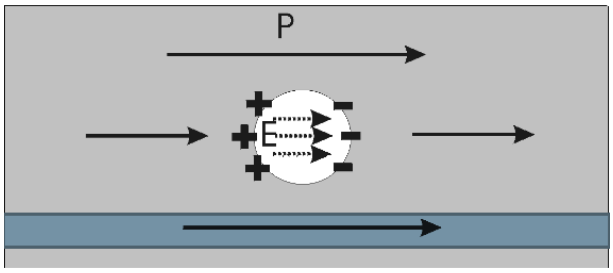

Figure 1.25: Local electric field in a cavity inside a ferroelectric,[2],[3]

denominator goes to zero. At this point the induced polarization will diverge. This divergence marks the onset of the ferroelectric instability [2],[3].

1.3.4 The Lyddane-Sachs-Teller (LST) Relation

This is a review section on the interaction of transverse optical (TO) phonon with electromagnetic waves in an ionic crystal [5], [21], [7]. To better understand this lets us consider the linear chain of ions as illustrated in figure (1.26). The black dots in this linear chain represent a series of positive ions and the grey dots represent negative ions. The waves are propagating along the z-direction. Since this a transverse mode, the atoms are displaced along the x and y directions.

The interaction between a transverse optical (TO) phonon with $q \approx 0$ and an infrared light of same frequency and wave vector is considered here.The spatial dependence of the AC electric field of the infrared light is represented by the solid line in figure(1.26). The phonon and the photon both have the

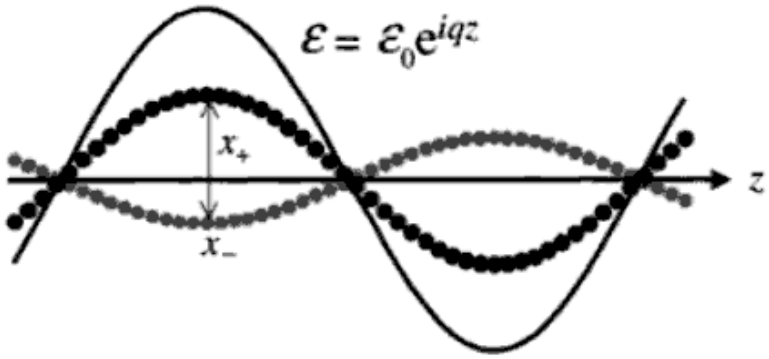

Figure 1.26: Interaction between a TO phonon mode propagating along the z direction with an electromagnetic wave with same wave vector. Positive ions are represented by the black circles and negative ions by grey circles. The spatial dependence of the electric field is given by the solid line,[5]

same wave vector at resonance. This implies that the light is a driving force acting on the positive and negative ions of the crystal and its in phase with the lattice vibration. At resonance, the interaction between the TO phonon and the AC field is strong. This interaction can be modeled by formulating the equations of motion for the displaced ions. Writing the displacement of the positive and negative ions in a TO mode as x_+ and x_- respectively (Fig.1.26), the equations of motion are [5]:

$$m_+ \frac{d^2 x_+}{dt^2} = -K\left(x_+ - x_-\right) + QE\left(t\right) \tag{1.38}$$

and

$$m_- \frac{d^2 x_-}{dt^2} = -K\left(x_- - x_+\right) - QE\left(t\right) \tag{1.39}$$

where m_+ and m_- are the masses of the positive and the negative ions respectively. K is the restoring constant of the medium and $E\left(t\right)$ is the external electric field due to light wave. $\pm Q$ is the effective charge per ion.

If we divide equation (1.38) with m_+ and equation (1.39) with m_- and then subtract, we get

$$\frac{d^2}{dt^2}\left(x_+ - x_-\right) = -\frac{K}{\mu}\left(x_+ - x_-\right) + \frac{Q}{\mu}E\left(t\right) \tag{1.40}$$

Here μ is the reduced mass given by

$$\frac{1}{\mu} = \frac{1}{m_+} + \frac{1}{m_-} \tag{1.41}$$

Substituting $x = x_+ - x_-$, equation (1.40) can be written as

$$\frac{d^2 x}{dt^2} + \omega_{TO}^2 x = \frac{Q}{\mu}E\left(t\right) \tag{1.42}$$

where $\omega_{TO} = K/\mu$ is the natural vibrational frequency of the TO mode at $q = 0$ in the absence of an external electric field. Equation (1.42) represents the equation of motion of the undamped lattice oscillation driven by the external electric field. To account for the damping, a phenomenological damping rate γ is introduced. Now equation (1.42) can be rewritten as [5]

$$\frac{d^2x}{dt^2} + \gamma\frac{dx}{dt} + \omega_{TO}^2 x = \frac{Q}{\mu}E(t) \tag{1.43}$$

This equation represents the response of a damped TO phonon mode to an external light wave at resonance. The electric field can be written as $E(t) = E_0 \mathrm{e}^{i\omega t}$

The formula for frequency dependent dielectric constant is

$$\varepsilon_r(\omega) = 1 + \chi + \frac{NQ^2}{\varepsilon_0\mu}\frac{1}{(\omega_{TO}^2 - \omega^2 - i\gamma\omega)} \tag{1.44}$$

where $\varepsilon_r(\omega)$ is the complex dielectric constant at angular frequency ω. χ represents the non-resonant susceptibility of the medium, and N is the number of unit cells per unit volume. The static dielectric constant $\varepsilon(0)$ and the high frequency dielectric constant $\varepsilon(\infty)$ can be defined as

$$\varepsilon(0) \equiv \varepsilon_r(0) = 1 + \chi + \frac{NQ^2}{\varepsilon_0\mu\omega_{TO}^2} \tag{1.45}$$

and

$$\varepsilon(\infty) \equiv \varepsilon_r(\infty) = 1 + \chi \tag{1.46}$$

Hence,

$$\varepsilon_r(\omega) = \varepsilon(\infty) + (\varepsilon(0) - \varepsilon(\infty))\frac{\omega_{TO}^2}{(\omega_{TO}^2 - \omega^2 - i\gamma\omega)} \tag{1.47}$$

If the system is lightly damped, then γ can be set to zero, giving us

$$\varepsilon_r(\omega) = \varepsilon(\infty) + (\varepsilon(0) - \varepsilon(\infty)) \frac{\omega_{TO}^2}{(\omega_{TO}^2 - \omega^2)} = \varepsilon(\infty) \left(\frac{\omega_L^2 - \omega^2}{\omega_T^2 - \omega^2} \right) \quad (1.48)$$

The zero of $\varepsilon_r(\omega)$ defines the frequency ω_L, as the pole of $\varepsilon_r(\omega)$ defines ω_T. The zero gives

$$\varepsilon(\infty)\omega_L^2 = \varepsilon(0)\omega_T^2 \quad (1.49)$$

or

$$\frac{\omega_L^2}{\omega_T^2} = \frac{\varepsilon(0)}{\varepsilon(\infty)} \quad (1.50)$$

which is the Lyddane-Sachs-Teller (LST) relation [5].

Chapter 2

SUPERCONDUCTIVITY

2.1 Introduction

Superconductivity is a phenomenon occurring in certain materials generally at low temperatures, characterized by exactly zero electrical resistance and the exclusion of the interior magnetic field (the Meissner effect).The electrical resistivity of many metals and alloys drop suddenly to zero when the specimen is cooled to a sufficiently low temperature, close to the liquid helium temperature range.At a critical temperature T_c, the specimen undergoes a phase transition from a state of normal electrical resistivity to a superconducting state. The phenomenon of superconductivity was first discovered in mercury by Dutch physicist Heike Kamerlingh Onnes in 1911. When he cooled it to the temperature of liquid helium, 4 degrees Kelvin (-452F, -269C), its resistance suddenly disappeared. Later, in 1913, he won the Nobel

Prize in physics for his research in this area.

The dc electrical resistivity goes to zero or approaches very close to zero in the superconducting state so that persistent electrical currents have been observed to flow without attenuation in superconducting rings forever in a closed loop of superconducting material, making it the closest thing to perpetual motion in nature. The magnetic properties of superconductors are equally interesting. A bulk superconductor in a weak magnetic field acts as a perfect diamagnet with zero magnetic induction in the interior of the sample.When a specimen is placed in a magnetic field and then cooled through the transition temperature for superconductivity, the magnetic flux originally present is ejected from the specimen. This phenomenon is called "'Meissner effect"' discovered by German physicists Walter Meissner and Robert Ochsenfeld in 1933.

The degree of flux expulson depends upon the material or the measurement conditions. The combination of zero resistance and perfect diamagnetism distinguishes a superconductor from a hypothetical 'perfect conductor'(which has the unique transport property of zero resistance).

The figure (2.2) illustrates the the response each would have if cooled below the transition temperature T_c. In the first case the magnetic field is applied after the samples are cooled to a temperature below T_c. In this case

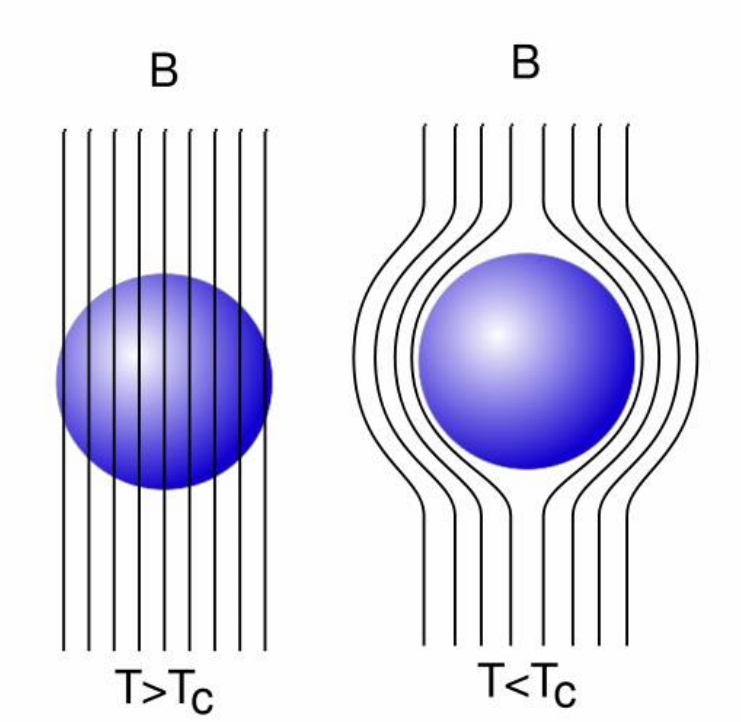

Figure 2.1: Meissner effect in a superconductor cooled in a constant applied magnetic field. When the temperature is below the transition temperature T_c, the lines of induction **B** are ejected from the sphere

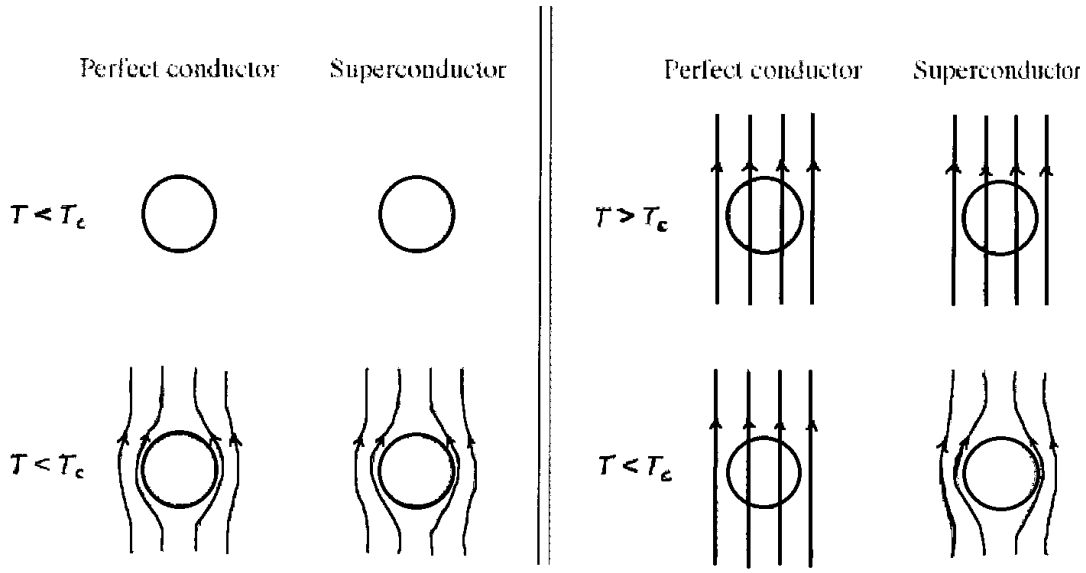

Figure 2.2: Hypothetical experiments showing the difference between a superconductor and a perfect conductor. In the first experiment, sample cooled in zero magnetic field after which the field is applied. In experiment two, sample cooled in applied magnetic field,[6]

both samples exclude the magnetic field. In the second case the samples are initially in a magnetic field and then the temperature is lowered below T_c. In this case only the superconductor ejects the magnetic flux from its interior while the 'perfect conductor' does not.It remains fully permeated by the field. These experimental surveys confirm that superconductivity is indeed a phase transition since an equilibrium thermodynamic state is characterized by its independent thermodynamic variables (in this case T and H) and does not depend on its history.

The superconducting state is an ordered state of the conduction electrons of the metal. The order is in the formation of loosely associated pairs of electrons. The electrons are ordered at temperatures below the transition temperature, and they are disordered above the transition temperature. The nature of the ordering was explained by Bardeen, Cooper and Schrieffer. The starting point was the consideration that phonons introduce an attractive interaction between electrons close to the Fermi surface (overscreening). The key idea is that an (isotropic) attractive interaction leads here to bound electron pair states (Cooper pairs). These pair states are no longer obliged to obey the Fermi-Dirac statistics, which enforced the electrons to occupy high kinetic energy single particle states due to the Pauli principle. The energy gain of the SC state with respect to the normal state does not result

from the small binding energy of the pairs but it is the condensation energy of the pairs merging into the macroscopic quantum state. It can be measured as an energy gap for electron excitations into single particle states [6], [7], [22].

2.2 Superconducting materials

We give a review of superconducting materials of interest to our research. following Narlikar [23], and Tinkaham [22]. Superconductivity can be observed in many metallic elements as well as in some alloys, intermetallic compounds and doped semiconductors. Superconductivity was discovered in Niobium Nitride (NbN) at $16K$ in 1941. Vanadium Silicon (V_3Si) was found to be a superconductor at $17.5K$ in 1953. In 1962, the first commercial superconducting wire made of an alloy of niobium and titanium ($NbTi$) was manufactured by researchers at Westinghouse. In the 1960's, the Rutherford-Appleton laboratory in the UK developed electromagnets made of copper clad niobium-titanium. These electromagnets were first used in a superconducting accelerator at the Fermilab Tevatron in 1987.

Although the BCS theory for superconductors is a highly successful theory, the discovery of the copper oxide high temperature superconductors (HTS) in 1986 required the development of a new type of theory. Before the

discovery of the HTS, the highest recorded temperature for the occurrence of superconductivity was $23K$. In some HTS, the T_c has been found to be as high as $138K$ under normal pressure. In layered cuprate HTS, there is a small magnitude of charge carriers($k_B T_c \sim E_{Fermi}$). These charge carriers have to be introduced in the insulating antiferromagnetic (AF) stoichiometric compound by appropriate doping. This gives us a 'bad' metal in which the charge and spin degrees of freedom are strongly correlated by Coulomb interaction. The metal-insulator, magnetic and superconducting transitions involved here require a far more complicated theory than that of a traditional superconductor. For HTS like cuprate, layered cobaltate and ruthenate compounds, the SC instability is believed to be of magnetic rather than phononic origin as in traditional superconductors [23].

Even before the discovery of HTS in 1986, a magnetic mechanism was already suspected for Heavy-Fermion superconductors discovered in 1979. These Heavy-Fermion superconductors are intermetallic compounds where the electronic degrees of freedom are responsible for superconductivity. The magnetic moments of the partially filled f-shells of the Ce or U atoms couple with the electronic degrees of freedom.

In 1960s, Ginzburg and Little came up with the idea that conductive polymer chains with polarizable molecular groups may be able to provide

a highly effective Cooper pair coupling for the electrons that run along the polymer chains. This coupling can be achieved by means of energy exchange via localized excitons. This propelled a search for organic superconductors and in 1980 the discovery of first organic superconductor with $T_c > 10K$ was made. However, the superconductivity in organic superconductors is not excitonic in nature as suggested by Ginzburg and Little. The π electrons in the stacked aromatic rings of the compound form one or two dimensional delocalized electron systems which are the reason behind superconductivity here. Like HTS, the strong Coulomb repulsion and restriction on effective dimensionality drive the system towards metal-insulator, magnetic and SC transitions [23].

Fullerenes ($C_{60}, C_{70}, ...$) were discovered in 1985 at Rice University and have been a much studied group of materials since then. Fullerenes are a modification of the elementary carbon and similar in structure to graphite. Superconductivity in C_{60} can be achieved by doping and intercalation of alkali-metal atoms. The value of T_c was found to be up to $33K$ under normal pressure. The conventional BCS theory fully explains the occurrence of superconductivity in fullerenes.

Researchers have investigated borides for superconductivity since the 1950s. Metal-rich borides such as MgB_2 exhibit superconductivity at T_c

$39K$. The discovery of superconductivity in MgB_2 in 2001 was a big surprise as its a very well known material since the 1950s and is available by metrical tons. The phonon interaction mechanism is only part of the story behind the superconductivity in such materials. Sodium Tungsten Bronze (Na_xWO_3) is another non-cuprate to exhibit superconductivity at T_c $90K$. A more recent (2008) surprise is the discovery of of superconductivity at $50K$ in Fe (iron) pnictides which are compounds of Fe and As. The discoveries of all these new type of superconducting materials require development of new theories, hence making the field of superconductivity a forefront of Physics and materials research for years to come [23].

2.3 Dependence on Magnetic Fields and Temperature

Superconductivity depends on the temperature as well as the applied magnetic field. It is possible to destroy superconductivity by the application of sufficiently high magnetic field. The field is temperature dependent and at critical field $H_c(T)$, the superconductivity disappears[8]. Figure (2.3) shows the variation of the critical field with respect to the temperature. At $T = T_c$, $H_c(T)$ goes to zero. The threshold curve separates the superconducting state(lower left of the figure) from the normal state(upper right

of the figure). There is also a discontinuous increase in the specific heat of the superconductor at $T = T_c$ because of the absence of latent heat at zero field. For $T < T_c$, the value of the specific heat drops rapidly and assumes an exponential form for low temperatures. The discontinuity in the specific heat is an identifying feature of second order phase transition.

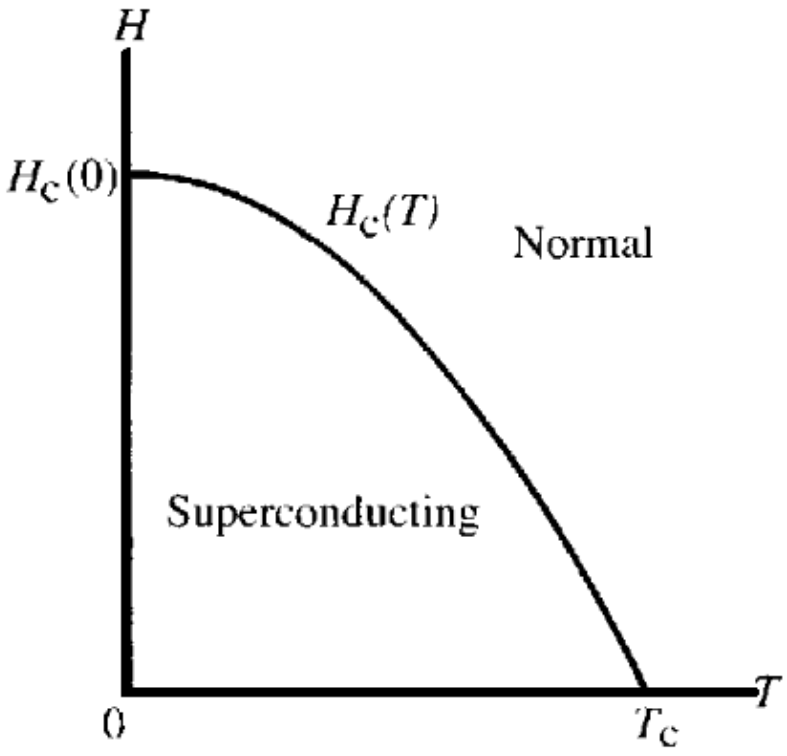

Figure 2.3: .
The temperature dependence of the critical field $H_c\,(T)$,[6]

2.4 Type I and Type II superconductors

When one studies the magnetization curve of a bulk superconductor vs the applied magnetic field, one can distinguish between the two types of superconductors,type I and type II.

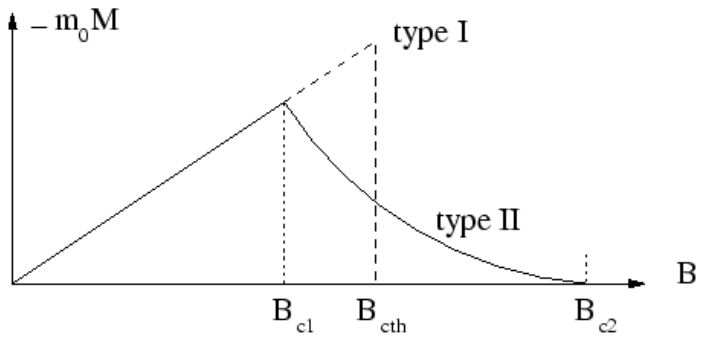

Figure 2.4: The dependence of the magnetization of a type II superconductor as function of the applied magnetic field.

Type I superconductors are superconductors that cannot be penetrated by magnetic flux lines (Meissner-Ochsenfeld effect). The magnetization versus applied magnetic field for a bulk type I superconductor exhibits complete Meissner effect or perfect diamagnetism. As such, they have only a single critical temperature at which the material ceases to super conduct, becoming resistive. The origin of their superconductivity is fully explained by BCS theory. Elementary superconductors, such as aluminum and lead are typical Type I superconductors.

As explained by BCS theory, type I superconductivity is exhibited by materials with a regularly structured lattice. This allows electrons to be coupled over a relatively large distance (compared to the size of an atom). These pairings are called Cooper pairs.

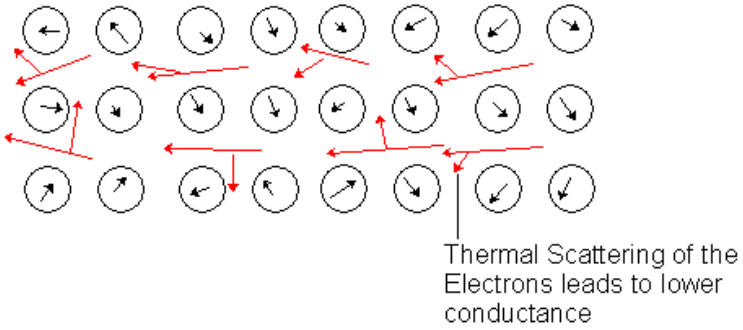

Figure 2.5: Schematic representation of the scattering of electrons as they pass through a vibrating lattice.

Though normally electrons exhibit Coulomb repulsion when displayed to each other, when they interact within a lattice, via a phonon interaction they display an attractive force. As this is not a normal state for an electron pair to be in, it is only achieved at very low temperatures. This is because, modeling it as a bond, it has a low bond energy, thus requiring very little force to break it. As such, if the temperature of the material is high, the energy in the vibrations of the lattice are sufficient to break the bond.

The reason for this force of attraction is an effect known as 'the mattress

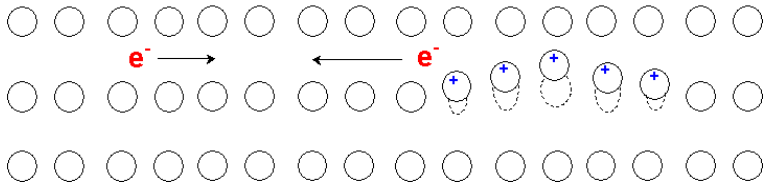

Figure 2.6: Schematic representation of the Cooper pair coupling model.

effect'. This comes about due to spins of electrons. As an electron passes through a lattice, the attractive forces between it and the protons in the nuclei of the atoms cause a ripple in the lattice structure. This means that there are ripples through much of the lattice. These ripples are vibrations called 'phonons'. The ripples induced throughout the lattice will affect other electrons passing through it. This creates the weak link between two electrons being affected by one phonon. This coupling means that even if one electron is presented with resistance the effect of the resistance is minimized as it is 'pulled along' by the other electron.

The extremely low value of H_c for type I superconductors renders them unsuitable for technical applications in coils and superconducting magnets.

A Type-II superconductor is a superconductor characterized by its gradual transition from the superconducting to the normal state within an increasing magnetic field. Typically they super conduct at higher temperatures and magnetic fields than Type-I superconductors. This allows them to conduct

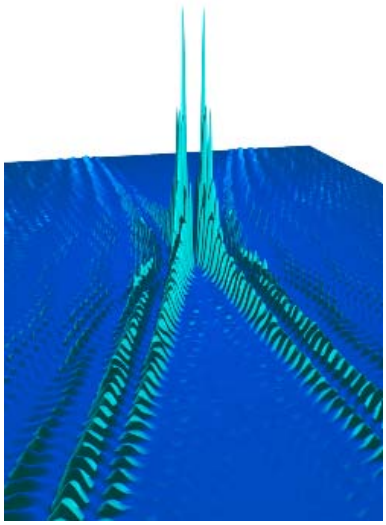

Figure 2.7: Cooper-pair states in real space p-wave

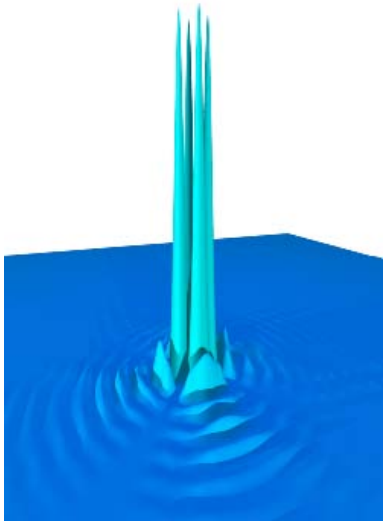

Figure 2.8: Cooper-pair states in real space d-wave

higher currents.

Type-II superconductors are usually made of metal alloys or complex oxide ceramics, whereas most pure metals are Type-I superconductors. All high temperature superconductors are Type-II superconductors, and (as of early 2008) are mostly complex copper oxide ceramics. While most pure metal or pure element superconductors are Type-I, Niobium, Vanadium, Technetium, Diamond and Silicon are pure element Type-II superconductors. Some metal alloy superconductors also exhibit Type-II behavior (eg. niobium-titanium, niobium-tin)

Other Type-II examples are the cuprate-perovskite ceramic materials which have achieved the highest temperatures to reach the superconducting state.These include $La_{1.85}Ba_{0.15}CuO_4$, BSCCO, and YBCO (Yttrium-Barium-Copper-Oxide), which is famous as the first material to achieve superconductivity above the boiling point of liquid nitrogen, as well as the highest temperature superconductor to date: mercury thallium barium calcium copper oxide ($Hg_{12}Tl_3Ba_{30}Ca_{30}Cu_{45}O_{125}$) with T_c of $123K$. Type II superconductors have superconducting electrical properties up to a field denoted by H_{c2}. The flux density is not zero i.e., $B \neq 0$ between the lower critical field H_{c1} and the upper critical field H_{c2}

2.5 Theoretical Survey of Superconductors

2.5.1 The London-London Equation

Many important results of superconductivity can be explained by phenomenological equations: the London equations and the Ginzberg-Landau equations.The older approach was used by F. London and H. London[24], [25] in 1935. It starts with Drude-Lorentz equations of motion for electrons in a metal.For an electron of mass m and charge e,moving in an electric field $\mathbf{E}$ with a velocity $\mathbf{v}$ we have [6]

$$m\left(\dot{\mathbf{v}}+\frac{1}{\tau}\mathbf{v}\right)=e\mathbf{E} \tag{2.1}$$

with a phenomenological viscous drag proportional to $\mathbf{v}/\tau$. For a perfect conductor $\tau \rightarrow \infty$. With $\mathbf{j} = ne\mathbf{v}$, where n is the conduction electron density,the above equation can be written as

$$\frac{d\mathbf{j}}{dt}=\frac{ne^2}{m}\mathbf{E} \tag{2.2}$$

This is referred to as the first London equation. Taking the time derivative of Maxwell's fourth equation (in cgs unit) we get

$$\nabla\times\frac{\partial\mathbf{H}}{\partial t}=\frac{4\pi}{c}\frac{\partial\mathbf{j}}{\partial t}+\frac{\varepsilon}{c}\frac{\partial^2\mathbf{E}}{\partial t^2} \tag{2.3}$$

where ε is the dielectric constant.Taking the curl of equation (2.3) and using equation (2.2) we have

$$\nabla \times \left(\nabla \times \frac{\partial \mathbf{H}}{\partial t} \right) = \left(\frac{4\pi n e^2}{me} + \frac{\varepsilon}{c} \frac{\partial^2}{\partial t^2} \right) \nabla \times \mathbf{E} \tag{2.4}$$

Using $\nabla \times \mathbf{E} = -\frac{1}{c} \frac{\partial \mathbf{H}}{\partial t}$, we have

$$\nabla \times \left(\nabla \times \frac{\partial \mathbf{H}}{\partial t} \right) + \left(\frac{1}{\lambda_L^2} + \frac{\varepsilon}{c^2} \frac{\partial^2}{\partial t^2} \right) \frac{\partial \mathbf{H}}{\partial t} = 0 \tag{2.5}$$

Here λ_L is called the London depth defined by $\frac{1}{\lambda_L^2} = \frac{4\pi n e^2}{mc^2}$. from equation (2.5) we can deduce that

$$\nabla \times (\nabla \times \mathbf{H}) + \left(\frac{1}{\lambda_L^2} + \frac{\varepsilon}{c^2} \frac{\partial^2}{\partial t^2} \right) \mathbf{H} = 0 \tag{2.6}$$

This is referred to as the second London equation also referred as the London equation.

Alternative derivation of the above equation is possible by considering the superconducting electrons to be a super fluid which has no viscosity.We assume that it is consisting of two fluids, a super fluid with no viscosity and a normal liquid with finite viscosity. We assume that the free energy of a super fluid consists of three parts [6]

$$F = F_N + E_{kin} + E_{mag} \tag{2.7}$$

where F_N is the free energy associated with the normal liquid, E_{kin} is the kinetic energy of the moving super fluid and E_{mag} is the energy of the magnetic field. We can write these quantities as

$$E_{mag} = \frac{1}{8\pi} \int H^2 (\mathbf{r}) d^3 r \tag{2.8}$$

and

$$E_{kin} = \frac{1}{2} \int \rho (\mathbf{r}) v^2 (\mathbf{r}) \, d^3 r \tag{2.9}$$

Here $\rho (\mathbf{r})$ is the mass density associated with the super fluid. With the use of $\rho = nm$, $\mathbf{v} = (1/ne) \mathbf{j}$ and the fourth Maxwell equation which is $\nabla \times \mathbf{H} = (4\pi/c) \mathbf{j}$, equation (2.9) becomes

$$E_{kin} = \frac{1}{8\pi} \int \frac{mc^2}{4\pi ne^2} (\nabla \times \mathbf{H})^2 \, d^3 r \tag{2.10}$$

Here n is the density of the superconducting electrons in the material. To minimize the free energy, the superconducting electrons adjust their motion. Hence, we get $\delta (E_{mag} + E_{kin}) = 0$ or

$$\int \left\{ \mathbf{H} (\mathbf{r}) \cdot \delta \mathbf{H} (\mathbf{r}) + \frac{mc^2}{4\pi ne^2} [\nabla \times \mathbf{H} (\mathbf{r})] \cdot [\nabla \times \delta \mathbf{H} (\mathbf{r})] \right\} d^3 r = 0 \tag{2.11}$$

Integrating by parts, we obtain [6]

$$\int \left[\mathbf{H}(\mathbf{r}) + \lambda_L^2 \nabla \times (\nabla \times \mathbf{H})\right] \cdot \delta\mathbf{H}(\mathbf{r})\, d^3r = 0 \tag{2.12}$$

Since $\delta\mathbf{H}(\mathbf{r})$ is arbitrary, the term in the bracket must vanish, hence

$$\frac{1}{\lambda_L^2}\mathbf{H}(\mathbf{r}) + \nabla \times (\nabla \times \mathbf{H}) = 0 \tag{2.13}$$

We can apply the above equation in the following two cases.

In the first case, lets consider the applied magnetic field perpendicular to the surface of the superconductor. The surface in consideration, say, lies in the xy-plane with no current flowing in the z-direction. From second Maxwell's equation $\nabla \cdot \mathbf{H} = 0$, we obtain $\partial H_z/\partial z = 0$ or $\mathbf{H} = const.$ From the fourth maxwell's equation, $\nabla \times \mathbf{H} = (4\pi/c)\,\mathbf{j}$, the first term in the equation (2.13) vanishes leaving $\mathbf{H} = 0$ the only solution.Therefore a superconductor exhibiting the Meissner effect cannot have a field component perpendicular to its surface [6].

Lets consider the following case as the second example. For a superconductor with the applied field parallel to the surface, say, $\mathbf{H} \parallel \hat{x}$ or $\mathbf{H} = H(z)\,\hat{x}$. Equation (2.13) can be written as

$$\frac{\partial^2 H_x}{\partial z^2} - \frac{1}{\lambda_L^2} H_x = 0 \tag{2.14}$$

Considering the superconductor occupies the region $z > 0$, we can write the solution to the above equation as

$$H(z) = \hat{x} H_x(0) e^{-z/\lambda_L} \tag{2.15}$$

Hence, a field parallel to the surface is possible, although it decays exponentially with a characteristic length λ_L. Depending on the material,λ_L can range from 500 to 1000 A° in the interior. A surface current density accompanies this parallel field and is responsible for shielding the magnetic field from the interior of the superconductor. The decrease of the magnetic induction described by (2.15) is a result of a screening of the external field by the superconducting currents. These currents flow within a surface layer of thickness λ_L.

The current density can be written as

$$\mathbf{j}(z) = -\frac{c}{4\pi\lambda_L} H_x(0) e^{-z/\lambda_L} \hat{y} \tag{2.16}$$

The length λ_L is denoted the 'London penetration length' [6], [8].

2.5.2 Pippard's Equation

A weak magnetic field $H < H_c$ generally does not penetrate a type-I superconductor on a microscopic scale. However, on a microscopic scale the field does penetrate a certain depth λ into the metal. This length is differ-

ent than the London penetration depth λ_L and represents a different scale affecting the behavior of a superconductor. It can be interpreted as a characteristic length which measures the spatial response of the superconductor to some perturbation. In other words it can be thought of as the distance over which the superconducting state develops at a normal metal-superconductor boundary [6],[22] .

London equation (2.13)can be re-written in the following manner. If we substitute $\nabla \times \mathbf{H} = (4\pi/c)\,\mathbf{j}$ in the London equation, we have

$$\nabla \times \mathbf{j} = -\frac{c}{4\pi\lambda_{\mathrm{L}}^2}\mathbf{H} = -\frac{ne^2}{mc}\mathbf{H} \tag{2.17}$$

However, this equation is not valid for superconductors of the first kind($\xi_0 > \lambda$). A more general approach is needed when dealing with the current and the fields. The equation should be applicable even when the current and the magnetic field have rapid variations in space.

The variable which is most convenient in this situation is the magnetic vector potential $\mathbf{A}$. We can write $\mathbf{H} = \nabla \times \mathbf{A}$. This equation with the supplementary condition

$$\nabla \cdot \mathbf{A} = 0 \tag{2.18}$$

and the boundary condition

$$A_n = 0 \tag{2.19}$$

where A_n is the component of $\mathbf{A}$ perpendicular to the sample surface, define $\mathbf{A}$ completely. Equation (2.18) is the London gauge. London's equation can be rewritten as

$$\mathbf{j} = -\frac{ne^2}{mc}\mathbf{A} \tag{2.20}$$

Insertion of the above conditions into equation (2.20) gives

$$\nabla \cdot \mathbf{j} = 0 \tag{2.21}$$

$$j_n = 0 \tag{2.22}$$

the first condition being the continuity equation. The latter condition which is vanishing of the normal component of the current is satisfactory if no external current is fed to the sample.

Equation (2.20) applies only when the variation of $\mathbf{A}$ and $\mathbf{j}$ is slow in space on the scale ξ_0. However, the current $\mathbf{j}(\mathbf{r})$ at point $\mathbf{r}$ also involves contributions from $\mathbf{A}(\mathbf{r}')$ at all neighboring points $\mathbf{r}'$ located in a volume

with a radius of order ξ_0 surrounding $\mathbf{r}$ or $|\mathbf{r}-\mathbf{r}'|<\xi_0$. A phenomenological relationship was proposed by Pippard; in the London gauge it has the form

$$\mathbf{j}(\mathbf{r}) = -C\int \frac{\mathbf{R}\left[\mathbf{R}\cdot\mathbf{A}(\mathbf{r}')\right]}{R^4} e^{-R/\xi} d\mathbf{r}' \tag{2.23}$$

Here the constant C is determined by the condition that when $\mathbf{A}$ varies slowly spatially over distances $\sim \xi_0$, it can be taken out of the integral and one must obtain the London equation.This gives

$$C\int \cos^2\theta d\Omega \int e^{-R/\xi_0} dR = \frac{ne^2}{mc} \tag{2.24}$$

from which we obtain $C = 3ne^2/4\pi\xi_0 mc$. The generalized London equation,by Pippard, can then be written as

$$\mathbf{j}(\mathbf{r}) = -\frac{3ne^2}{4\pi\xi_0 mc}\int \frac{\left[\mathbf{A}(\mathbf{r}')\cdot\mathbf{R}\right]\mathbf{R}}{R^4} e^{-R/\xi_0} d^3r' \tag{2.25}$$

Substituting $\mathbf{H} = \nabla\times\mathbf{A}$ in the fourth Maxwell's equation we obtain

$$\nabla\times(\nabla\times\mathbf{A}) = \frac{4\pi}{c}\mathbf{j} \tag{2.26}$$

Equation (2.25) is valid for a bulk superconductor.If the penetration phenomena near a sample surface is to be studied, the relationship between $\mathbf{j}$ and $\mathbf{A}$ needs modification. In equation (2.25), the integration can be modified by integrating over points $\mathbf{r}'$ restricted to the interior of the superconductor and

more restrictively to points $\mathbf{r}'$ from which an electron can travel in a straight to a point $\mathbf{r}$. In the case of a highly contoured surface, its possible that two points near the surface separated by about a coherence length cannot be connected by a straight electron trajectory without passing through the vacuum. Or if there is a small empty cavity in the metal,one must exclude the "'shadow"'of the cavity[7] as shown in the figure (2.9). We restrict ourselves

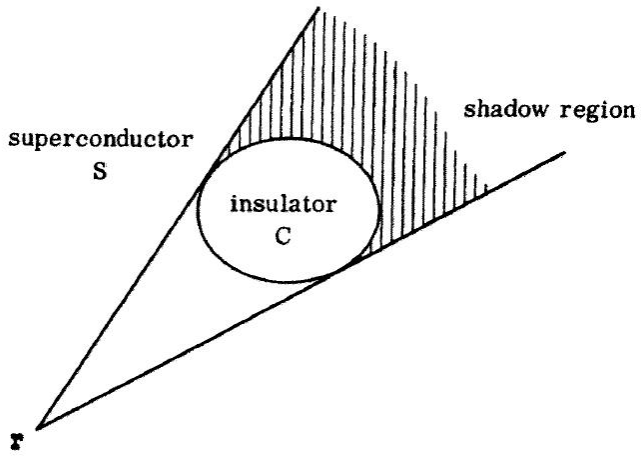

Figure 2.9: Shadow Effect,[7]

to plane boundaries which we take to be normal to the z direction.

In the limit of $\lambda_L \gg \xi_0$, equation (2.25) reduces to the London equation.In the opposite limit $\lambda_L \ll \xi_0$, $\mathbf{A}(r)$ varies rapidly. Assume that $A(r)$ is non zero only in a small thickness or characteristic length λ. When $\lambda < \xi_0$, the value of the integral reduces to

$$\mathbf{j}(\mathbf{r}) = -\frac{\lambda}{\xi_0}\frac{ne^2}{mc}\mathbf{A}(\mathbf{r}) \tag{2.27}$$

Using this relation along with $\nabla \times \mathbf{h} = (4\pi/c)\, j$, equation (2.27) can be written as

$$\nabla \times \nabla \times \mathbf{h} + \frac{\lambda}{\xi_0 \lambda_L^2}\mathbf{h} = 0 \tag{2.28}$$

Solving equation (2.28), we get an approximate penetration law of the form $h(z) = h(0)\, e^{-z/\lambda}$ where λ is defined by

$$\frac{1}{\lambda^2} = \frac{4\pi ne^2}{mc^2}\frac{\lambda}{\xi_0} \tag{2.29}$$

or $\lambda^3 = \lambda_L^2 \xi_0$. A more rigorous calculation gives $\lambda^3 = 0.62\lambda_L^2\xi_0$.The conclusion that can be drawn is that in the Pippard limit, λ becomes larger than the London value $(\lambda/\lambda_L) \sim (\xi_0/\lambda_L)^{1/3} > 1$, but λ remains much smaller than the coherence length $(\lambda/\xi_0) \sim (\lambda_L/\xi_0)^{2/3} < 1$.

If impurities are present inside the metal, then the relationship between the vector potential and the current will be modified. To account for the electron scattering, Pippard modified the coherence length in the exponent of equation of (2.25) such as $1/\xi_0 \rightarrow (1/\xi_0) + (1/l)$ where l is the electron mean free path.

In the limit of $\lambda \gg (l, \xi_0)$, the current can be written as

$$\mathbf{j}(\mathbf{r}) = -\frac{ne^2}{mc}\frac{1}{\frac{1}{\xi_0}+\frac{1}{l}}\mathbf{A}(\mathbf{r}) \tag{2.30}$$

In the case of very dirty metal, the current can be written as

$$\mathbf{j}(\mathbf{r}) = -\frac{ne^2}{mc}\frac{l}{\xi_0}\mathbf{A}(\mathbf{r}) \tag{2.31}$$

The effective penetration depth then can be written as

$$\lambda = \left(\frac{\lambda_L^2 \xi_0}{l}\right)^{1/2} \tag{2.32}$$

If $\lambda \ll (l, \xi_0)$, we continue to use $\lambda^3 = \lambda_L^2 \xi_0$. The magnetic response of a superconductor depends on the relationship between λ and ξ. Type I superconductors are characterized by $\lambda < \xi$ and for Type II superconductors $\lambda > \xi$.

2.5.3 Ginzberg-Landau Theory

Ginzburg-Landau theory was proposed in 1950 by Vitaly Lazarevich Ginzburg and Lev landau. This phenomenological theory describes some macroscopic mechanism of a both classical and high temperature superconductors with the help of general thermodynamical principles. This section gives a brief review of the theory following Ginzberg [26], Bennenman [27] and Poole [8].

According to the GL theory, the super current in the superconducting state is carried by 'super electrons' of mass m^*, charge e^*, and density n^*. Here $m^* = 2m^*$, $e^* = 2e$, and $n^* = \frac{1}{2}n_S$. m, e and n_S are the mass, charge and the density for free electron. The complex order parameter $\varphi(r)$ is [8]

$$\varphi(r) = |\varphi(r)| e^{i\theta} \tag{2.33}$$

The super electron density is defined as the square of the order parameter such as

$$n_S = |\varphi|^2 \tag{2.34}$$

For a uniform homogeneous field n_S and φ can be taken as constants. For the temperature above T_c, the value of φ is zero. As the temperature goes below T_c, the value of φ increases as shown in the figure (2.10 a). The first Ginzburg-Landau equation is obtained by expanding the Gibb's free energy per unit volume G_s in terms of the order parameter φ and then minimizing it with respect to it. The condition here is that the temperature is less than but close to T_c and London gauge $\nabla \cdot A = 0$ is satisfied. The first GL equation is

$$(1/2m^*)\left[\hbar^2\nabla^2\varphi - 2i\hbar e^* A \cdot \nabla\varphi - e^{*2}A^2\varphi\right] - a\varphi - b|\varphi|^2\varphi = 0 \tag{2.35}$$

If we minimize the free energy G_s with respect to the vector potential A, we

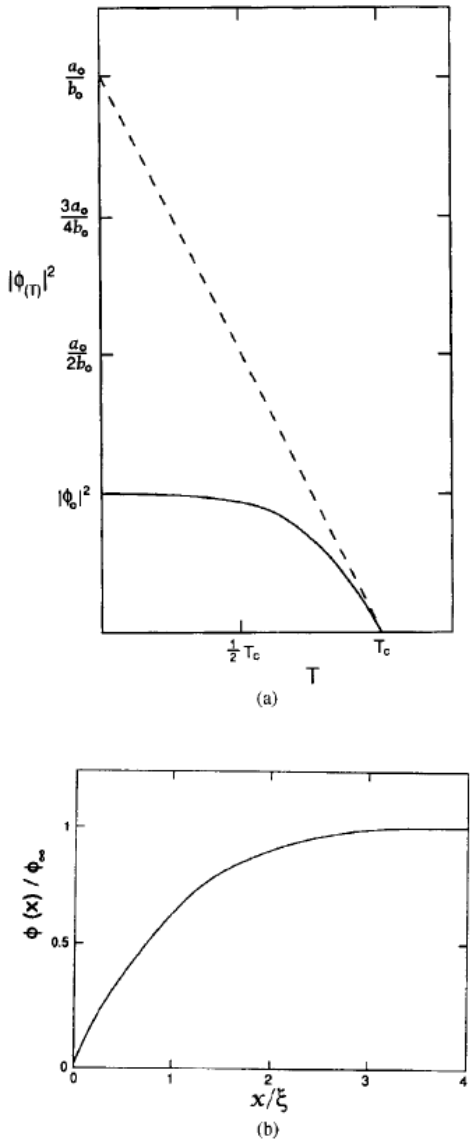

Figure 2.10: (a) Temperature dependence of GL parameter, (b) variance of order parameter w.r.t. coherence length,[8]

obtain the second GL equation

$$\nabla \times (\nabla \times A) + \frac{i\hbar e^*}{2m^*} (\varphi^* \nabla \varphi - \varphi \nabla \varphi^*) + \frac{e^{*2}}{m^*} A |\varphi|^2 = 0 \tag{2.36}$$

The macroscopic properties of a superconducting state can be determined with the help of these two equations. The coefficients a and b are determined in the following manner. When the temperature is below but near T_c, the dependence of a on T is linear and can be written as [8]

$$a(T) \approx a_0 [(T/T_c) - 1] \tag{2.37}$$

b is independent of temperature. The value of $a(T)$ is negative below T_c, hence

$$|\varphi|^2 = n_s^* = -a/b = (a_0/b_0 [1 - (T/T_c)]), \tag{2.38}$$

The temperature dependence of the oder parameter is given in the figure (2.10a) and the dependence on coherence length ξ is given in (2.10b). Coherence length is the characteristic length over which the order parameter varies and it is written as [8]

$$\xi^2 = \hbar^2 / 2m^* |a|. \tag{2.39}$$

The condensation energy of the super electrons can be written as

$$E_{cond} = \frac{1}{2} \left(a^2/b\right) = B_c^2 / 2\mu_0 \tag{2.40}$$

When an external magnetic field is applied the flux Φ enclosed in a path given by the line integral of $J/|\phi|^2$ around a closed path is

$$\left(m\mu_0/e^{*2}\right) \oint \left(J/|\phi|^2\right) \cdot dl + \Phi = n\Phi_0, \tag{2.41}$$

where n is an integer and the quantum of flux Φ_0 has the value

$$\Phi_0 = h/e^*. \tag{2.42}$$

If the applied magnetic field $B(x)$ is parallel, the field as well as the current density $J(x)$ decay exponentially with the distance x within the surface of the superconductor such as

$$B(x) = B_0 e^{-x/\lambda_L} \tag{2.43}$$

and

$$J(x) = J_c e^{-x/\lambda_L} \tag{2.44}$$

where the London penetration depth λ_L, the second fundamental length scale, is given by

$$\lambda_L^2 = \frac{m^*}{\mu_0 e^{*2} |\varphi_\infty|^2}, \tag{2.45}$$

The ratio $\kappa = \lambda/\xi = 1/\sqrt{2}$ divides superconductors into two types

$\kappa \leq 1/\sqrt{2}$ (Type (I)) and $\kappa \geq 1/\sqrt{2}$ (Type (II)) Type II superconductor have lower, thermodynamic, and upper critical fields given by

$$B_{c1} = \frac{\varphi_0 \ln \kappa}{4\pi\lambda_L^2}, B_c = \frac{\varphi_0}{2\sqrt{2}\pi\xi\lambda_L}, B_{c2} = \frac{\varphi_0}{2\pi\xi^2}, \tag{2.46}$$

respectively, where $B_{c1}B_{c2} = B_c^2 \ln \kappa$. Complete Meissner effect occurs when $B_{app} < B_{c1}$. With the increase in the applied field above the first critical field B_{c1}, flux lines penetrate the material in form of vortices. Magnetization continues to increase with the increase in field. When the field crosses the threshold B_{c2}, the vortex cores almost overlap and the superconductivity is destroyed. In case of a thin sheath, residual superconductivity may persist up to a higher critical field B_{c3} where $B_{c3} = \sqrt{3}B_{c2}$. Above B_{c3}, the sample is in a truly normal state [8].

2.5.4 Vortices

An identifying feature of a superconductor is the expulsion of magnetic field from its interior which is the Meissner effect. However, with a sufficiently strong magnetic field, flux lines enter the some superconductors (Type II) in form of vortices. each vortex carries a quantized amount of magnetic flux through the superconductor. Meanwhile, the superconducting state is maintained in the regions around the vortex. Over some enclosed area A,

the magnetic flux is [8]

$$\int B \cdot dA = \Phi_0 \tag{2.47}$$

and it equals to the flux quantum Φ_0,

$$\Phi_0 = h/2e = 2.0678 \times 10^{-15} Tm^2 \tag{2.48}$$

This flux quantum Φ_0 is associated with the Hall effect quantum of resistance R_H,

$$R_H = h/e^2 = 2\Phi_0/e = 25,813\Omega \tag{2.49}$$

For cuprates, where κ has a high limit, $\lambda_L >> \xi$. In this case, for $r > \xi$, the local magnetic field due to the vortex $B(r)$ and the shielding current $J_s(r)$ outside the vortex core are radially dependent and can be written as [8]

$$B\left(r\right) = \frac{\Phi_0}{2\pi\lambda_L^2} K_0\left(r/\lambda_L\right) \tag{2.50}$$

$$J_s\left(r\right) = \frac{\Phi_0}{2\pi\mu_0\lambda_L^3} K_1\left(r/\lambda_L\right) \tag{2.51}$$

where $K_0(r/\lambda_L)$ and $K_1(r/\lambda_L)$ are the zero order and first order modified Bessel functions, respectively, with the properties that $K_1(r) \gg K_0(r)$ for small $r \ll \lambda_L$, and $K_1(r) \approx K_0(r)$ for larger $r \gg \lambda_L$.

For $r \leq \xi$, or inside the vortex core, the magnetic field can assumed to be a constant and the current $J_s(r) = 0$. The field can be written as [8]

$$B(r) = \frac{\Phi_0}{2\pi\lambda^2} K_0 \left(r/\lambda_L\right) \tag{2.52}$$

Near the core, equations (2.50) and (2.51) behaves asymptotically

$$B\left(r\right) = \frac{\Phi_0}{2\pi\lambda_L^2} \ln\left(1.123\lambda_L/r\right), r \ll \lambda_L \tag{2.53}$$

$$J_s\left(r\right) = \frac{\Phi_0\lambda_L}{2\pi\mu_0\lambda_L^3 r}, r \ll \lambda_L \tag{2.54}$$

and far away from the core

$$B\left(r\right) = \frac{\Phi_0}{2\sqrt{2\pi}\lambda^2} \frac{e^{(-r/\lambda_L)}}{\sqrt{(r/\lambda_L)}}, r \gg \lambda_L \tag{2.55}$$

$$J_s\left(r\right) = \frac{\Phi_0}{2\sqrt{2\pi}\mu_0\lambda_L^3} \frac{e^{(-r/\lambda_L)}}{\sqrt{(r/\lambda_L)}}, r \gg \lambda_L \tag{2.56}$$

where the numerical factor 1.123 in equation (2.53) is $2e^{-\gamma}$ and $\gamma = 0.57721566..$ is the dimensionless Euler-Mascheroni constant.

Vortices generally arrange themselves in a hexadic pattern as shown in the figure (2.11). The distance between the cores of each flux line is d and the area occupied by each vortex is $\frac{\sqrt{3}}{2}d^2$. The separation between vortices

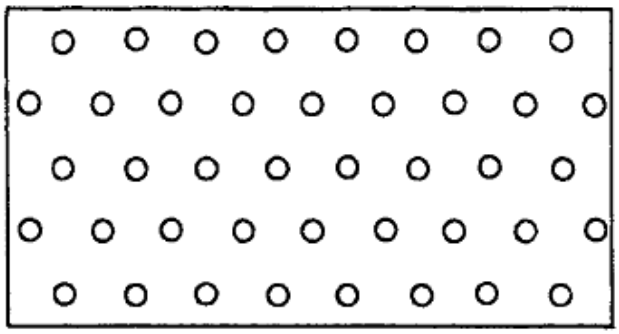

Figure 2.11: Hexagonal vortex lattice,[8]

changes with the change in the applied field. Near B_{c1}, $d \approx 2\lambda$ and near B_{c2}, $d \approx 2\xi$. The average field B_{in} inside the superconductor is given by

$$B_{in} = \frac{\Phi_0}{\left(\sqrt{3}/2\right) d^2} = N_A \Phi_0 \tag{2.57}$$

where N_A is the number of vortices per unit area [8]. A superconductor is not really superconducting when vortices are present. Vortices move inside the field and this creates a resistance to the flow of current. If the material has enough flaws to 'pin' down the vortices, then the resistance goes to zero and a well defined vortex lattice is formed.

2.6 Magnetic Properties of Superconductors

The magnetic properties of a superconductor is greatly affected by the vortex structure. The macroscopic properties of a superconductor due to the vortex structure are discussed here. The vortex structure depends on the shape of

the superconductor. It also affects the super current inside the sample.

2.6.1 Internal Fields and Magnetization

The fields B and H are related to each other as

$$B = \mu_0 (H + M) = \mu H = \mu_0 H (1 + \chi), \tag{2.58}$$

This relationship holds true for both inside and outside of the sample. Here M is the magnetization which can be defined as the magnetic moment per unit volume, χ is the magnetic susceptibility and μ_0 is the permiability of free space. When an external magnetic field $B_{app} = H_{app}/\mu_0$ is applied, the magnetization M is obviously zero outside the sample. Inside the sample [8],

$$B_{in} = \mu_0 H_{in} (1 + \chi), \tag{2.59}$$

where the dimensionless susceptibility χ

$$\chi = M/H_{in} \tag{2.60}$$

For an ideal Type I superconductor $\chi = -1$. Assuming that no demagnetizing effect are present, the B field and the magnetization M can be written

as [8]

$$B_{in} = 0$$

$$M = -H_{in} = -B_{app}/\mu_0 \tag{2.61}$$

B and M for an ideal Type-I superconductor are plotted in figure (2.12).

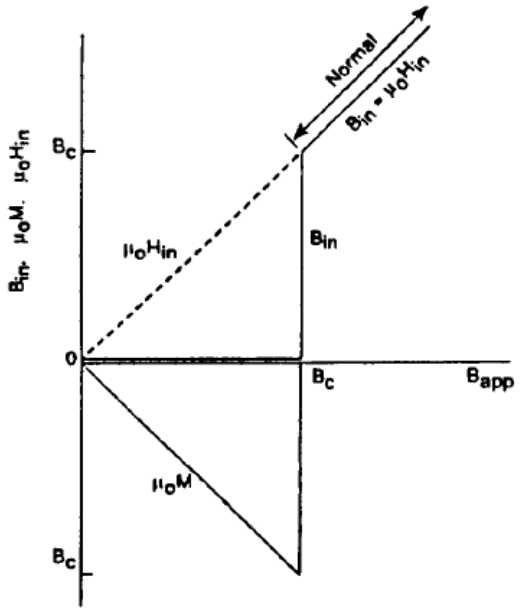

Figure 2.12: Internal field and magnetization for ideal Type I superconductor,[8]

In case of a Type-II superconductor, the vortex state exists between the lower critical field B_{c1} and the upper critical field B_{c2}. The expressions for

the field and magnetization are

$$\begin{aligned} B_{in} &= 0 \\ 0 \leq B_{app} &\leq B_{c1} \\ M = -H_{in} &= -B_{app}/\mu_0 \end{aligned} \tag{2.62}$$

The plot for the internal field and the magnetization for the Type-II superconductor is given in the figure (2.13). The critical field B_c corresponds to

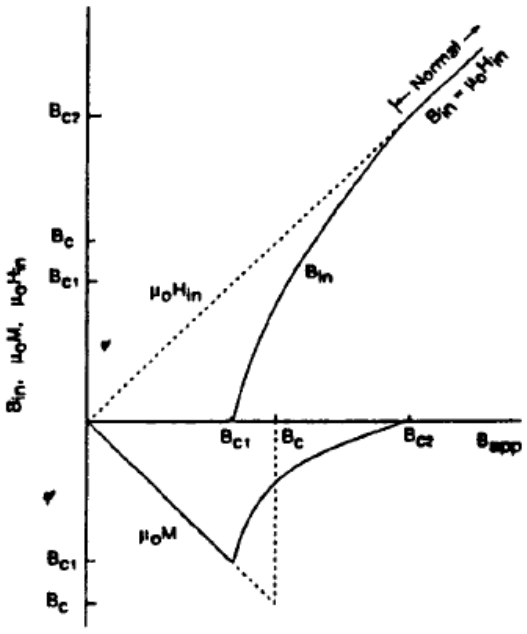

Figure 2.13: Internal fields B_{in}, H_{in} and magnetization M for an ideal Type II superconductor,[8].

the integral

$$\int_{B_{c1}}^{B_c} (B_{app} + \mu_0 M)\, dB_{app} = \mu_0 \int_{B_c}^{B_{c2}} (-M) dB_{app} \tag{2.63}$$

Here M is a negative quantity and energetically B_c involves the difference between the Gibbs free energies of the normal and the superconducting states,

$$G_n - G_s = B_c^2/2\mu_0 \tag{2.64}$$

where $B_c^2/2\mu_0$ is the condensation energy. This expression is valid for both Type-I and Type-II superconductors. The magnetization shows hysteresis as shown in the figure(2.14). Figures (2.15) and (2.16) give the variation of

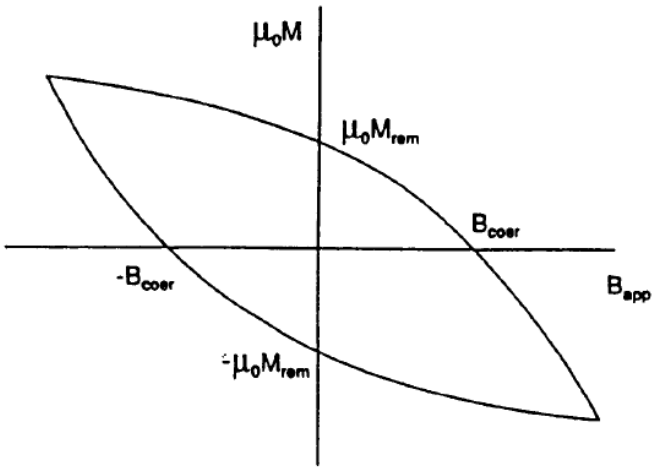

Figure 2.14: Low field hysteresis loop showing the coercive field B_{coer} where the magnetization is zero, and the remnant magnetization M_{rem} that remains when the applied field has been reduced to zero,[8].

some low-field and high-field hysteresis loops respectively.

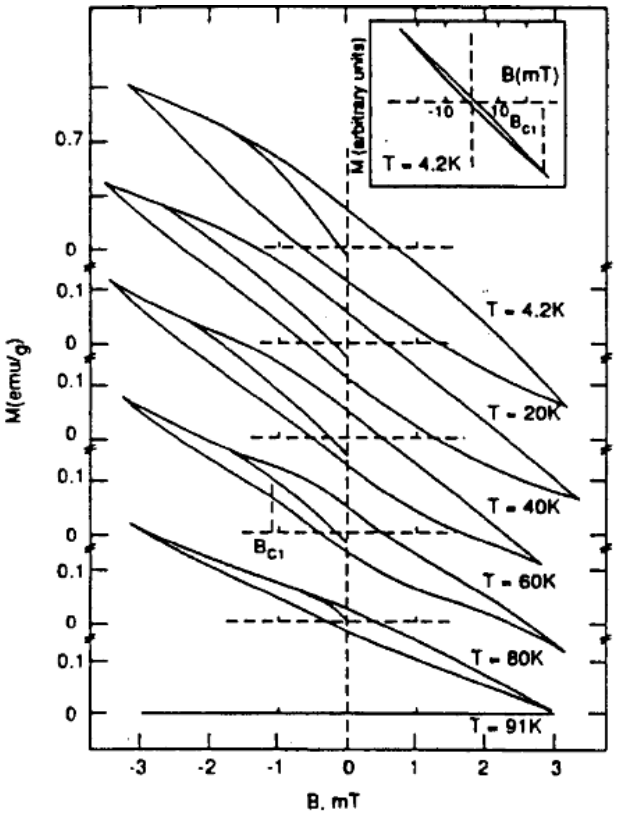

Figure 2.15: Low field hysteresis loop of $YBa_2Cu_3O_7$ cycled over the same field scan, $-3mT \leq B_{app} \leq 3mT$, for several temperatures. The loops gradually collapse as the temperature increases,[8].

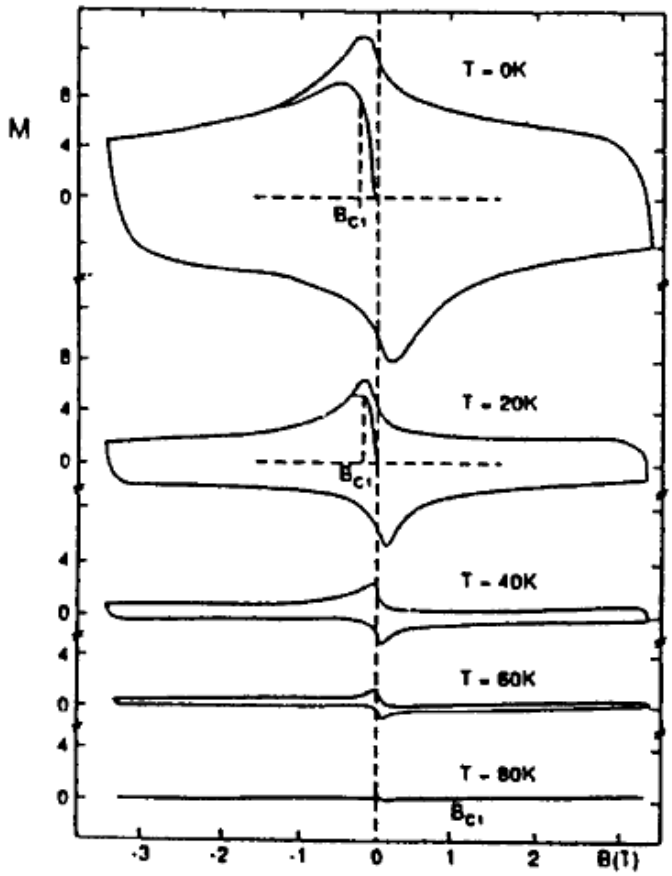

Figure 2.16: High field hysteresis loop of $YBa_2Cu_3O_7$ cycled over the same field scan $-3mT \leq B_{app} \leq 3mT$ for several temperatures. The loops gradually collapse as the temperature increases,[8].

2.6.2 Critical Fields

For an isotropic Type-II superconductor, the lower and upper critical fields can be written as

$$B_{c1} = \frac{\Phi_0 \ln \kappa}{4\pi\lambda^2} \tag{2.65}$$

and

$$B_{c2} = \frac{\Phi_0}{2\pi\xi^2} \tag{2.66}$$

Here λ is the penetration depth and ξ is the coherence length. The thermodynamic critical field can be defined as

$$B_c = \frac{\Phi_0}{2\sqrt{2}\pi\lambda\xi} \tag{2.67}$$

The upper and lower critical fields can be written in terms of B_c such as

$$B_{c1} = \frac{B_c \ln \kappa}{\sqrt{2}\kappa} \tag{2.68}$$

and

$$B_{c2} = \sqrt{2}\kappa B_c. \tag{2.69}$$

Here $\kappa = \lambda/\xi$ is called the Ginzburg-Landau parameter. B_c, B_{c1} and B_{c2} are represented in figure (2.13) [8].

Chapter 3

NEARLY FERROELECTRIC SUPERCONDUCTORS

3.1 Introduction

In 2001, Prof. Joseph Birman and Dr. Natalya Zimbovskaya of the City College, CUNY published an article in PRB regarding Nearly Ferroelectric Superconductors which gave us a theoretical understanding of these materials [9]. An NFE-SC material exhibits superconductivity (SC) and is in a nearly ferroelectric (NFE) state. Its a material that is a typical soft-mode phonon Cochran-Anderson system[18], with high-static dielectric constant. Examples of materials in this class include the sodium tungsten bronze (Na_xWO_3) and n or p doped $SrTiO_3$ systems.

Sodium tungsten bronze (Na_xWO_3) with $x \sim 0.05$ is a high-temperature superconductor[28] with $T_c \sim 90K$. For $0.1 < x < 1$, Mattheis and collab-

orators long ago reported superconductivity[29]. However, the temperature reported by them was $T_c \sim 1 - 3K$. Mattheis and Wood were also among the first to report ferroelectricity in a host of Tungsten Oxide (WO_3) system. Its long since known that a superconductor can be created by increasing the density of charge carriers (electrons or holes) in the solid to high levels. Chemical doping is one route to achieve this. For example, n or p doped $SrTiO_3$ exhibits superconductivity with $T_c \sim 1 - 3K$. $SrTiO_3$ can be regarded as a "nearly ferroelectric material". It is of particular interest because of its unusual properties at low temperatures. It has been shown that $SrTiO_3$ possesses a static dielectric constant $\varepsilon(0)$ of the order of 10^4 in the temperature range where superconductivity occurs.

The Nearly Ferroelectric Superconductor considered here is an ionic lattice with a high static dielectric coefficient $\varepsilon(0)$. The assumption taken here is that the induced or injected charge careers to boost up the superconducting property of the host fully condensate into $s-$wave Cooper pair[30]. Conventional BCS superconductors are characterized by a standard $s-$wave, spin singlet pairing state with $s = 0$ and $l = 0$ Cooper pairs. The two electrons of a pair have equal and opposite momenta $\vec{k}$ and $-\vec{k}$ so that the center of mass momentum of a Cooper pair is zero. For an attractive electron-electron interaction, the bound state is symmetric upon exchange of electron positions,

so it must be an antisymmetric singlet upon exchange of electron spins to satisfy the pauli exclusion principle. Thus, at any instant of time, one can think of the electrons in a Cooper pair as being in state $\left(\vec{k}_i \uparrow, -\vec{k}_i \downarrow\right)$, and the wave function describing the pair consists of all states i occupied by the pair during its lifetime. An attractive interaction between electrons results in a potential energy contribution which is negative, and thus lowers the total energy of the system. The negative potential energy associated with the Cooper pair is the binding energy of that pair.

In metallic superconductors , the attractive interaction between electrons originates from the electron-phonon interaction, which is short range and retarded in space-time. The lattice deformation resulting from the first electron takes a finite time to relax and thus a second electron can be influenced by the lattice deformation at a later time. The attraction arising from the electron-electron interaction overcomes the screened Coulomb repulsion between the electrons due to the presence of other electrons and ions in the solid. This screening aids in reducing the natural Coulomb repulsion between two electrons, leading to an effective interaction which is relatively short range compared with the unscreened Coulomb potential.

Since its considered that the free electrons condense into Cooper pairs, its logical to assume that the free charge density $\rho_e = 0$ and the free current

density $\mathbf{J}_e = 0$. While treating the problem of a nearly ferroelectric superconductor, one needs to take into account both superconducting and ferroelectric properties. The equations for lattice vibration (Born-Huang equations) are coupled with the equations for superconducting electrons in a local London approximation and the transverse electromagnetic field. The NFE-Sc materials considered are Type II where $\lambda_L > \xi$. λ_L is the well known London penetration depth and ξ is the coherence length. In this work, Birman and Zimbovskaya did not consider the effect of the high background dielectric on a vortex in this system.

3.2 The Model

The NFE-SC material is subjected to a transverse electric field. Maxwell's equations for the transverse macroscopic fields can be written as [31]

$$\begin{aligned} \nabla \cdot \mathbf{B} = 0; \nabla \cdot \mathbf{D} = 0; \\ \nabla \times \mathbf{E} + \frac{1}{c}\frac{\partial \mathbf{B}}{\partial t} = 0; \\ \nabla \times \mathbf{H} - \frac{1}{c}\frac{\partial \mathbf{D}}{\partial t} = 0, \end{aligned} \tag{3.1}$$

with the corresponding equations of the medium taken as $\mathbf{B} = \mathbf{H} + 4\pi\mathbf{M}$

and $\mathbf{D} = \mathbf{E} + 4\pi\mathbf{P} = \varepsilon(\omega)\,\mathbf{E}$.

A diatomic basis is considered for the host diatomic lattice. For the diatomic ionic lattice under discussion, the macroscopic theory is fully embodied in the following pair of equations[32];

$$\begin{aligned} \frac{d^2\mathbf{w}}{dt^2} &= b_{11}\mathbf{w} + b_{12}\mathbf{E}; \\ \mathbf{P} &= b_{21}\mathbf{w} + b_{22}\mathbf{E}, \end{aligned} \tag{3.2}$$

where $\mathbf{P}$ and $\mathbf{E}$ are the dielectric polarization and the electric field, as defined by the Maxwell's equations (3.1.) Here $\mathbf{w}$ is the relative displacement vector of the positive and negative ions, $\mathbf{w} = \mathbf{u}_+ - \mathbf{u}_-$. The linearity of the equations of motion for the diatomic lattice is an assumption analogous to Hooke's law in the theory of elasticity. The coefficients b_{ij} are frequency dependent . A plane wave solution is sought for equation (3.2) in the form $\exp(i\mathbf{k}\cdot\mathbf{r} - i\omega t)$ in the Long wave approximation. For these transverse waves, in the ionic medium with a single resonance frequency ω_{TO} the expression for the dielectric function is obtained as

$$\varepsilon(\omega) = \varepsilon_\infty \frac{(\omega_{LO}^2 - \omega^2)}{(\omega_{TO}^2 - \omega^2)} \tag{3.3}$$

The b coefficients in equation (3.2) are expressed in terms of measurable

constants as follows:

$$\begin{aligned} b_{11} &= -\omega_0^2, \\ b_{12} = b_{21} &= \left(\frac{\varepsilon_0 - \varepsilon_\infty}{4\pi}\right)^{1/2} \omega_0, \\ b_{22} &= \frac{\varepsilon_\infty - 1}{4\pi}. \end{aligned} \tag{3.4}$$

In perovskites, cuprates or bronzes, one has to take into account the other non-soft LO and TO modes. This is achieved by renormalizing ε_∞ to some effective value ε'_∞ [33] where $\varepsilon'_\infty = \varepsilon_\infty \prod_i{}' \omega_{Li}^2/\omega_{Ti}^2$. The primed product includes all oscillations except the soft mode. In this case, equation(3.3) is modified with ε_∞ replaced by ε'_∞. The generalized Lyddane-sachs-Teller (LST) relation[17], [33] is

$$\frac{\varepsilon_0}{\varepsilon_\infty} = \prod_i \frac{\omega_{Li}^2}{\omega_{Ti}^2} \tag{3.5}$$

In this generalized relation, all the oscillators, including the soft mode are included in the product.

London equation[22] can be written as

$$\nabla \times \mathbf{M} = \frac{1}{c}\mathbf{J}_s = -\frac{1}{c^2\Lambda}\mathbf{A} = -\frac{n_s e^2}{m^* c^2}\mathbf{A} \tag{3.6}$$

In this equation, **A** is the vector potential which obeys the London gauge

$$\frac{\partial \mathbf{A}}{\partial t} = -c\mathbf{E}, \nabla \times \mathbf{A} = \mathbf{B} \tag{3.7}$$

Combining the equation (3.1), (3.6) and (3.7) the equation for the electric field is obtained

$$\nabla \times (\nabla \times \mathbf{E}) = -\frac{1}{c^2}\varepsilon(\omega)\frac{\partial^2 \mathbf{E}}{\partial t^2} - \frac{4\pi}{c^2\Lambda}\mathbf{E} \tag{3.8}$$

This is a coupled equation between the soft-mode NFE oscillators and the London supercurrent.

Reminding ourselves that the fields considered here are transverse and a plane wave solution is sought here, we can write $\nabla \times \nabla \times \mathbf{E} = -\nabla^2 E$, equation (3.8) can be written as

$$-\nabla^2 E = k^2 E \tag{3.9}$$

where

$$k^2 = \frac{\omega^2}{c^2}\varepsilon(\omega) - \frac{4\pi}{c^2\Lambda} \tag{3.10}$$

In this equation if the London term is absent, it is the usual equation for transverse phonon polaritons; on the other hand , if the displacement term due to the polarization is absent , then the field attenuates at a distance $\lambda_L^{-1} = \sqrt{4\pi/c^2\Lambda}$, where λ_L is the London penetration depth.

Solution of equation (3.10) produces interesting results. Depending on the sign of k, it is either real and the electromagnetic waves propagate through the medium or imaginary and the wave damps with frequency dependent penetration depth λ_L^* where

$$\lambda_L^* = \lambda_L \Big/ \left(\left| 1 - \frac{\omega^2}{c^2} \varepsilon(\omega) \lambda_L^2 \right| \right)^{1/2} \tag{3.11}$$

Figure 3.1 illustrates this. When $\omega = 0$, $\lambda_L^* \to \lambda_L$, the usual London

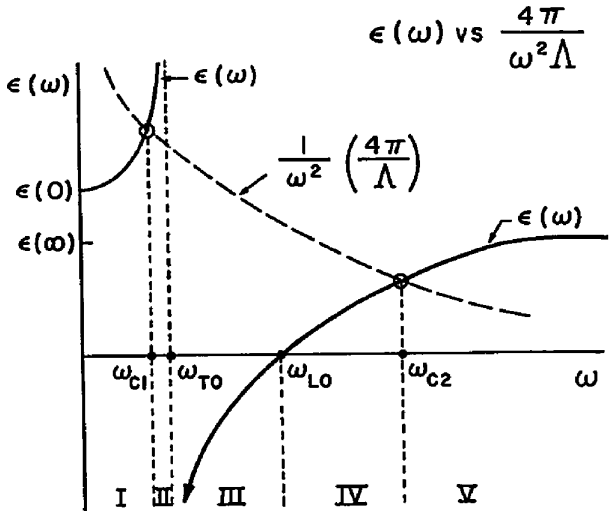

Figure 3.1: Solution of the dispersion equation (3.10) for zero damping. The intervals $\omega_{c1} < \omega < \omega_{TO}$ and $\omega > \omega_{c2}$ correspond to real root of the equation,[9]

penetration depth. With the increase in frequency, λ_L^* increases as well. At $\omega = \omega_{c1}$, $k^2(\omega_{c1}) = 0$ and $\lambda_L^*(\omega_{c1})$ becomes infinite. This makes the field uniform within the medium. For $\omega_{c1} < \omega < \omega_{TO}$, $k^2 < 0$. In this case the penetration depth again depends upon the frequency. This is equivalent to

the Meissner effect. At $\omega = \omega_{LO}$, $\varepsilon(\omega_{LO}) = 0$. Hence, $\lambda_L^*(\omega_{LO}) \to \lambda_L$. For $\omega_{c1} < \omega_{LO} < \omega_{c2}, k^2 < 0$ giving increasing $\lambda_L^*(\omega)$, and at $k^2(\omega_{c_2}) = 0$, a uniform field. For $\omega > \omega_{c2}, k^2 > 0$ and the wave propagates in the medium again, as in a dielectric.

In short, equation (3.10) can be summarized as a function of frequency and it describes the interesting behavior of the medium switching between dielectric and superconducting as the frequency of the applied electromagnetic field changes. For the frequency ranges described in the paragraph above, the material behaves like a superconductor with frequency dependent penetration depth $\lambda_L^*(\omega)$. For $x > \lambda_L^*(\omega)$, magnetic field $\mathbf{B}$ is excluded from the sample. With change in frequency, the material switches to dielectric behavior where the field propagates through the material with frequency dependent real wave number as in a real dielectric material. One can conclude that a quantum phase transition occurs between these two states driven by the changing frequency.

In order to include damping, equation (3.3) can be modified by adding a phenomenological damping coefficient Γ such as

$$\varepsilon(\omega) = \frac{\varepsilon'_\infty(\omega_{L0}^2 - \omega^2)}{(\omega_{T0}^2 - \omega^2) - 2i\omega\Gamma} \tag{3.12}$$

As shown on figure (3.2), including "moderate" damping Γ of the soft-

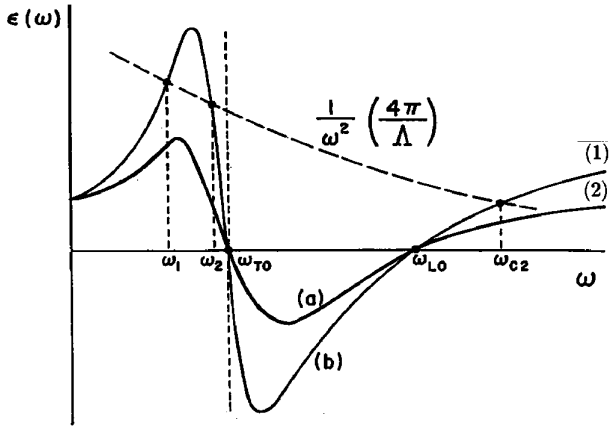

Figure 3.2: Solution of the dispersion equation (3.10) for non-zero damping coefficient. For moderate damping, the 'anomalous' frequency range still exists. This is demonstrated in curve 1. With enhancement in Γ, such frequency intervals disappear,[9]

mode oscillator changes the results quantitatively but the above qualitative features remain the same.

The roots of this equation are,

$$\omega_{1,2} = \omega_{T0}\sqrt{\frac{1}{2}N_1 - \frac{2\Gamma^2}{\omega_{T0}^2(1+a^2)} \pm \frac{1}{2}\sqrt{N_2^2 - \frac{4\Gamma^2}{\omega_{T0}^2(1+a^2)}N_1}} \qquad (3.13)$$

Here $N_1 = \left[1 + (1+a^2)^{-1}\right]$, $N_2 = \left[1 - (1+a^2)^{-1}\right]$ and $a^2 = \omega_{LO}\varepsilon'\Lambda/4\pi$ is a dimensionless that can take on values of the order of unity in nearly ferroelectric materials such as $n - SrTiO_3$. Birman and Zimbovskaya go on to study a semi-infinite medium and a thin film of the NFE-SC material. The material of their choice is $n - SrTiO_3$ for which the lattice, dielectric and electronic data are available. In the following chapters, we study structure

of vortices in NFE-SC thin film and film of finite thickness as well as the non-local effects in the NFE-SC film. Hence its logical for us to give a review of the electromagnetic theory of the NFE-SC film as proposed by Birman and Zimbovskaya.

3.3 A Thin Nearly-Ferroelectric Superconducting Film

The film in consideration here occupies the region $0 \leq z \leq L$. It has thickness L and the term 'thin' here indicates an infinite surface area (xy-plane) rather than an infinitesimally thin film. An electromagnetic wave is propagating in a direction normal to the film (along the z axis) at interface $z = 0$. The electric field $\mathbf{E}$ is polarized along the x axis and the magnetic field $\mathbf{B}$ is polarized along the y axis and have z dependence. The electromagnetic field can be expanded in a Fourier series[34]

$$E(z) = \frac{2}{L}\sum_{N=0}^{\infty}\left(1 - \frac{1}{2}\delta_{N0}\right)E_N \cos(k_N z) + \frac{2}{L}\sum_{N=1}\tilde{E}_N \sin(k_N z) \qquad (3.14)$$

The expressions E_N and $\tilde{E}_N$ are

$$E_N = \int_0^L E(z)\cos(k_N z)dz;$$

$$\tilde{E}_N = \int_0^L E(z)\sin(k_N z)dz; \quad k_N = \frac{\pi N}{L}.$$

Combined with the dispersion equation (3.10), the expressions become

$$E_N = \frac{\lambda_L^{*2}}{\mp\lambda_L^{*2}k_N^2 - 1}\big[E'(0) - (-1)^N E'(L)\big];$$

$$\tilde{E}_N = \frac{\lambda_L^{*2}}{k_N(\mp\lambda_L^{*2}k_N^2 - 1)}\big[E(0) - (-1)^N E(L)\big]. \tag{3.15}$$

In equation (3.15), the $'-'$ sign is used for frequency ranges where $k^2 < 0$ and the $'+'$ sign is when $k^2 > 0$. Here the frequency range considered is when $k^2 > 0$, and $\delta\omega = \omega_{C1} - \omega_{TO}$. The material exhibits dielectric like behavior in this frequency range. No damping effect is considered here. Substitution of equation (3.15) into (3.14) produces

$$\begin{aligned} E_x(0) &= \frac{i\omega\lambda_L^*}{c}B_y(0)\cot\left(\frac{L}{\lambda_L^*}\right) - \frac{i\omega\lambda_L^*}{c}B_y(L)\sin^{-1}\left(\frac{L}{\lambda_L^*}\right); \\ E_x(L) &= \frac{i\omega\lambda_L^*}{c}B_y(0)\sin^{-1}\left(\frac{L}{\lambda_L^*}\right) - \frac{i\omega\lambda_L^*}{c}B_y(L)\cot\left(\frac{L}{\lambda_L^*}\right) \end{aligned} \tag{3.16}$$

For the magnetic field, the solutions are

$$B_y(0) = \frac{ic}{\omega\lambda_L^*}E_x(0)\cot\left(\frac{L}{\lambda_L^*}\right) - \frac{ic}{\omega\lambda_L^*}E_x(L)\sin^{-1}\left(\frac{L}{\lambda_L^*}\right);$$
$$B_y(L) = \frac{ic}{\omega\lambda_L^*}E_x(0)\sin^{-1}\left(\frac{L}{\lambda_L^*}\right) - \frac{ic}{\omega\lambda_L^*}E_x(L)\cot\left(\frac{L}{\lambda_L^*}\right). \qquad (3.17)$$

The boundary conditions that govern the system at the interfaces $z = 0$ and $z = L$ are fairly standard and can be written as

$$E_{ix}(0) + E_{rx}(0) = E_{tx}(0);$$

$$E_{ix}(0) - E_{rx}(0) = B_y(0);$$

$$E_x(L) = B_y(L) \qquad (3.18)$$

These boundary conditions combined with equation (3.17) gives the expression for the reflection coefficient and transmission coefficient as

$$R = \frac{1}{1 + \rho^2(\omega)\sin^{-2}(L/\lambda_L^*)};$$
$$T = \frac{\rho^2(\omega)\sin^{-2}(L/\lambda_L^*)}{1 + \rho^2(\omega)\sin^{-2}(L/\lambda_L^*)}, \qquad (3.19)$$

where the function $\rho\,(\omega)$ can be written as

$$\rho(\omega) = \frac{2ck^*}{\omega}\frac{1}{1 - c^2k^{*2}/\omega^2}. \qquad (3.20)$$

Here $k^* = 1/\lambda_L^*$ is the solution of the dispersion equation (3.10) in the 'anamalous' frequency range $\omega_{C1} < \omega < \omega_{TO}$. When ω is very close to ω_{TO}, then $k \cong (\omega/c)\sqrt{\varepsilon}$. This corresponds to a polariton-phonon transverse wave.

Plots of the reflection coefficient and the transmission coefficient vs. normalized frequency (ω/ω_{TO}) produces very interesting result when $\lambda_L^* = L/(\pi N)$ or the effective London penetration depth is in resonance with the Fourier component $k = k_N$. At resonance $\sin(L/\lambda*) \to 0$ in equations (3.19) and (3.20) making the reflection coefficient $R = 0$ and the transmission coefficient $T = 1$. At this point the film becomes totally transparent to the propagating electromagnetic wave. In general when the quantity $\sqrt{\varepsilon(\omega) - 4\pi/\omega^2\Lambda} = \sqrt{\tilde{\varepsilon}(\omega)} \equiv \tilde{n}(\omega)$, the "effective reflective index" of the film, goes to unity the electromagnetic field goes through the film with zero reflection. Other situations when $R = 0$ are when $k = k_0 = \omega/c$.

With the inclusion of damping, near the resonances, the expressions for R and T are

$$R = \frac{1}{1 + \rho^2(\omega) + S^2(\omega)\sin^{-2}(L/\lambda_L^{*\prime})}; \tag{3.21}$$

$$T = \frac{\rho^2(\omega)\sin^{-2}(L/\lambda_L^{*\prime})}{1 + \rho^2(\omega) + S^2(\omega)\sin^{-2}(L/\lambda_L^{*\prime})}, \tag{3.22}$$

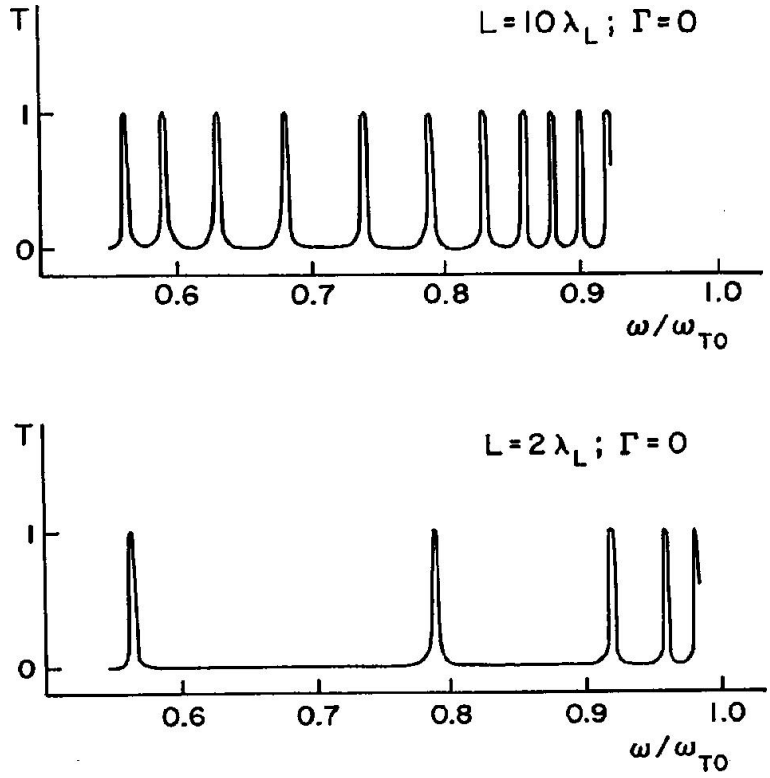

Figure 3.3: Transmission coefficient vs. normalized frequency for an NFE-Sc film of thickness L in the anamalous frequency range $\omega_{c1} < \omega < \omega_{TO}$. The parameters for $SrTiO_3$ are used,[9].

where

$$S(\omega) = \rho(\omega)\cos\left(\frac{L}{\lambda_L^{*\prime}}\right) + \sqrt{1+\rho^2(\omega)}\sinh\left(\frac{L}{\lambda_L^{*\prime\prime}}\right) \tag{3.23}$$

and $1/\lambda_L^* = 1/\lambda_L^{*\prime} + i/\lambda_L^{*\prime\prime}$.

Here

$$\frac{1}{\lambda_L^{*\prime}} \approx \sqrt{\frac{\omega^2}{c^2}\varepsilon'(\omega) - \frac{1}{\lambda_L^2}} \tag{3.24}$$

$$\frac{1}{\lambda_L^{*\prime\prime}} \approx \left(\frac{2\omega\Gamma}{\omega_{TO}^2 - \omega^2}\right)^{1/2} \frac{1}{\lambda_L} \tag{3.25}$$

With the inclusion of damping the anamalou effects in the frequency range $\delta\omega$. It only slightly modifies the sharp resonances occurring at $k = k_N$ and $k = k_0$.

3.4 Application to $N - SrTiO_3$

$n{-}SrTiO_3$ can be considered a prototype of the NFE-SC material. the lattice parameters, dielectric and electronic data are known for $n - SrTiO - 3$. It is a widely studied material. The parameters[35], [36], [37] are

$$\varepsilon_\infty = 5.5, \quad \omega_{LO} = 5.2 \times 10^{12} s^{-1}, \quad \frac{\Pi_i' \omega_{Li}^2}{\omega_{Ti}^2} = 4.1.$$

Using the LST relation , at ∼1K

$$\omega_{TO} = 1.6 \times 10^{11} s^{-1}$$

and at 1K

$$\varepsilon(0) \sim 2.25 \times 10^{4}.$$

The damping constant for the soft TO mode from equation (3.13) is measured from optical line width $\Gamma^2/\omega_{T0}^2 \sim 0.2$

The effective mass is $m^* \sim 10m_e$. Here m_e is the free electron mass. For doping, $n_s = 9 \times 10^{17} cm^{-3}$

Figure (3.3) represents the transmission coefficient of $n - SrTiO_3$ for $L = 2\lambda_L$ and $L = 10\lambda_L$. The peaks arise due to the complete propagation of the transverse mode corresponding to the solution of the dispersion equation (3.10). It is reasonable to predict that these picks can be observed experimentally in any NFE-SC material in the appropriate frequency range and temperature below the transition temperature T_c. Although the calculations presented in this chapter are for $n - SrTiO_3$, the general theory developed by Birman and Zimbovskaya can be applied to any NFE-SC material such as sodium tungsten bronzes and possibly high temperature cuperates. The main assumption here is that all free careers condense into Cooper pairs, hence the resulting coupled modes can be treated as "phonon polaritons dressed by the

supercurrent or electromagnetic waves in a London superconductor dressed by the transverse optic waves (TO phonon)". the system can be considered undergoing a phase transition between the superconducting and the dielectric states with the change in frequency.

Chapter 4

VORTEX STRUCTURE IN NFE-SC: LONDON LIMIT

4.1 Introduction

The experimental report of high temperature superconductivity at $T_c \sim 90K$ in the 'Sodium Tungsten Bronze' materials in 1999 resulted in renewed interest in the coexistence and competition of Superconductivity and 'Near-Ferroelectricity' . These bronzes are non-cuprates typified by Na_xWO_3 with reported superconducting transition temperature around 90K for $x \approx 0.05$; other reported examples involve K, and Cs substituting for Na, with T_c's in the same range. It has long been known that the host tungsten oxide material WO_3 is ferroelectric with several phase transitions reported . Also many years earlier Mattheis et.al. reported superconductivity in the *bronzes* with much larger values of $x \approx 1$ and T_c's in the 3-5K range. Other well known

cases of low temperature($T_c \approx 1\ K$) superconductivity in impurity doped perovskites such as $n-SrTiO_3$ are also examples of 'Nearly-Ferroelectric Superconductors' (NFE-SC). We use this term to describe materials which have high background static (or low frequency) dielectric coefficients($\varepsilon(0) \propto 10^3$ in $SrTiO_3$) and which become superconducting when doped n or p.

Theoretical studies of microscopic mechanisms for superconductivity in doped semiconductors including perovskite (high dielectric coefficient) dielectrics were also initiated in the 1960's by M.L. Cohen and collaborators in the framework of Eliashberg theory, and have continued. In some recent work a microscopic 'dynamical symmetry' model for NFE-SC was proposed which predicted, inter alia, a new magnetoelectric effect .

In this previous work on electrodynamics of NFE-SC, Birman and Zimbovskaya investigated the frequency-dependent optical response of such a material especially near to the infra-red resonance frequency of the Transverse Optical(lattice mode). In that work they found highly unusual behavior of the London penetration depth of the fields depending on frequency: the material can be tuned by changing the electromagnetic frequency to behave as a conventional dielectric , a 'mixed' dielectric superconductor, or a London superconductor with more conventional Meissner effect. The predicted frequency-dependent reflectivity showed a 'comb-like' structure of peaks and

dips.

In the present work we generalize the electromagnetic theory of a nearly ferroelectric superconductor by including the vortices. General vortex structure as well as the interaction between the vortices are investigated.Properties of vortices in the NFE-SC system in the framework of local 'London' electrodynamics are considered. In this chapter we take into account nearly ferroelectric superconducting films of various thicknesses, namely, thin and finitely thick. We explore the structure of a single vortex and the vortex-vortex interaction in a nearly ferroelectric medium. The nearly-ferroelectric nature of the matter with a high background dielectric constat renders significant changes to the structure of the vortices in the material.

Although much work has been done on the electrodynamics of the NFE-SC material, to the best of our knowledge the structure of a single vortex or vortex-vortex interaction in such materials have not been investigated. This work fills this gap.

4.2 Structure of a Single Vortex in an NFE-SC Thin Film

A thin film is a film where the thickness of the film d is smaller than the London penetration depth λ_L. In such thin films we consider the structure

of the vortices as point vortices, similar to the Pearl vortices. London theory assumes that all vortex cores (of radius $\sim \xi$, the coherence length) to be separated and the Ginzberg-Landau (GL) parameter $\kappa = \left(\lambda/\xi\right) \gg 1$ to be large. Hence the London theory is applicable to infinitely large superconductors. In this chapter we investigate the structure of Pearl-like vortices [38] and their interactions in a two dimensional scenario.

We consider a NFE-SC thin film of thickness d. A transverse magnetic field $\mathbf{H}$ is applied to the film. The applied field considered here is strong enough to form vortex structure in the film. The magnetic flux quanta $\phi_0 = ch/2e$ penetrate into the film in form of a single vortex.

We make the usual London assumption that the vortex is represented as a one dimensional line singularity. With inclusion of the vortex the London-like equation for the NFE-SC thin film can be written as[39], [40], [38]

$$\mathbf{h} + \frac{4\pi\lambda\left(\omega\right)^2}{c}\nabla \times \mathbf{j} = \phi_0 \delta_2\left(r\right)\hat{z} \tag{4.1}$$

where $\mathbf{j}$ is the current density and $\hat{z}$ is the unit vector normal to the film. $\delta_2\left(r\right) = \delta\left(r\right)/\pi r$ is the two dimensional delta function in cylindrical coordinates. Here

$$\lambda\left(\omega\right) = \frac{\lambda_L}{\sqrt{\left|1 - \frac{\omega^2}{c^2}\varepsilon\left(\omega\right)\lambda_L^2\right|}}$$

as discussed in chapter three of this thesis[9]. Its the modified London pen-

etration depth due to the presence of background dielectric.

The current density $j(x,y,z)$ in thin films is nearly independent of the z coordinate (perpendicular to the film) and the sheet current in the film is thus $\mathbf{J}(x,y) = \int_{-d/2}^{d/2} \mathbf{j}(x,y,z)\,dz \approx \mathbf{j}d$. For a thin film its reasonable to assume that $d \ll \lambda$. Also the magnetic field can be written in therms of the vector potential $\mathbf{A}$ such as $\mathbf{h} = \nabla \times \mathbf{A}$.

Considering these assumptions, equation (4.1) can be written as

$$\mathbf{A} + \frac{4\pi\lambda(\omega)^2}{c}\frac{\mathbf{J}}{d} = \hat{\phi} \tag{4.2}$$

where $\hat{\phi} = (0, \phi_0/2\pi r, 0)$.

Equation (4.2) can be written as

$$\mathbf{J} = \frac{cd}{4\pi\lambda(\omega)^2}\left(\hat{\phi} - \mathbf{A}\right) \tag{4.3}$$

In the thin film limit, one can replace the film with an infinitely thin current carrying sheet in the plane $z = 0$. Te current density can then be written as $\mathbf{J}\delta(z)$ Taking the curl of equation (4.2), we have the equation expressed in London gauge as

$$-\nabla^2\mathbf{A} = (\varphi - \mathbf{A})\frac{d}{\lambda(\omega)^2}\delta(z) \tag{4.4}$$

We intend to take a Fourier transformation of the vector potential $\mathbf{A}$. The three dimensional Fourier transformation of the vector potential gives

us

$$A_{qk} = \int A_{xyz} \exp\left(iq_x x + iq_y y + ikz\right) dxdydz$$

and the two dimensional Fourier transformation is

$$A_q = \int A_{xyz} \delta\left(z\right) \exp\left(iq_x x + iq_y y\right) dxdydz$$

. Using the property $\frac{d^n f(t)}{dt^n} = (i\omega)^n F(\omega)$ of Fourier transform[41], the LHS of equation (4.4) gives us

$$F_{qk}\left[\nabla^2 \mathbf{A}\left(x,y,z\right)\right] = \left(i\mathbf{q}\right)^2 A_{qk} = -\left(q^2 + k^2\right) A_{qk}$$

. Fourier transform of the first term of the RHS of equation (4.4) leads to

$$\begin{aligned} & F_{qk}\left[\phi\left(x,y\right)\frac{d}{\lambda^2\left(\omega\right)}\delta\left(z\right)\right] \\ &= \frac{d}{\lambda^2\left(\omega\right)}\int \phi\left(x,y\right)\delta\left(z\right)\exp\left\{-i\left(q_x x + q_y y + kz\right)\right\} dxdydz \\ &= \frac{d}{\lambda^2\left(\omega\right)}\int \phi\left(x,y\right)\exp\left\{-i\left(q_x x + q_y y\right)\right\} dxdy \\ &= \frac{d}{\lambda^2\left(\omega\right)}\int \phi\left(x,y\right)\exp\left\{-i\left(\mathbf{q}\cdot\mathbf{r}\right)\right\} dxdy \\ &= \frac{d}{\lambda^2\left(\omega\right)}\int \frac{\phi_0}{2\pi r}\exp\left(-iq_r r\right) rdrd\theta = \frac{d}{\lambda^2\left(\omega\right)}\frac{i\phi_0}{q} \end{aligned}$$

Fourier transform of the second term of the RHS of equation (4.4) gives us the following :

$$F_{qk}\left[\mathbf{A}\left(x,y,z\right)\frac{d}{\lambda^{2}\left(\omega\right)}\delta\left(z\right)\right]$$
$$=\frac{d}{\lambda^{2}\left(\omega\right)}\int\mathbf{A}\left(x,y,z\right)\delta\left(z\right)\exp\left\{-i\left(q_{x}x+q_{y}y+kz\right)\right\}dxdydz$$
$$=\frac{d}{\lambda^{2}\left(\omega\right)}\int\mathbf{A}\left(x,y\right)\delta\left(z\right)\exp\left\{-i\left(q_{x}x+q_{y}y\right)\right\}dxdy$$
$$=\frac{d}{\lambda^{2}\left(\omega\right)}A_{q}$$

Combining all the Fourier transformed terms, we obtain

$$\left(q^{2}+k^{2}\right)A_{qk}=\frac{d}{\lambda^{2}\left(\omega\right)}\left(\phi_{q}-A_{q}\right) \tag{4.5}$$

Solving equation (4.5), we get

$$A_{q}=\phi_{q}\frac{1}{1+2qd/\lambda^{2}\left(\omega\right)} \tag{4.6}$$

From this expression of the vector potential, one can extract all the necessary information regarding the magnetic field and the current in the material.

The magnetic field can be calculated[22] by using

$$h_{zq}=\left|i\mathbf{q}\times\mathbf{A}_{q}\right|$$
$$=\frac{\phi_{0}}{1+2q\lambda^{2}\left(\omega\right)/d}\sim\frac{\varphi_{0}}{2q\lambda^{2}\left(\omega\right)/d} \tag{4.7}$$

From the previous work by Birman and Zimbovskaya[9], we recall comb-like structure at resonances. The material properties are highly dependent on the frequency of the applied field. At resonances the electromagnetic wave passes through the material without reflection. Even though the film has a thickness d, with the change in frequency the film behaves as if the thickness fluctuates to accommodate or repel the external electromagnetic field. We recall that $\lambda(\omega)$ includes the effect of the background dielectric. Hence, we can modify the thickness of the film into something called "effective thickness", from d to $L(\omega)$ such that the effective thickness is proportional to the reflection coefficient

$$L(\omega) = dR = \frac{d}{1 + \rho(\omega)^2 \sin^{-2}(d/\lambda(\omega))} \tag{4.8}$$

Here R is the reflection coefficient as for the thin film as described in chapter three.Taking into account the modified thickness of the film, the magnetic field can be written as

$$h_z(r) = \frac{\phi_0 d}{4\pi\lambda^2(\omega)\, r\left[1 + \rho(\omega)^2 \sin^{-2}(d/\lambda(\omega))\right]} \tag{4.9}$$

We take the normalized frequency $\omega/\omega_{TO} = x$ and plot the dimensionless magnetic field versus x. Here the damping constant Γ is taken as zero. The plots are given in figures (4.1) and (4.2)

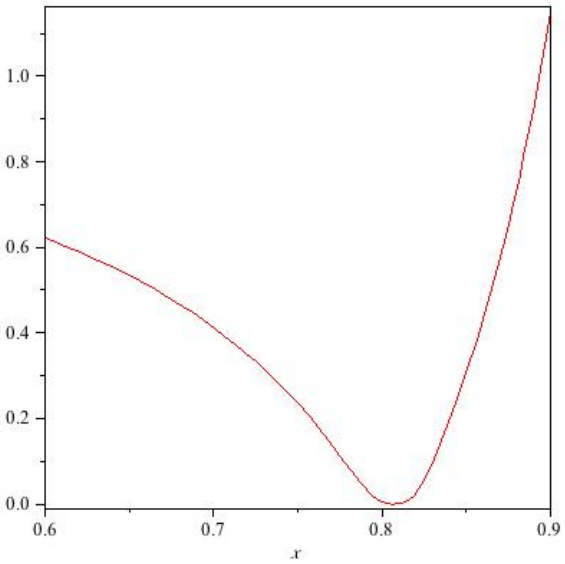

Figure 4.1: A two dimensional view of the magnetic field vs. the normalized frequency. At resonance the magnetic field goes to zero. The thickness of the film considered here is $d = 0.1\lambda_L$

4.3 Vortex-Vortex Interaction in an NFE-SC Thin Film

In a superconductor, Pearl vortices interact mainly via their stray field which extends far into the vacuum and which in the film causes a current density j that decreases as $1/r$ at large distances r. The force between two such Pearl vortices with one quantum of flux ϕ_0 is unscreened and of long range. In case of a NFE-Sc film,the cores are normal electron (currents) which feel each others effect through the dielectric function.

We consider two parallel line vortices on the z axis situated at $\mathbf{r_1} = (x_1, y_1)$

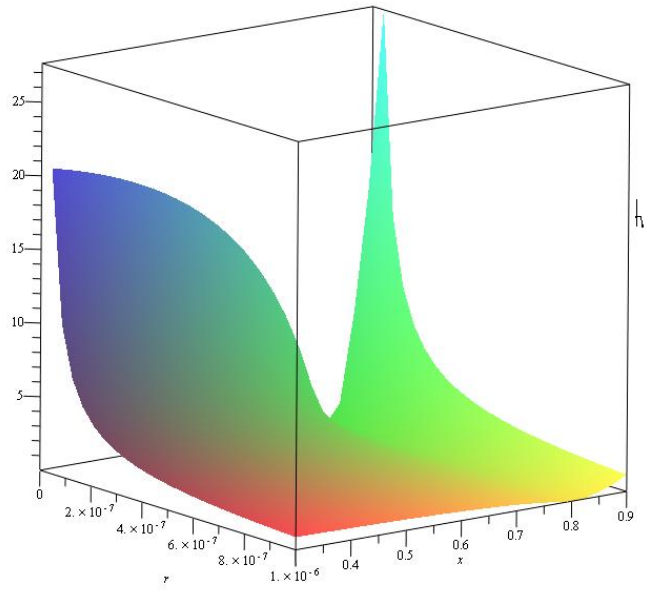

Figure 4.2: In this plot($L(\omega) = Rd$) the magnetic field goes to zero at certain frequencies. At these frequencies the vortex disappears and the material behaves like a regular dielectric.

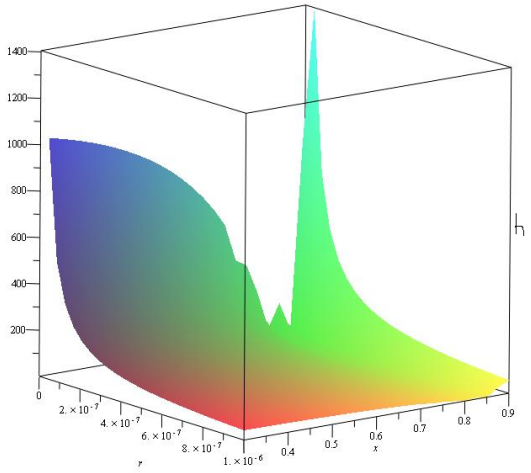

Figure 4.3: In this figure, magnetic field h is plotted as a function of normalized frequency x and the distance from the vortex core r. The thickness of the film here is $d = 5\lambda_L$. With the increase in thickness, the resonances become more pronounced.

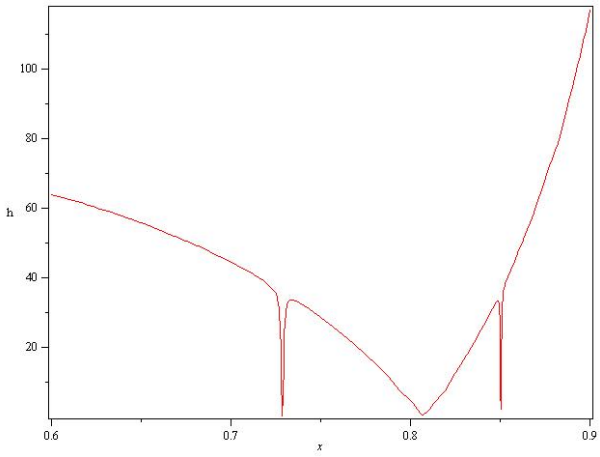

Figure 4.4: In this figure, magnetic field h is plotted as a function of normalized frequency x . The thickness of the film here is $d = 10\lambda_L$.

and $\mathbf{r_2} = (x_2, y_2)$. With two vortices equation (4.1) can be generalized as

$$\mathbf{h} + \lambda(\omega)^2 \nabla \times \nabla \times \mathbf{h} = \varphi_0 \left[\delta(\mathbf{r} - \mathbf{r_1}) + \delta(\mathbf{r} - \mathbf{r_2})\right] \tag{4.10}$$

The resulting magnetic field is a superposition of the individual fields due to the filaments (1) and (2) such as

$$\mathbf{h}(\mathbf{r}, \omega) = \mathbf{h_1}(\mathbf{r}, \omega) + \mathbf{h_2}(\mathbf{r}, \omega) \tag{4.11}$$

Solution for the magnetic field can be written as[38]

$$h_1(r, \omega) = \frac{\varphi_0}{2\pi\lambda(\omega)^2} K_0\left(\frac{r - r_1}{\lambda(\omega)}\right) \tag{4.12}$$

If one sets

$$h_{12} = h_1(r_2, \omega) = h_2(r_1, \omega) = \frac{\varphi_0}{2\pi\lambda(\omega)^2} K_0\left(\frac{r_1 - r_2}{\lambda(\omega)}\right) \tag{4.13}$$

then the energy of interaction can be written as

$$U_{12} = \frac{\varphi_0}{4\pi} h_{12}(r, \omega) \tag{4.14}$$

4.4 Generalized Vortex Structure in an NFE-SC Film of Finite Thickness

In this section we try a more generalized approach towards the NFE-SC material by considering an NFE-SC film of finite thickness. We follow Agassi and Cullen[10] who gave the expression for the magnetic field for a superconducting film of finite thickness. The approach here is based based on combining London equation and Ampere law along with the transverse optical lattice vibration. We modify the theory for a Nearly ferroelectric Superconductor taking into account the high background static dielectric constant of the material.

We consider a single pancake vortex with its core aligned along the z axis and pointing in the $\varphi\hat{z}$ direction ($\varphi = \pm 1$). The pancake vortex considered here is cylindrical in geometry, hence we consider the cylindrical system of coordinates here.

The symmetry between the domains makes it possible to consider only domains (I) and (II). Here $h_z^I(\rho, z) = h_z^{III}(\rho, -d - z)$ and $h_\rho^I(\rho, z) = -h_\rho^{III}(\rho, -d - z)$ The structure of vortex implies that the field needs to be investigated only in the tangential ρ and the normal z directions. In case of a nearly ferroelectric superconductor, the background dielectric effect is contained in the

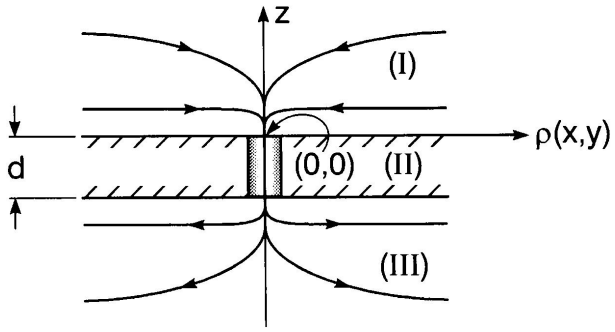

Figure 4.5: Schematic diagram of an NFE-SC film in the presence of a single vortex. Shown are the chosen cylindrical system, the domains (I), (II) and (III), the thickness d, the induction $\vec{h}\,(\vec{r})$ field-lines flow and the cylindrical shaft around the core-line at $\{x, y, z\} = \{0, 0, -d \leq z \leq 0\}$,[10]

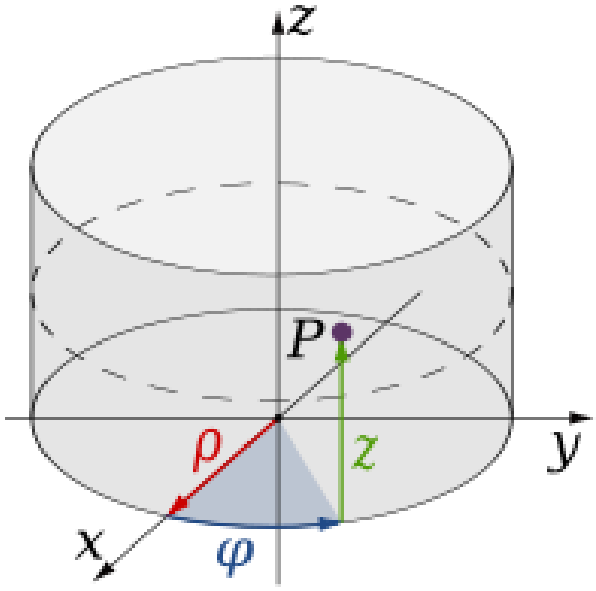

Figure 4.6: Cylindrical coordinate system

effective London penetration depth or the frequency dependent penetration depth $\lambda(\omega)$. Incorporating this factor, the equations for the magnetic field h[22],[10] in regions I and II can be written as

$$\begin{aligned} \nabla^2 h^I_{\rho,z}(\rho,z) &= 0 \\ \left(\nabla^2 - \beta(\omega)^2\right) h^{II}_z(\rho,z) &= -\varphi\phi_0\beta(\omega)^2\delta(\rho) \\ \left(\nabla^2 - \beta^2\right) h^{II}_\rho(\rho,z) &= 0 \end{aligned} \tag{4.15}$$

where

$$\beta(\omega) = \frac{1}{\lambda(\omega)}$$

and the frequency dependent penetration depth, as discussed in the chapter for NFE-SC materials,

$$\beta(\omega) = \frac{\lambda_L}{\sqrt{\left|1 - \frac{\omega^2}{c^2}\epsilon(\omega)\lambda_L^2\right|}}$$

λ_L is the usual London penetration depth. From the condition $\vec{\nabla}\cdot\vec{h} = 0$, it can be concluded that the tangential and the normal components of the magnetic induction are related, and thsi relationship can be found by considering the vector potential in the London gauge [22] $\vec{A} = (A_\rho = 0, A_\varphi(\rho,z), A_z = 0)$. From calculations[10]

$$h_\rho = -\frac{1}{\rho}\int_0^\rho dr \frac{\partial h_z(r,z)}{\partial z} r \tag{4.16}$$

The boundary conditions complementing the equation above are the continuity of h_ρ and h_z across the $z = 0$ surface and that no field exists at $|z| \to \infty$. The set of equation (4.15) are solved by a Fourier-Bessel transformation. The transformation takes into account the symmetries and the boundary conditions. As shown in figure (4.5) and in coordinate system, the transformations are[10]

$$h_z^I(\rho, z) = \int_0^\infty J_0(q\rho) e^{-qz} h_z^I(q)\, dq$$

$$h_z^{II}(\rho, z, \omega) = \varphi \frac{\phi_0 \beta(\omega)^2}{2\pi} K_0(\beta(\omega)\rho) + \int_0^\infty J_0(q\rho) \times \frac{\cosh(D[q,\omega](z + d/2))}{\cosh(D[q,\omega]d/2)} h_z^{II}(q)\, dq \tag{4.17}$$

where

$$D[q, \omega] = \sqrt{q^2 + \beta(\omega)^2}$$

Here $K_0(z)$ and $J_0(z)$ are the modified and regular Bessel function of order zero respectively. The effect of finite thickness of the film is contained in the second term of equation (4.17) for $h_z^{II}(\rho, z, \omega)$. Utilizing the integral results [42], [10]

$$\int_0^\infty dx \frac{xJ_0(\rho x)}{x^2+\beta^2} = K_0(\beta\rho)$$
$$\int xJ_0(x)dx = xJ_1(x) \tag{4.18}$$

the magnetic field for the domains I and II can be written as [10]

$$h_z^I(q,\omega) = \varphi\frac{\phi_0\beta^2}{2\pi} \times \frac{q\tanh(D[q,\omega]d/2)}{D[q,\omega](q+D[q,\omega]\tanh(D[q,\omega]d/2))}$$
$$h_z^{II}(q,\omega) = -\varphi\frac{\phi_0\beta^2}{2\pi} \times \frac{q^2}{D^2[q](q+D[q,\omega]\tanh(D[q,\omega]d/2))} \tag{4.19}$$

Inserting equation (4.19) into equation (4.16) and 4.18) yields

$$h_\rho^I(\rho,z,\omega) = \int_0^\infty J_1(q\rho)e^{-qz}h_z^I(q,\omega)\,dq$$
$$h_\rho^{II}(\rho,z,\omega) = -\int_0^\infty \frac{J_1(q\rho)}{q}\frac{\sinh(D[q,\omega](z+d/2))}{\cosh(D[q,\omega]d/2)} \times D[q,\omega]h_z^{II}(q,\omega)\,dq \tag{4.20}$$

Equations (4.18), (4.19) and (4.20) constitute the vortex structure in a film of arbitrary thickness d.

4.4.1 The Half space Limit

For the half-space limit, we consider $\delta = d/\lambda \to \infty$. In this limit $\tanh[z] \to 1$ and $\cosh(D[q,\omega](z+d/2)) \to \exp[D[q,\omega]z]$ can be replaced in equation (4.17) , The expression for the dimensionless tangential and vertical components are [10].

$$\frac{h_z^{II}(\tilde{\rho},\varsigma)}{\phi_0\beta^2/2\pi} = K_0[\tilde{\rho}] - \int_0^\infty dv J_0(v\tilde{\rho}) e^{D[v]\varsigma} \times \left\{ \frac{v^2}{D^2[v](v+D[v])} \right\} \tag{4.21}$$

and

$$\frac{h_\rho^{II}(\tilde{\rho},\varsigma)}{\phi_0\beta(\omega)^2/2\pi} = \int_0^\infty J_1(v\tilde{\rho}) e^{D[v]\varsigma} \left\{ \frac{v}{D[v](v+D[v])} \right\} dv \tag{4.22}$$

where $D[v] = \sqrt{v^2+1}$. $\tilde{\rho} = \beta\rho \geq 0$, $\varsigma = \beta(\omega) z \leq 0$ are the dimensionless coordinates.

When $|z|/\lambda \gg 1$,deep inside the film only the first term of the equation(4.17) survives. This is Abrikosov-like vortex structure. This effect is Meissner-like in its nature. The delocalization effect due to the weakened screening capacity are accounted for by substituting $\varsigma = 0$ in(4.17). Using standard integral results [42],[10] yields

$$\frac{h_z^{II}\left(\rho, z=0; d=\infty\right)}{\phi_0\beta^2/2\pi} = \frac{1}{2}\left\{I_0\left[\frac{\tilde{\rho}}{2}\right]K_0\left[\frac{\tilde{\rho}}{2}\right] - I_1\left[\frac{\tilde{\rho}}{2}\right]K_1\left[\frac{\tilde{\rho}}{2}\right]\right\} \tag{4.23}$$

and

$$\frac{h_\rho^{II}\left(\rho, z=0; d=\infty\right)}{\phi_0\beta^2/2\pi} = \frac{1}{8\tilde{\rho}^2}\left\{\begin{array}{l} I - 8e^{-\tilde{\rho}}\left(1+\tilde{\rho}\right) \\ +\tilde{\rho}^2\left(-I_2\left[\frac{\tilde{\rho}}{2}\right]K_0\left[\frac{\tilde{\rho}}{2}\right] + I_0\left[\frac{\tilde{\rho}}{2}\right]K_2\left[\frac{\tilde{\rho}}{2}\right]\right) \\ \end{array}\right\} \tag{4.24}$$

The graphs represent a single vortex structure near the surface of the film. As we can see, due to resonance, the magnetic field goes to zero at certain point resulting the expulsion of the vortex from the material.x is the normalized frequency. There is a mix of ferroelectric, superconducting and Meissner-like effects here which needs further investigation.

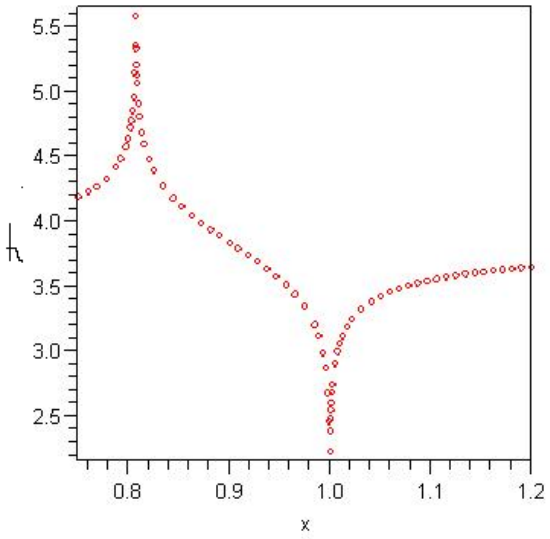

Figure 4.7: A single vortex in NFE-SC film of finite thickness. The magnetic field goes to zero at resonance frequency thus expelling the vortex out of the material

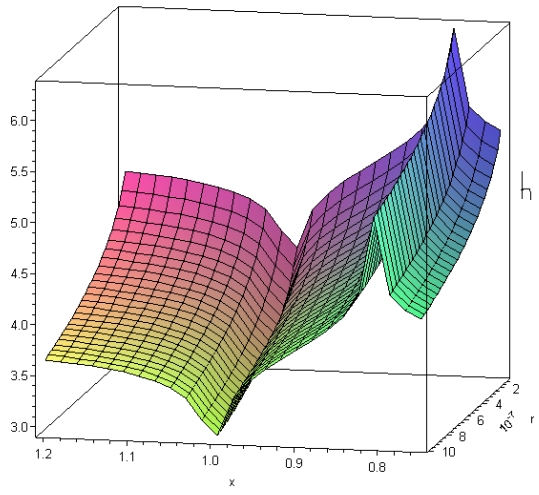

Figure 4.8: Variation of magnetic field with respect to the distance from the vortex core as well as the frequency .

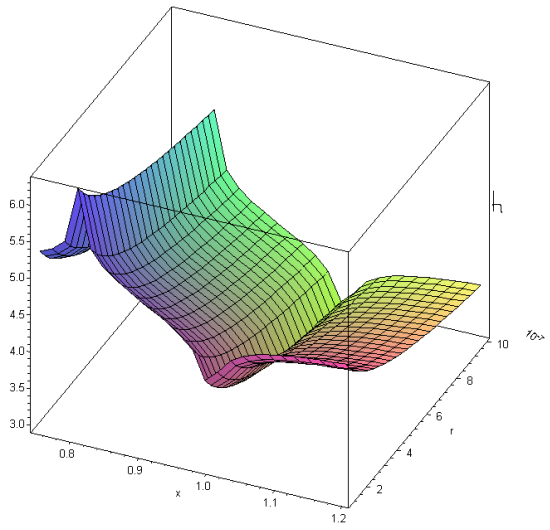

Figure 4.9: Magnetic field vs. r and the normalized frequency x.

Chapter 5

NFE-SC THIN FILM IN NONLOCAL PIPPARD LIMIT

In chapters three and four we discussed the electrodynamics of nearly ferroelectric superconductors in London limit. The approach was local, effects from the surrounding were not considered. In this chapter we generalize this theory further by considering a non-local approach. Scrieffer [11] investigated specular and random scattering for superconducting films subjected to a steady external magnetic field H_0.

For a superconductor, a weak external magnetic field acts as a perturbation on the ground state. Within the perturbation expansion one can show that the following non-local relation between the supercurrent density $\mathbf{j}$ and the vector potential $\mathbf{A}$ holds (in Coulomb gauge $\nabla \cdot \mathbf{A} = 0$)[43]:

$$j_\alpha(r) = -\sum_\beta \int \left[R_{\alpha\beta}(r-r') - \frac{e^2 n_S}{m^*}\delta(r-r')\,\delta_{\alpha\beta} \right] A_\beta(r')\,dr'$$
$$= -\sum_\beta \int G_{\alpha\beta}(r-r')\,A_\beta(r')\,dr' \qquad (5.1)$$

where e is the electron charge, n_S is the super carrier density, m^* is the effective electron mass and $\nabla \times \mathbf{A} = \mathbf{B}$[6]. The first term in the square brackets, $R_{\alpha\beta}$, describes the paramagnetic response, whereas the second reflects the diamagnetic one. $G_{\alpha\beta}$ is called the kernel. If the wave function of the electronic ground state were "rigid" with respect to all perturbations (rather than only those which lead to transverse excitations), $R_{\alpha\beta}$ would be identically zero and equation (5.1) would reduce to the local $\mathbf{j} - \mathbf{A}$ relation

$$j_\alpha(r) = -\frac{1}{\mu_0 \lambda_L^2} A_\alpha(r) \qquad (5.2)$$

with μ_0 the magnetic permeability of the vacuum[22][44]. This combined with the London equation $\nabla \times \mathbf{M} = \frac{1}{c}\mathbf{J_S}$ yields, at a plane superconductor-vacuum interface, the result of an exponentially suppressed magnetic field

$$B(z) = B_{ext} \exp(-z/\lambda_L) \qquad (5.3)$$

with the London penetration depth $\lambda_L = \sqrt{\frac{m^*}{\mu_0 e^2 n_S}}$, which is the well known result[22].

However. $R_{\alpha\beta}$ has a range of the order parameter of the Cooper pairs, i.e., of the coherence length ξ. The magnetic penetration depth sets the length scale for the decay of the magnetization; for $\lambda \gg \xi$ the spatial variation of the vector potential $\mathbf{A}$ over the superconducting pairs is negligible and the one-parameter local description of equation (5.2) holds. If $\xi \geq \lambda$ the full non-local description has to be taken into account.

Using the Maxwell equations and the relation between $\mathbf{A}$ and $\mathbf{B}$, equation (5.1) transforms to an integro-differential equation

$$[\nabla \times \nabla \times \mathbf{A}]_{\alpha}(r) = -\sum_{\beta} \int G_{\alpha\beta}(r - r') A_{\beta}(r') d^3 r' \tag{5.4}$$

In the non-local Pippard electrodynamics the current is generally written as[45],[46],

$$\mathbf{J}_s(\mathbf{r}) = \frac{-3}{4\pi\xi_0\Lambda c} \int \frac{\mathbf{R}[\mathbf{R} \cdot \mathbf{A}(\mathbf{r}')]}{R^4} e^{-R/\xi} d\vec{r}' \tag{5.5}$$

and

$$\begin{aligned} \mathbf{J}(\mathbf{k}) &= -\left[\frac{3\pi^2}{\xi_0\Lambda ck}\right] \frac{2}{(\xi k)^2} \left\{\left[1 + (\xi k)^2\right] \tan^{-1} \xi k - \xi k\right\} \mathbf{A}(\mathbf{k}) \\ &\simeq -\left[\frac{3\pi^2}{\xi_0\Lambda ck}\right] \mathbf{A}(\mathbf{k}), \xi k \gg 1 \end{aligned} \tag{5.6}$$

where $\mathbf{R} = \mathbf{r} - \mathbf{r}'$ and $\frac{1}{\xi} = \frac{1}{\xi_0} + \frac{1}{l}$, l=mean free path in the normal state

and ξ_0=coherence length.

Equation (5.4) can be solved if the boundary conditions are known. For two different boundary conditions a modified version of equation (5.4) has been discussed which are specular reflection and random or diffuse scattering[11]. The equation is modified because we consider a nearly ferroelectric superconductor here.

In case of specular reflection, the electrons, Cooper pairs are perfectly reflected from the interface where the incoming angle is equal to the outgoing angle. In this case a Fourier transform method simplifies equation (5.4) for us.

In case of diffuse scattering or random scattering, the electrons, Cooper pairs loose all their memory upon scattering on the interface. This type of scattering is mathematically the more difficult one.

We consider the electromagnetic wave propagating along the z-direction with electric field $\mathbf{E}(\mathbf{r})$ polarized along the x-direction and the magnetic field $\mathbf{B}(\mathbf{r})$ polarized along the y-direction. Lattice equations not including the damping are[32],[47]

$$\frac{d^2\mathbf{w}}{dt^2} = b_{11}\mathbf{w} + b_{12}\mathbf{E}, \mathbf{P} = b_{21}\mathbf{w} + b_{22}\mathbf{E} \tag{5.7}$$

where[32]

$$\varepsilon(\omega) = \varepsilon_\infty \frac{(\omega_{LO}^2 - \omega^2)}{(\omega_{TO}^2 - \omega^2)} \tag{5.8}$$

London gauge is

$$\nabla \times \mathbf{A} = \mathbf{B}\ , \frac{\partial \mathbf{A}}{\partial t} = -c\mathbf{E} \tag{5.9}$$

Considering there are no free careers and all the careers in the system have condensed into Cooper pairs, we have

$$\nabla \times \mathbf{M} = \frac{1}{c}\mathbf{J}_s \tag{5.10}$$

Taking curl of Maxwell's equation, we get

$$\nabla \times \left(\nabla \times \mathbf{E} + \frac{1}{c}\frac{\partial \mathbf{B}}{\partial t} \right) = 0 \tag{5.11}$$

Further substitution gives us

$$-\nabla^2 \mathbf{E} + \frac{1}{c^2}\varepsilon(\omega)\frac{\partial^2 \mathbf{E}}{\partial t^2} + \frac{4\pi}{c^2}\frac{\partial \mathbf{J}_s}{\partial t} = 0 \tag{5.12}$$

Considering the London gouge $\frac{\partial \mathbf{A}}{\partial t} = -c\mathbf{E}$ we can write down equation (5.12) as

$$\nabla^2 \mathbf{A} + \frac{\omega^2}{c^2}\varepsilon(\omega)\mathbf{A} - \frac{3}{\xi_0 \Lambda c^2}\int \frac{\mathbf{R}(\mathbf{R}\cdot\mathbf{A})}{R^4} e^{-R/\xi} d\mathbf{r}' = 0 \tag{5.13}$$

This is the general integro-differential equation for the non-local nearly ferroelectric superconductors. We aspire to solve this for a thin film (where the thickness is much smaller compared to the available surface area.)

5.1 Specular Reflection in NFE-SC Thin Film

were not considered. In this chapter we generalize this theory further by considering a non-local approach. Schrieffer [11] investigated specular and random scattering for superconducting films subjected to a steady external magnetic field H_0. Although we follow Schrieffer's approach, our approach is significantly different in terms of the material studied, application of the field and solving the system of equations numerically.

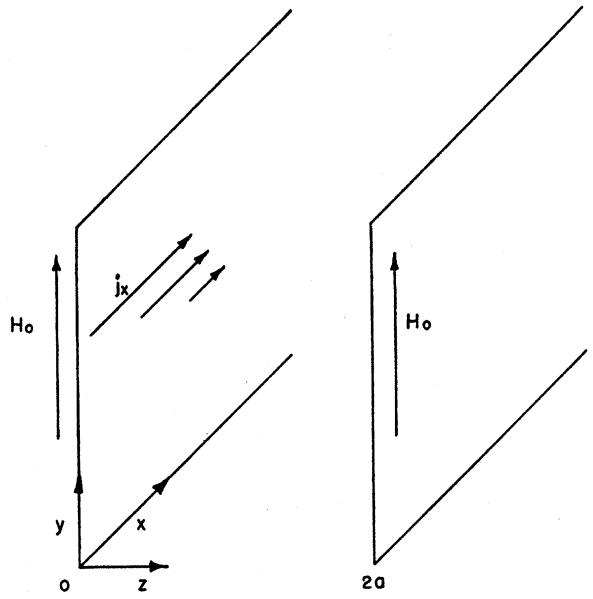

Figure 5.1: An NFE-SC film of thickness $2a$ is placed in an externally applied magnetic field $H(z,t)$. Supercurrent j_x shields the interior,[11]

We consider an NFE-SC film of finite thickness $2a$ and infinite surface area with normal to the surface in the z-direction. An external electro-magnetic

field is applied parallel to the film surface in the direction y .The incident electro magnetic field is also taken in the symmetrical form as[31]:

$$\mathbf{E}_i(z,t) = \hat{\mathbf{x}}\left(E_i \exp\left(i(k_z z - \omega t)\right) + E_i^{\star} \exp\left(-i(k_z z - \omega t)\right)\right) \tag{5.14}$$

The applied magnetic field can be written as $H\left(z,t\right) = H_0 e^{ikz - i\omega t}$

This external electric field creates nonlocal Pippard current in the sample. Diamagnetic super currents are established along the x direction which shield the interior of the film. Maximas for image current densities are established at $z = 0, \pm 2a, \pm 4a, ...$ etc[48],[11].

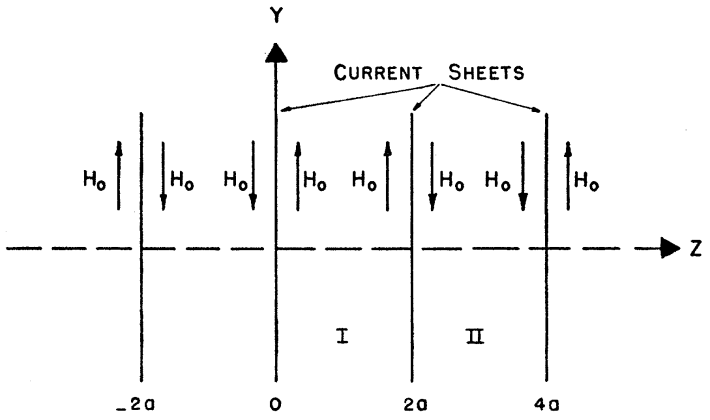

Figure 5.2: An array of image current sheets are induced because of the supercurrent at positions $z = 0, \pm 2a, \pm 4a, ..$ etc,[11]

Magnitude of the image surface current can be written as

$$\sigma = \frac{cH_0}{2\pi} \cos\left(kz\right) e^{-i\omega t} \tag{5.15}$$

Fourier analysis of the image current sources give us the expression for the source current density

$$j_x^{\sigma}(z) = \frac{-cH_0}{2\pi a}\sum_{n=0}^{\infty} e^{-i\omega t}\cos(kz)\cos(q_n z) \tag{5.16}$$

where $q_n = (2n+1)\pi/a$

Substituting the expressions above in the Maxwell's equation

$$\nabla \times \mathbf{H} = \frac{1}{c}\frac{\partial \mathbf{D}}{\partial t} + \frac{4\pi}{c}\mathbf{J}_e \tag{5.17}$$

we get

$$\frac{1}{c}\frac{\partial \mathbf{D}}{\partial t} = \frac{1}{c}\frac{\partial}{\partial t}(\varepsilon(\omega)\mathbf{E}) \tag{5.18}$$

Substituting equation (5.9) leads us to

$$\frac{1}{c}\frac{\partial \mathbf{D}}{\partial t} = -\frac{\omega^2}{c^2}\varepsilon(\omega)\mathbf{A} \tag{5.19}$$

The momentum space relation between J and A can be written as[22]

$$J(q) = \frac{-c}{4\pi}K(q)a(q) \tag{5.20}$$

and

$$\nabla \times \mathbf{H} = \nabla \times \nabla \times \mathbf{A} = q_n^2 A_x(q_n) \tag{5.21}$$

Combining all these terms, in momentum space,

$$q_n^2 A_x(q_n) = -\varepsilon(\omega)\frac{\omega^2}{c^2}A_x(q_n) - \frac{2H_0}{a}e^{-i\omega t} - K(q_n)A(q_n) \tag{5.22}$$

Solving the equation gives us the expression for the vector potential

$$A_x(z) = -\frac{2H_0}{a}\sum_{n=0}^{\infty} e^{-i\omega t}\frac{\cos(kz)\cos(q_n z)}{q_n^2 + K(q_n) + \frac{\omega^2}{c^2}\varepsilon(\omega)} \tag{5.23}$$

We shall calculate the magnetic susceptibility[49] of the thin film which is given by

$$\frac{\kappa}{\kappa_0} = \frac{1}{2a}\int_{-a}^{a}\frac{H_0 e^{ikz-i\omega t} - H_y(z)}{H_0 e^{ikz-i\omega t}}dz \;= 1 - \frac{e^{i\omega t}}{2aH_0}\int_{-a}^{a} e^{-ikz}\frac{\partial A}{\partial z}dz \tag{5.24}$$

For the thin film we can take the approximation $e^{ikz} \sim 1$. This gives us

$$-4\pi\kappa = 1 - \frac{e^{i\omega t}}{2aH_0}\int_{-a}^{a}\frac{\partial A}{\partial z}dz = 1 - \frac{e^{i\omega t}A(a)}{aH_0} \tag{5.25}$$

where $\kappa_0 \equiv -1/4\pi$ and we have used $A_x(a) = -A_x(-a)$ due to symmetry. With the increase in the thickness of the film , there would be more corrections to the susceptibility and the integration in equation (5.24) has to be calculated numerically.

Substituting the expression for $A_x(z)$ in the equation above we obtain the expression for magnetic susceptibility of a thin NFE-SC film for specular reflection, such as

$$-4\pi\kappa = 1 - \frac{2\cos(2ka)}{a^2}\sum_{n=0}^{\infty}\frac{1}{q_n^2 + K(q_n) + \frac{\omega^2}{c^2}\varepsilon(\omega)} \tag{5.26}$$

where $\cos(q_n z)|_{z=2a} \to 1$

5.2 Random Scattering

Due to symmetry, equation (5.13) can be reduced to an one dimensional problem as

$$\frac{d^2 A_x(z)}{dz^2} + \frac{\omega^2}{c^2}\varepsilon(\omega) A_x(z) - \int_{-a}^{a} G(z-z') A_x(z')\, dz' = 0 \tag{5.27}$$

where $G(z-z')$ is the Pippard kernel which in this case is defined as[45], [46]

$$G_P(z-z') = \frac{3\pi}{\xi_0 \Lambda c} \int_{|z-z'|}^{\infty} \left(\frac{1}{\eta} - \frac{|z-z'|^2}{\eta^3} \right) e^{-\eta/\xi} d\eta \tag{5.28}$$

With separation of variables for A_{xi},A_{xr} and A_{xt} (incident,reflected and transmitted or inside the film)

$$\frac{d^2 A_{xr}(z)}{dz^2} + \frac{\omega^2}{c^2}\varepsilon_0 A_{xr}(z) = 0 \tag{5.29}$$

$$\frac{d^2 A_{xt}(z)}{dz^2} + \frac{\omega^2}{c^2}\varepsilon(\omega) A_{xt}(z) - \int_{-a}^{a} G(z-z') A_{xt}(z') dz' = 0 \tag{5.30}$$

The boundary conditions are

$$B_i + B_r = B_t,$$

$$B_i - B_r = E_t \tag{5.31}$$

which could also be written as

$$2B_i = B_t + E_t = \left.\frac{\partial A_{xt}}{\partial z}\right|_{z=a} + \left(-\frac{1}{c}\right)\left.\frac{\partial A_{xt}}{\partial t}\right|_{z=a}$$

or

$$2B_0 e^{ika-i\omega t} = \left.\frac{\partial A_{xt}}{\partial z}\right|_{z=a} + \left.\frac{i\omega}{c}A_{xt}\right|_{z=a} \tag{5.32}$$

We assume that at the boundary the plane wave part is still dominant.We are looking for the vector potential $A_{xt}(z)$ inside the medium. So we have the integro-differential equation only for A_{xt}. At this point we can drop the suffix t for the transmitted wave and we are left with

$$\frac{d^2 A_x(z)}{dz^2} + \frac{\omega^2}{c^2}\varepsilon(\omega) A_x(z) - \int_{-a}^{a} G(z-z') A_x(z')\, dz' = 0 \tag{5.33}$$

for the vector potential $A_x(z)$ inside the medium.

At this point let us introduce the following functional:

$$F(x, A(x), A'(x)) = \frac{1}{2}\left(\frac{dA}{dx}\right)^2 - \frac{1}{2}\frac{\omega^2}{c^2}\varepsilon(\omega) A^2 + \tag{5.34}$$
$$+\frac{1}{2}\int_{-a}^{a} A(x) A(y) G(x-y)\, dy - 2B_0 e^{ika-i\omega t}\left(\frac{dA}{dx} + \frac{i\omega}{c}A\frac{dA}{dx}\right)$$

A variational equivalent of equation (5.33) with the boundary conditions (5.32) can be written as

$$\delta I = \delta \int_{-a}^{a} F(x, A(x), A'(x)) dx = 0 \tag{5.35}$$

where the use of the functional F in the Euler-Lagrange equation[50], [51] leads us back to equations (5.32) . We have used the following condition

$$\frac{\partial F\left(a\right)}{\partial y_1'}+\frac{\partial F\left(a\right)}{\partial y_2'}+\frac{\partial g\left(a\right)}{\partial y_1}+\frac{\partial g\left(a\right)}{\partial y_2}=0 \tag{5.36}$$

with $g(a)=0$ in our case. Substituting F in equation (5.35) we get

$$\begin{aligned}&\delta\left\{\frac{1}{2}\int_{-a}^{a}\left(\frac{dA}{dx}\right)^{2}dx-\frac{1}{2}\frac{\omega^{2}}{c^{2}}\varepsilon\left(\omega\right)\int_{-a}^{a}A^{2}dx\right\}\\&+\delta\left\{\frac{1}{2}\int_{-a}^{a}\int_{-a}^{a}A\left(x\right)A\left(y\right)G\left(x-y\right)dxdy\right\}\\&-\delta\left\{2B_{0}e^{ika-i\omega t}\int_{-a}^{a}\left(\frac{dA}{dx}+\frac{i\omega}{c}A\frac{dA}{dx}\right)dx\right\}=0\end{aligned} \tag{5.37}$$

We choose a trial function of the form

$$A\left(z\right)=\sum_{n,odd}C_{n}z^{n} \tag{5.38}$$

After substituting into equation 5.37, we have the algebraic equation

$$\sum_{n,odd}C_{n}\left(\sum_{m,odd}C_{m}\left(\frac{nma^{n+m-1}}{n+m-1}-\frac{\omega^{2}}{c^{2}}\varepsilon\left(\omega\right)\frac{a^{n+m+1}}{n+m+1}+G_{mn}\right)-4B_{0}e^{ika-i\omega t}a^{n}\right)=0 \tag{5.39}$$

or

$$\sum_{m,odd}C_{m}\left(\frac{nma^{n+m-1}}{n+m-1}-\frac{\omega^{2}}{c^{2}}\varepsilon\left(\omega\right)\frac{a^{n+m+1}}{n+m+1}+G_{mn}\right)=4B_{0}e^{ika-i\omega t}a^{n} \tag{5.40}$$

where

$$G_{mn} = \int_{-a}^{a}\int_{-a}^{a} x^m y^n G\left(x-y\right) dxdy$$

Within the non-local theories such as BCS and Pippard, there is no analytical formula available for the magnetic field $h\left(z\right)$. It has to be calculated numerically. Equation (5.40) can lead to approximate solution for the vector potential and ultimately the magnetic field. But we solved the integro-differential equation (5.27) using powerful programming techniques in Mathematica, which lead us to elegant solution for the magnetic field inside the sample.

We start with the integro-differential equation (5.27)

$$\frac{d^2 A_x\left(z\right)}{dz^2} + \frac{\omega^2}{c^2}\varepsilon\left(\omega\right) A_x\left(z\right) - \int_{-a}^{a} G\left(z-z'\right) A_x\left(z'\right) dz' = 0$$

with the Pippard Kernel given by equation(5.28) as

$$G_P\left(z-z'\right) = \frac{3\pi}{\xi_0 \Lambda c}\int_{|z-z'|}^{\infty}\left(\frac{1}{\eta} - \frac{\left|z-z'\right|^2}{\eta^3}\right) e^{-\eta/\xi} d\eta$$

We introduce a set of dimensionless variables such as [12]

$$\begin{aligned} &s = \eta/\xi \\ &\Delta = 2a/\xi \\ &\alpha = 3\pi\xi^3/(\xi_0 \Lambda c) \\ &F\left(s\right) = A_x\left(z\right)/(\xi H_{ext}) \\ &k\left(|s|\right) = \xi_0 \Lambda c G\left(|z|\right)/(3\pi) \end{aligned}$$

and

$$\omega_{LO}^2/\omega_{TO}^2 = \varepsilon_0/\varepsilon_\infty = \varepsilon'$$
$$\omega/\omega_{LO} = \omega'$$
$$\beta'' = \omega_{LO}^2 \varepsilon' \xi H_{ext} \varepsilon_\infty / c^2 = \omega_0^2 \varepsilon_0 \xi H_{ext}/c^2$$
$$\beta(\omega) = \beta'' \omega'^2 (1-\omega'^2)/(1-\varepsilon'\omega'^2)$$

which transforms the integro-differential equation (5.27)

$$F''(s) - \beta(\omega) F(s) = \alpha \int_0^\Delta k(|s-\tilde{s}|) F(\tilde{s})\, d\tilde{s} \tag{5.41}$$

$$F'(0) = F'(\Delta) = 1 \tag{5.42}$$

$$F(0) = 1/2 \tag{5.43}$$

where the prime symbol 'on F indicates the derivative w.r.t. s. $F(s)$ can be written as[49], [52],[12]

$$F(s) = \psi(s) - \psi(\Delta - s) \tag{5.44}$$

The film thickness Δ is divided into n intervals such as $l = \Delta/n$ [53]. For convenience, we write $\psi(k.l) = \psi_k, (k = 0, ..., n)$. The second derivative of this expression can be approximated as

$$\psi_k'' \simeq \frac{1}{l^2}(\psi_{k+1} - 2\psi_k + \psi_{k-1}) + \frac{\beta(\omega)}{c^2}\psi_k \tag{5.45}$$

The following identities are used [54], [53], [55]:

$$v(s) = -v(-s) = \int_0^s k(|t|)dt$$
$$= \frac{2}{3} + \frac{1}{6}e^{-s}\left[s(s-1) - 4\right] - \frac{1}{6}s\left(s^2 - 6\right)\Gamma(0,s) \tag{5.46}$$

We also define

$$w(s) = w(-s) = \int_0^s v(t)\,dt$$
$$= \frac{1}{12}(8s-3) + \frac{1}{24}e^{-s}\left(s^3 - s^2 - 10s + 6\right) - \frac{1}{24}s^2\left(s^2 - 12\right)\Gamma(0,s) \tag{5.47}$$

for $s \geq 0$. The gamma function is defined as

$$\Gamma(a,s) = \int_s^\infty t^{a-1}e^{-t}dt \tag{5.48}$$

The behavior of the w, v and Γ function are presented in figure (5.3) From the identities above, it follows that $k(s) = v'(s) = w''(s)$, hence

$$\int_0^\Delta k(|s-\tilde{s}|)\psi(\tilde{s})\,dt = v(|s-\tilde{s}|)\psi(\tilde{s})|_0^\Delta - \int_0^\Delta k(|s-\tilde{s}|)\psi(\tilde{s})\,dt$$
$$= v_{n-i}\psi_n - v_{-i}\psi_0 - \sum_{k=0}^{n-1}\frac{1}{l}(\psi_{k+1} - \psi_k)(w_{k+1-i} - w_{k-i}) \tag{5.49}$$

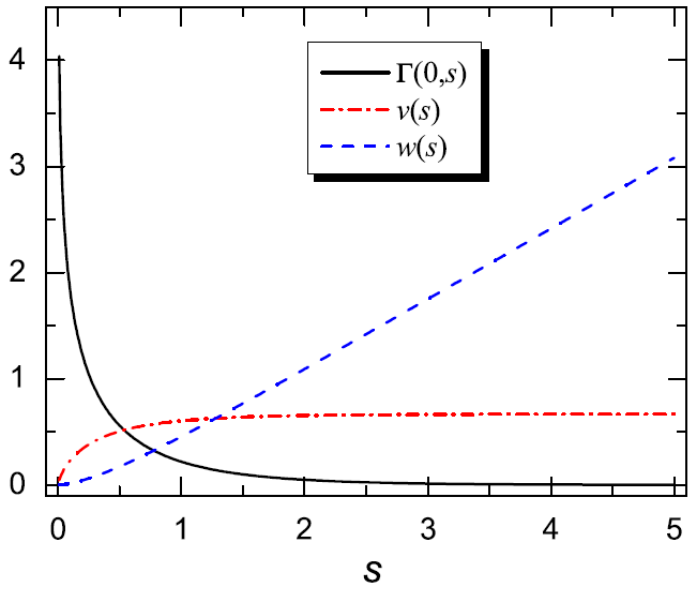

Figure 5.3: Behavior of w, v and Γ functions used in the calculation, [12]

Equations (5.46) and (5.49) together with equation (5.41) lead us to the set of linear equations such as

$$\frac{1}{\alpha l^2}\left[\psi_{i+1} - \left(2 + \beta'' \omega'^2 \frac{1-\omega'^2}{1-\varepsilon'\omega'^2}\right)\psi_i + \psi_{i-1}\right] = \psi_0\left[-v_{-i} + \frac{1}{l}\left(w_{1-i} - w_{-i}\right)\right] + \sum_{k=0}^{n-1} \psi_k \frac{1}{l}\left[w_{k+1-i} - 2w_{k-i} + w_{k-1-i}\right] + \psi_n\left[v_{n-i} - \frac{1}{l}\left(w_{n-i} - w_{n-i-1}\right)\right] \quad (5.50)$$

The boundary conditions should be formulated in such a manner so as to

satisfy the condition that the current should remain in the boundary of the sample. It can be written as

$$\psi'(0) = \frac{1}{2l}\left[-3\psi_0 + 4\psi_1 - \psi_2\right] = 0 \tag{5.51}$$

$$\psi'(\Delta) = \frac{1}{2l}\left[-3\psi_n - 4\psi_{n-1} + \psi_{n-2}\right] = 1 \tag{5.52}$$

The equations can be written in the matrix form as

$$(D - C)\,\psi = d \tag{5.53}$$

where

$$D = \frac{1}{\alpha l^2}\begin{bmatrix} 0 & 0 & 0 & . & . & . & 0 & 0 & 0 \\ 1 & -2+f(\omega) & 1 & 0 & . & . & . & 0 & 0 \\ 0 & 1 & -2+f(\omega) & 1 & 0 & . & . & . & 0 \\ . & . & . & . & . & . & . & . & . \\ . & . & . & . & . & . & . & . & . \\ . & . & . & . & . & . & . & . & . \\ 0 & 0 & . & . & . & 0 & 1 & -2+f(\omega) & 1 \\ 0 & 0 & 0 & . & . & . & 0 & 0 & 0 \end{bmatrix} \tag{5.54}$$

Here

$$f(\omega) = \beta'' \omega'^2 \frac{1-\omega'^2}{1-\varepsilon'\omega'^2} \tag{5.55}$$

The C matrix can be written as

$$C = \begin{bmatrix} -3/(2l) & 4/(2l) & -1/(2l) & 0 & . & . & . & 0 & 0 \\ a_1 & c_{11} & c_{21} & c_{31} & . & . & . & c_{n-1,1} & b_1 \\ a_2 & c_{12} & c_{22} & c_{32} & . & . & . & c_{n-1,2} & b_2 \\ . & . & . & . & . & . & . & . & . \\ . & . & . & . & . & . & . & . & . \\ . & . & . & . & . & . & . & . & . \\ a_{n-1} & c_{1,n-1} & c_{2,n-1} & c_{3,n-1} & . & . & . & c_{n-1,n-1} & b_{n-1} \\ 0 & 0 & . & . & . & 0 & 1/(2l) & -4/(2l) & 3/(2l) \end{bmatrix} \tag{5.56}$$

Matrix elements a, b, and c in the C matrix are the following:

$$\begin{aligned} a_i &= \left[-v_{-i} + \frac{1}{l} \left(w_{1-i} - w_{-i} \right) \right] \\ b_i &= \left[v_{n-i} - \frac{1}{l} \left(w_{n-i} - w_{n-i-1} \right) \right] \\ c_{ki} &= \left[w_{k+1-i} - 2w_{k-i} + w_{k-1-i} \right] \end{aligned} \tag{5.57}$$

The d matrix in equation (5.53) is

$$d = \begin{bmatrix} 0 & 0 & 0 & . & . & . & 0 & 0 & 1 \end{bmatrix} \tag{5.58}$$

with $n + 1$ elements.

We solved this system of equations using Mathematica. To the best of our knowledge, the software developed here is one of the most efficient methods to solve integro-differential equations and the results given here represent

the distribution of current in an NFE-SC Thin film in various frequency range. The plots are normalized current vs. normalized frequency. In standard superconducting film in the non-local Pippard limit, supercurrent does not penetrate inside the sample and has the highest value at the boundary. However, in an NFE-SC material with its high background dielectric, the current enters the medium unlike a regular superconductor. At certain frequencies, the magnetic field is expelled from the interior of the NFE-SC film thus making it behave like a standard superconductor. We have given all the numerical parameters and data for the current here, which can be verified by any suitable experiment on NFE-SC films.

We also compare the nature of current inside an NFE-SC sample to that of a regular superconductor to show the stark difference between these two similar yet different materials. Figure (5.7) represents the current potential A within a superconducting film. The value of A inside the sample remains zero indicating exclusion of magnetic filed from the interior.

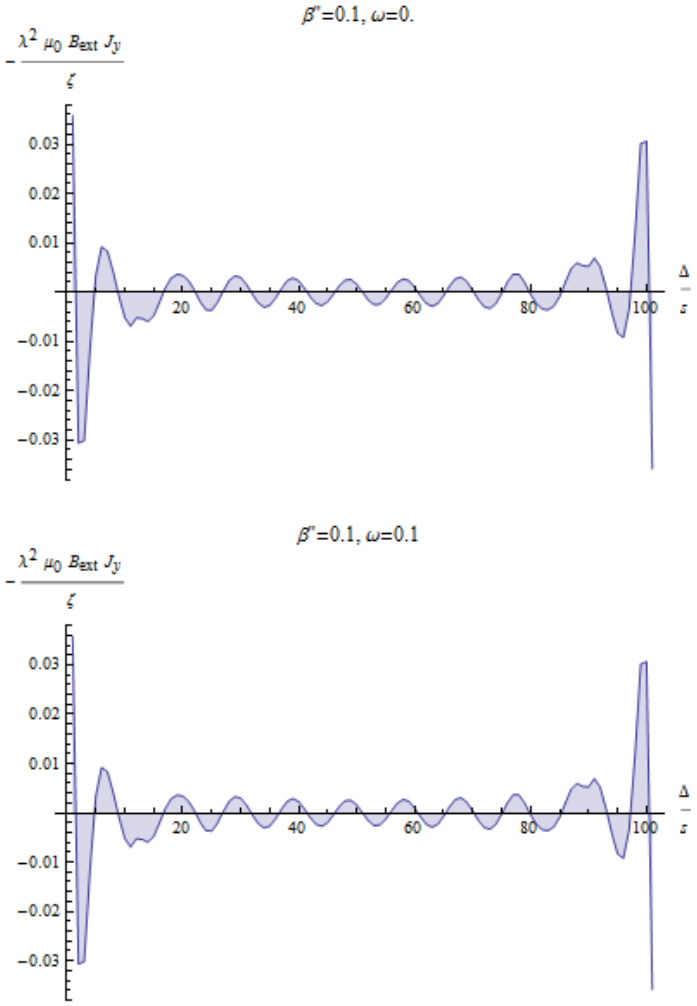

Figure 5.4: Normalized current vs. normalized frequency for $\omega = 0$ and $\omega = 0.1$. As can be seen here, near the boundary of the sample, the current has a higher value. Inside the sample, the current penetrates unlike a standard superconductor.

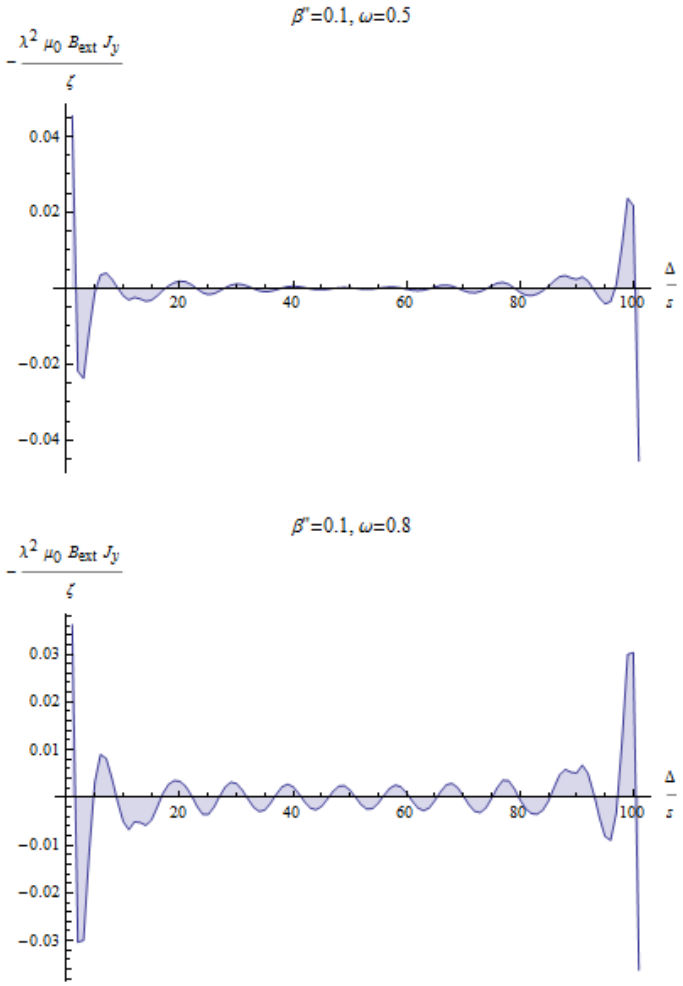

Figure 5.5: Normalized current vs. normalized frequency for the normalized frequencies $\omega = 0.5$ and $\omega = 0.8$. At $\omega = 0.5$, the current is nearly expelled from the sample like a standard superconductor.

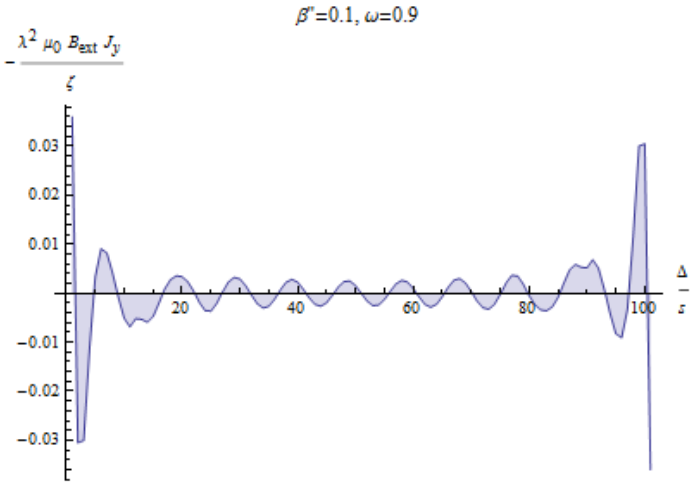

Figure 5.6: Normalized current vs. normalized frequency for $\omega = 0.9$. The current maintains a non-zero value inside the sample.

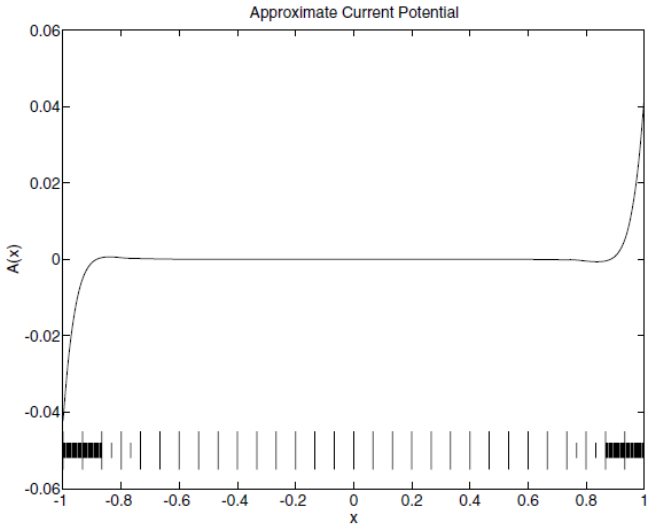

Figure 5.7: A linear finite approximation to the current potential in Pippard's nonlocal superconductivity model. Image source [13]

Summary

We explored the vortex structure in a nearly-ferroeletric thin film and film of finite thickness in London limit. The NFE-SC material having a high back ground dielectric expels the vortex structure from the sample at resonances thus exhibiting the nearly-ferroelectric behavior. In our work on NFE-SC material in nonlocal Pippard limit, we studied the specular and random reflection for a thin film. We found that the current penetrates the sample unlike a standard superconductor. At certain frequencies it gets nearly-expelled from the sample thus rendering its behavior superconductor-like.

Appendix A

Codes used in solving Non-local Random Reflection

The numerical implementation of the equations in Chapter 4 is done in Mathematica and the codes are given below:

```
Solution for the current in an NFE-SC Thin film in the Pippard limit.


PsiOmega[CapitalDelta_, bEta_, NumberOfItterations_, \[Omega]_] :=
 Module[
   {v, w,
    lEngth = CapitalDelta/NumberOfItterations,
    a, b, c,
    DMatrix, dMatrix, CMatrix, aa, bb, cc},
```

```
v[s_ /; s > 0] := 2/3 + Exp[-s]/6 (s (s - 1) - 4) -
  (s (s^2 - 6))/6 Gamma[0, s];
v[s_ /; s < 0] := -(2/3 + Exp[s]/6 (-s (-s - 1) - 4) -
    (-s (s^2 - 6))/6 Gamma[0, -s]);
v[0] = 0;
w[s_ /; s > 0] := 1/12 (8 s - 3) + 1/24 Exp[-s] (s^3 - s^2 - 10 s + 6) -
  1/24 s^2 (s^2 - 12) Gamma[0, s];
w[s_ /; s < 0] :=
 1/12 (8 (-s) - 3) + 1/24 Exp[s] ((-s)^3 - s^2 + 10 s + 6) -
  1/24 s^2 (s^2 - 12) Gamma[0, -s];
w[0] = 0;


a = Array[(-v[-#*lEngth] + (w[1 - #*lEngth] - w[-#*lEngth])/lEngth) &,
   NumberOfItterations - 1] // N;
b = Array[(v[
       NumberOfItterations - #*
         lEngth] - (w[NumberOfItterations - #*lEngth] -
         w[NumberOfItterations - 1 - #*lEngth])/lEngth) &,
   NumberOfItterations - 1] // N;
c = Array[(w[#2*lEngth +
```

```
          1 - #1*lEngth] - (2 + (bEta*(\[Omega]^2)*(1 - \[Omega]^2)/(1 -
                4.1*\[Omega]^2)))*w[#1*lEngth - #2*lEngth] +
       w[#1*lEngth - 1 - #2*lEngth])/lEngth &, {NumberOfItterations - 1,
    NumberOfItterations - 1}] // N;
DMatrix =
 SparseArray[{{1, 1} -> 0, {1, 2} ->
    0, {NumberOfItterations + 1, NumberOfItterations + 1} -> 0,
   {NumberOfItterations + 1, NumberOfItterations} -> 0, Band[{1, 1}] -> -2,
    Band[{2, 1}] -> 1, Band[{1, 2}] -> 1}, {NumberOfItterations + 1,
   NumberOfItterations + 1}];
dMatrix =
 SparseArray[(NumberOfItterations + 1) -> 1, NumberOfItterations + 1];
Module[
 {tempMatrixUpper =
   SparseArray[{1 -> -3, 2 -> 4, 3 -> -1},
     NumberOfItterations + 1]/(2 lEngth),
  tempMatrixLower =
   SparseArray[{(NumberOfItterations + 1) -> 3,
      NumberOfItterations -> -4, (NumberOfItterations - 1) -> 1},
     NumberOfItterations + 1]/(2 lEngth)},
```

```
    CMatrix =
     Prepend[Append[Transpose[Prepend[Append[c, b], a]], tempMatrixLower],
      tempMatrixUpper]];
   LinearSolve[DMatrix - CMatrix, dMatrix]
   ];


GraphicsColumn[
 Table[ListLinePlot[
   PsiOmega[10, 0.1, 100, \[Omega]] -
    Reverse[PsiOmega[10, 0.1, 100, \[Omega]]], Filling -> Axis,
   PlotRange -> All,
   AxesLabel -> {\[CapitalDelta]/
      s, ( -Subscript[\[Mu], 0] \[Lambda]^2/\[Zeta] Subscript[B,
        ext]) Subscript[J, y]},
   PlotLabel ->
    "\[Beta]''=" <> ToString[0.1] <> ", \[Omega]=" <>
     ToString[\[Omega]]], {\[Omega], {0.0, 0.1, 0.5, 0.8, 0.9}}]]
```

Bibliography

[1] M. Hargittai and I. Hargittai. *Symmetry through the Eyes of a Chemist*. Springer Verlag, 1995.

[2] P. Chandra and P. Littlewood. A Landau primer for ferroelectrics. *Physics of Ferroelectrics*, pages 69–116, 2007.

[3] K.M. Rabe, C.H. Ahn, and J.M. Triscone. *Physics of ferroelectrics: a modern perspective*. 2007.

[4] K.C. Kao. *Dielectric phenomena in solids*. Elsevier Academic Press San Diego, CA, 2004.

[5] M. Fox. *Optical properties of solids*. Oxford University Press, USA, 2010.

[6] J.B. Ketterson and S.N. Song. *Superconductivity*. Cambridge University Press, UK, 1999.

[7] Charles Kittel. *Introduction to Solid State Physics* . John Wiley and Sons, Inc, New York, 1986.

[8] Charles P. Poole Jr. *Handbook of Superconductivity* . Academic Press, 2000.

[9] Joseph L. Birman and Natalya A. Zimbovskaya. Electrodynamics of nearly ferroelectric superconductors. *Phys. Rev. B*, 64(14):144506, Sep 2001.

[10] D. Agassi and J.R. Cullen. Single-vortex structure in a superconductor film and strip. *Physica C*, 334:274–282, February 2000.

[11] J. R. Schrieffer. Evaluation of some nonlocal theories for a thin superconducting film. *Phys. Rev.*, 106(1):47–50, Apr 1957.

[12] Andreas Suter. Pippard's non-local effect in the case of diffuse scattering. June 2004.

[13] T. Lin and R.C. Rogers. Accurate computation of the field in Pippards nonlocal superconductivity model. *J. Integral Equations Appl*, 7:167–192, 1995.

[14] C.H. Rabe, Karin M. Ahn and J. Triscone. *Physics of Ferroelectrics: A Modern Prospective*. Springer-Verlag, Berlin, 2007.

[15] Istvan Hargittai and Magdolna Hargittai. *Symmetry through the Eyes of a Chemist* . Plenum Press,New York, 1995.

[16] David Y. Curtin and Iain C. Paul. Chemical consequences of the polar axis in organic solid-state chemistry. *Chemical Reviews*, 81(6):525–541, 1981.

[17] Richard J.D. Tilley. *Understanding Solids: The Science of Materials*. John Wiley and Sons Ltd, UK, 2004.

[18] M.E. Lines and A.M. Glass. *Principles and applications of ferroelectrics and related materials*. Clarendon Press, Oxford, 1977.

[19] L.D. Landau and E.M. Lifshitz. *Statistical Physics* . Pergamon,Oxford, 1959.

[20] A. F. Devonshire. Xcvi. theory of barium titanate – part i. *Philosophical Magazine Series 7*, 40:1040–1063, 1949.

[21] F. Wooten and F. Stern. Optical properties of solids. *Physics Today*, 26:60, 1973.

[22] M. Tinkham. *Introduction to Superconductivity* . McGraw Hill, New York, 1996.

[23] A. Narlikar. *Frontiers in Superconducting materials*. Springer-Verlag, Berlin, 2004.

[24] F. London. *Superfluids, Volume 1, Macroscopic Theory of Superconductivity*. New York: Dover, 1961.

[25] F. London and H. London. The electromagnetic equations of the supraconductor. *Proceedings of the Royal Society of London. Series A, Mathematical and Physical Sciences*, 149(866):71–88, 1935.

[26] V.L. Ginzburg and E.A. Andryushin. *Superconductivity: Revised Edition* . Plenum, new York, 2004.

[27] K.H. Bennemann and J.B. Ketterson. *Superconductivity* . Springer-Verlag, Berlin, 2008.

[28] S. Reich and Y. Tsabba. Possible nucleation of a 2d superconducting phase on wo3 single crystals surface doped with na+. *Euro. Phys.J. B.*, 9:1–4, May 1999.

[29] Ch. J. Raub, A. R. Sweedler, M. A. Jensen, S. Broadston, and B. T. Matthias. Superconductivity of sodium tungsten bronzes. *Phys. Rev. Lett.*, 13(25):746–747, Dec 1964.

[30] J.L. Birman and M. Weger. Theory of coexistence of superconductivity and ferroelectricity: A dynamical symmetry model. *Physical Review B*, 64(17):174503, 2001.

[31] J.D. Jackson and R.F. Fox. Classical electrodynamics. *American Journal of Physics*, 67:841, 1999.

[32] M. Born and K. Huang. *Dynamical theory of crystal lattices*. Oxford University Press, USA, 1988.

[33] PA Fleury and JM Worlock. Electric-Field-Induced Raman Scattering in SrTiO_{3} and KTaO_{3}. *Physical Review*, 174(2):613–623, 1968.

[34] A. Abrikosov. Fundamentals of the Theory of Metals.(Translation). *Elsevier Science Publishers, 1988,*, page 630, 1988.

[35] RA Cowley. Temperature dependence of a transverse optic mode in strontium titanate. *Physical Review Letters*, 9(4):159–161, 1962.

[36] T. Mitsui and WB Westphal. Dielectric and X-ray studies of CaxBa1-xTiO3 and CaxSr1-xTiO3. *Physical Review*, 124:1354–1359, 1961.

[37] A. Baratoff and G. Binnig. Mechanism of superconductivity in SrTiO/sub 3. *Name: Physica B+ C (Amsterdam*, 1981.

[38] J. Pearl. Current distribution in superconducting films carrying quantized fluxoids. *Applied Physics Letters*, 5(4):65–66, 1964.

[39] P.G. De Gennes. *Superconductivity of metals and alloys*. 1999.

[40] P.G. de Gennes. *Superconductivity of Metals and Alloys*. W. A. Benjamin, Inc.,New York, 1966.

[41] I.N. Sneddon. *Fourier transforms*. Dover Pubns, 1995.

[42] I.S. Gradshteyn, I.M. Ryzhik, A. Jeffrey, and D. Zwillinger. *Table of integrals, series, and products*. Academic press New York, 1980.

[43] A.B.Pippard. *Proc. Roy. Soc.*, A216, 1953.

[44] J.R. Schrieffer. *Theory of Superconductivity*. Addision Wesley, San Francisco, 1964.

[45] AB Pippard. An experimental and theoretical study of the relation between magnetic field and current in a superconductor. *Proceedings of the Royal Society of London. Series A, Mathematical and Physical Sciences*, 216(1127):547–568, 1953.

[46] M. R. Schafroth and J. M. Blatt. Phenomenological equations for superconductors. *Phys. Rev.*, 100(4):1221–1222, Nov 1955.

[47] K. Huang. Lattice vibrations and optical waves in ionic crystals. 1951.

[48] JM Lock. Penetration of Magnetic Fields into Superconductors III. Measurements on Thin Films of Tin, Lead and Indium. *Proceedings of the Royal Society of London. Series A, Mathematical and Physical Sciences*, pages 391–408, 1951.

[49] W. Liniger and F. Odeh. Susceptibilities and Critical Fields of Superconducting Films. *Physical Review Letters*, 10(2):47–48, 1963.

[50] O.P. Agrawal. Formulation of Euler-Lagrange equations for fractional variational problems. *Journal of Mathematical Analysis and Applications*, 272(1):368–379, 2002.

[51] M. Crampin. On the differential geometry of the Euler-Lagrange equations, and the inverse problem of Lagrangian dynamics. *Journal of Physics A: Mathematical and General*, 14:2567, 1981.

[52] C.T.H. Baker. *The numerical treatment of integral equations*. Clarendon press Oxford, 1977.

[53] LM Delves and JL Mohamed. *Computational methods for integral equations*. Cambridge Univ Pr, 1988.

[54] K.E. Atkinson. *The numerical solution of integral equations of the second kind*. Cambridge Univ Pr, 1997.

[55] H. Brunner and PJ van der Houven. *The numerical solution of Volterra equations*. Amsterdam, 1986.